Max-Planck-Institut für molekulare Zellbiologie und Genetik
Direktor: Prof. Dr. Marino Zerial

Characterisation of hepatic polarity formation and its contribution to liver architecture emergence during mouse development

Dissertationsschrift

zur Erlangung des akademischen Grades
Doctor of Philosophy (Ph.D.)
vorgelegt
der Medizinischen Fakultät Carl Gustav Carus
der Technischen Universität Dresden

von

Julien Delpierre, MSc

aus Paris, Frankreich.

Dresden 2021

Abstract

Hepatocytes, the parenchymal cells of the liver are polarized in a unique way. This polarity contributes to the fine architecture of the organ. These cells are forming a continuous secretory network of bile canaliculi and all of them are in contact with the vascular network. The advances in microscopy and clearing techniques have led to a better understanding of the adult liver architecture. However, our knowledge of the establishment of this structure during development remains elusive.

In this study we aimed at identifying and characterizing the key steps in bile canaliculi network formation and hepatocyte polarity acquisition.

With this goal we performed deep tissue imaging on mouse embryonic liver sections to look at polarized trafficking and junctional markers to follow polarity establishment. We looked at ECM and cell division markers to correlate cues susceptible to guide polarization. We also performed in vitro experiments to further explore the hypotheses formulated along the way based on in vivo observations.

We found that multipolar polarity arises from both lumen tubular elongation and multiple lumen formation. The formation of multiple lumina involves the synchronized movement of a Rab11 vesicular cluster and the centrosome. Our study also suggests that ZO-1 could be involved in the synchronization between vesicular cluster movement and junction plate formation. Finally, we could correlate fibronectin distribution to potential early polarization events

Table of Contents

List of Figures

List of Tables

List of abbreviations

E(number) - number of days of mouse embryonic development
FGF - Fibroblast Growth Factor
BMP - Bone Morphogenic Protein
HNF6 - Hepatocyte Nuclear Factor 6
ECM - Extracellular Matrix
TGFβ - Transforming Growth Factor β
CD(number) - Cluster of Differentiation number
TJ - Tight Junctions
PAR - Partition-defective
CRB - Crumbs
SCRIB - Scribble
NAFLD - Non-Alcoholic Fatty Liver Disease
MDCK - Madin-Darby Canine Kidney
ZO-1 - Zonula Occludens 1
AMIS - Apical Membrane Initiation Site
ARE - Apical Recycling Endosome
PAP – Pre-Apical Patch
DPPIV - Dipeptidyl Peptidase IV
MRP2 - Multidrug Resistance Protein 2
EM - Electron Microscopy
KD - Knock-Down
siRNA - Small Interfering Ribonucleic Acid
VAC - Vacuolar Apical Compartment
RT-qPCR - Reverse transcription-quantitative polymerase chain reaction
GFP - Green Fluorescent Protein
EGFP - Enhanced Green Fluorescent Protein
CARE - Content Aware Image Restoration
FLK1 - Foetal Liver Kinase 1
FRAP - Fluorescence Recovery After Photobleaching
E-Cadherin - Epithelial Cadherin
PBS - Phosphate Buffered Saline
PFA - Paraformaldehyde
BSA - Bovine Serum Albumin
SeeDB - See Deep Brain
DNAse I - Deoxyribonuclease I
MACS - Magnetic Cell Isolation
Dlk1 - Delta Like Non-Canonical Notch Ligand 1
mAb – Monoclonal Antibody
FITC - Fluorescein isothiocyanate
IE-HPLC - Ion-Exchange High Performance Liquid Chromatography
LC-MS - Liquid chromatography–mass spectrometry

1 Introduction

1.1 Liver Architecture

The liver holds multiple essential function. Among them, multiple are key for metabolic homeostasis maintenance. All these functions are distributed within a functional unit called the liver lobule. Structurally the lobule is defined by the axis (called metabolic axis) between the portal triad (blood input and bile output) and the central vein (blood output) (Figure 1.1-1). The venous blood from the gut, loaded with nutrients, enter the organ via the portal vein, it is then mixed with oxygen rich blood coming from the portal artery in the portal area. The blood then runs through a network of capillaries called sinusoids. Before reaching the Central vein to exit the organ. In the other direction bile is secreted through a second network formed by hepatocytes, the bile canaliculi network. Bile then flows toward the collecting bile duct in the portal area. The bile is then sent to the gall bladder before it reaches the gut to digest dietary lipids.

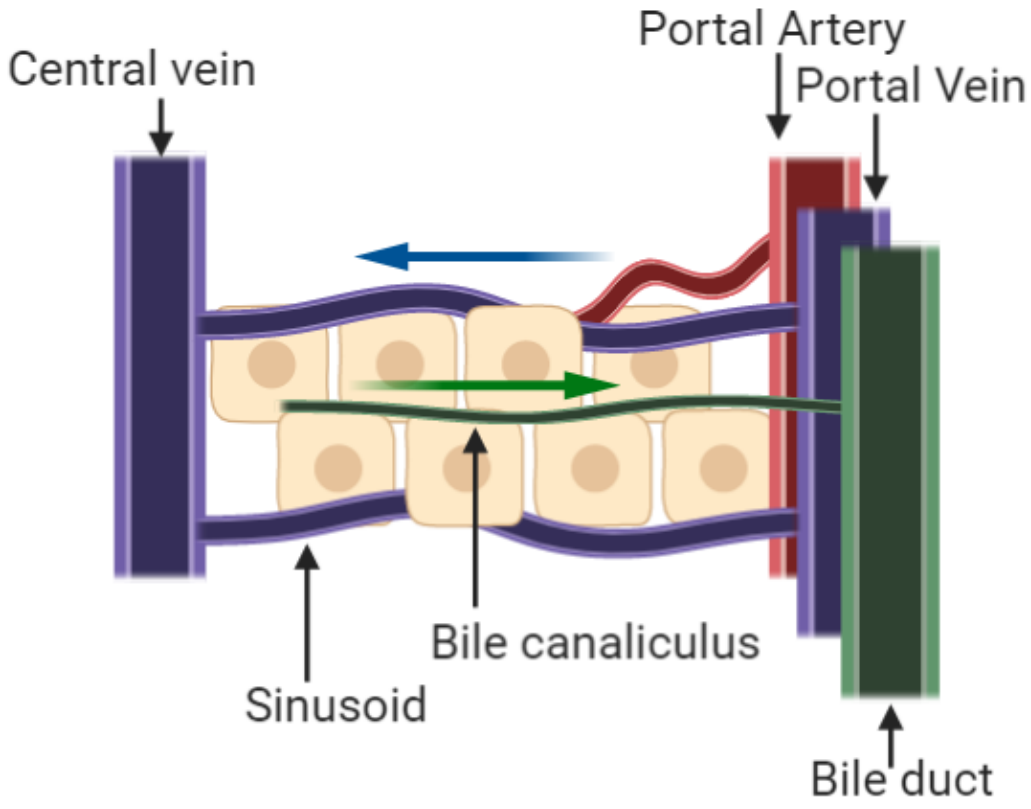

Figure 1.1-1: Schematic of the liver metabolic axis

The metabolic axis is defined as the tissue region situated between the portal triad and the central vein. Sinusoids are shown in purple and blood flow direction by a blue arrow. A canaliculus is shown in green and the bile flow direction by a green arrow. Hepatocytes are shown as yellow squares, all of them contact both sinusoids and contribute to the canaliculus.

Within a 2-dimensional (2D) plane these axes are in general viewed as arranged in a hexagonal shape (Rappaport et al., 1954) with one central vein in the middle and six portal veins on the edges. Since its first description in 1949 (Elias, 1949) the lobule shape has been controversial (Sasse et al., 1992). The general organisation pattern seems to be present and quite well conserved among mammals (Kruepunga et al., 2019). However, a closer look to the fine architecture reveals differences to the general model and between species (Bhunchet & Wake, 1998). Recent progress in microscopy, clearing, segmentation and reconstruction techniques are allowing us to study this structure at an unprecedented resolution in 3 dimensions (3D) (Morales-Navarrete et al., 2015). This type of study led our lab to the identification of intra-lobular cell organisation (Morales-Navarrete et al., 2019). This work led the way to several projects. For instance, the exact shape of the lobule is currently investigated taking into consideration the multiple scales of cellular arrangements. At the single cell scale, this study provided tools to quantify and better understand hepatocyte polarity.

Hepatocytes are polarized cells; cell polarity refers to the asymmetric spatial organisation of a cell. From a structural perspective this allows cells to separate two compartments and in general the inside and the outside of an organism. Hepatocytes are in contact with both the sinusoids (inner milieu) and form the bile canaliculi network (in continuity with the outside of the body). The establishment of hepatocyte polarity during development is poorly understood but the afore mentioned tools and understanding will soon allow us to gain new insight into this process.

Hepatocytes originate from the mesodermal layer. At 8.5 days of mouse embryonic development (E8.5), fibroblast growth factor (FGF) signal from the developing heart (Jung et al., 1999) and bone morphogenic protein (BMP) signal from the septum transversum (Rossi et al., 2001) reaches the ventral foregut endoderm (Douarin, 1964). This induction leads to a morphological change from a cuboidal epithelium to a pseudostratified and ultimately delamination of the hepatocytes precursors (hepatoblasts) (Bort et al., 2006).

This morphogenetic process is conserved across vertebrates and the liver appears as an anatomically distinct organ only in vertebrates. However, in closely related species like the cephalochordate *Branchiostoma lanceolatum* (Lancelet), the midgut presents a diverticulum that clusters the functions of both the pancreas and the liver. This diverticulum is vascularized by a capillary net between two veins, it has therefore been proposed for a long time that this arrangement is a homologous precursor to the portal vein/liver system in vertebrates (Willey, 1894). Interestingly in invertebrates with an open circulatory system liver functions appear to be distributed in several tissues (Monahan-Earley et al., 2013).

This strong connections between the vascularisation pattern and the organ function appears clearly during development. It has been shown that the emergence of the liver primordium from the gut requires endothelial cells before their vascular function in mouse (Matsumoto et al., 2001). The induction mechanism is still unclear, however, at this point hepatoblasts start expressing specific transcription factors (such as Hepatocyte Nuclear Factor 6 (HNF6) (Margagliotti et al., 2007)). Along with these changes hepatoblasts start expressing matrix metalloproteases, allowing them to delaminate across the basement membrane into the mesenchyme (Margagliotti et al., 2008) and form the liver bud.

Hepatoblasts in the liver bud are progenitors of two cell types, hepatocytes and cholangiocytes (Haruna et al., 1996; Yang et al., 2017). In the adult liver cholangiocytes are forming the collecting bile duct in the portal area of the lobule and have a distinct polarity phenotype from hepatocytes. The cell fate decision between these two cell types is associated with local signalling cues. The combination of factors observed in the portal area leading to cholangiocytes fate includes several Notch ligands, transforming growth factor β (TGFβ) and a specific extracellular matrix (ECM) composition (Kaylan et al., 2016). Notch ligand and Notch (Zong et al., 2009) as well as TGFβ signals (Antoniou et al., 2009) come from hepatoblasts. Although it has been shown that hepatocytes and other liver cells can produce ECM (Bedossa, 1993), most of both ECM production and degradation is thought to come from stellate cells (Li et Friedman, 1999).

Stellate cells (Ito cells/Fat storing cells) are first detected in the embryonic liver at E10,5 (Suzuki et al., 2008). They originate from the mesothelium at the periphery of the organ and migrate inwards to spread across the liver (Asahina et al., 2009). In the adult, these cells are present in the space of Disse, between hepatocytes and sinusoidal cells. Their long cytoplasmic extensions in contact with the vasculature as well as their pivotal role in angiogenesis regulation has led them to be considered the equivalents of pericytes in the liver (Lee et al., 2007). Stellate cells also regulate erythropoiesis. During development, this process occurs in the liver (between E12,5 and E16,5), liver macrophages are at the core of erythroblastic islands and keep progenitors within the tissue (Isern et al., 2008). Whereas stellate cells, around these islands, secrete growth factors (Kubota et al., 2007) and maintain a suitable environment for erythroblast differentiation. Their function in this process is crucial to the point that they can be compared to bone marrow mesenchymal stem cells (Kordes et al., 2013). In turn the hematopoietic cells (positives for the protein Cluster of Differentiation 45 (CD45+)) secrete oncostatin M and promote hepatocyte differentiation (Kamiya et al., 1999). In addition stellate cells secrete hepatocyte growth factor (Kubota et al., 2007) and directly promote hepatoblasts differentiation (Nagai et al., 2002).

1.2 Hepatocyte Polarity

In their differentiation process, hepatoblasts acquire hepatocytes features, for instance secretory vesicles can be found in their cytoplasm (Luzzatto, 1981). Polarized proteins can also be detected early on (Feracci et al., 1987), however, hepatocyte polarity is complex its establishment is not yet fully understood.

Cell polarity is characterized by structural and functional asymmetries within the cell. In epithelial cells (like hepatocytes) this asymmetry is visible through the formation of two distinct cellular surface regions: an apical and a basolateral surface with distinct protein and lipid composition. These two surfaces are established and maintained by distinct vesicular trafficking routes and their physical separation is mediated by tight junctions.

Tight junctions are sealing the epithelia and prevent diffusion across the epithelial barrier. Permeability barriers are found in all multicellular organisms, two main types can be distinguished: Septate junctions and Tight junctions (TJ). Septate junctions are the main type of paracellular insulator found in invertebrates and similar structure can be found in paranodal regions that flank the nodes of Ranvier in myelinated axons of vertebrates (Banerjee et al., 2006). In vertebrates, tight junctions are present in all epithelia.

Tight junctions are cellular structures composed of several layers of dense protein networks (Shin et al., 2006; Zihni et al., 2016) (Figure 1.2-1). A first layer is composed of transmembrane proteins connecting two cells. They are effectively preventing paracellular diffusion and can act as specific channels for some compounds (Tsukita et al., 2019). This transmembrane complex also prevent lipid and transmembrane protein diffusion between the apical and the basolateral cell membrane (van Meer & Simons, 1986). Beyond the structural aspects the junctional transmembrane proteins have been shown to interact with polarity complexes (Partition-defective (PAR) complex (Ebnet et al., 2001) and possibly Crumbs (CRB) complex (Hamazaki et al., 2002)). A second layer located of proteins interact with the transmembrane layer and is composed of soluble proteins located on the cytoplasmic side of the tight junction. These proteins are also interacting with the cytoskeleton (Maiers et al., 2013) and the CRB polarity complex (Roh et al., 2002).

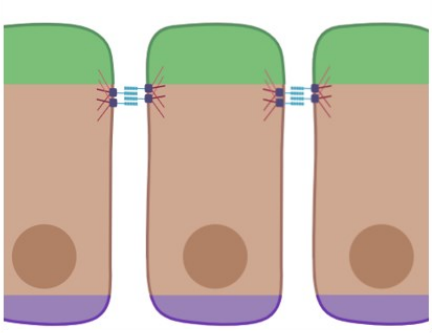

Figure 1.2-1: Schematic of the apico-basal polarity structure

The apical surface of each cell is shown as a green area. A tight junction fence prevents diffusion of apical components to the lateral membrane (in brown). The basal surface is shown as a purple area.

The three polarity complexes (PAR, CRB and Scribble (SCRIB)), transmembrane and cytoplasmic part of the tight junctions all contribute to the establishment and maintenance of polarity. Due to the large number of interactions and potential organism and tissue specificity the exact function of individual component is still unclear. However it seems that polarity complexes tend to initiate and regulate functional aspects of polarity through trafficking (Román-Fernández & Bryant, 2016). Whereas tight junctions seem to have a role in structural aspects and cell behaviour (Garcia et al., 2018).

Hepatocyte polarity, from a structural perspective, allows to separate blood and bile. Hepatocytes can therefore extract xenobiotics from the blood and excrete them along with the bile into the bile canaliculi network. Hepatocytes also maintain nutrient composition in the blood and impact gut absorption through variation in bile composition. In adults, some conditions (genetic and epigenetic predispositions along with excessive caloric intake (Marchesini et al., 2016)) can result in lipid accumulation in liver. Our lab has recently shown that in the Non-Alcoholic Fatty Liver Disease (NAFLD) context the bile canaliculi network is disrupted, and these alterations can explain some aspects of the disease physiopathology (Segovia-Miranda et al., 2019).

Developmental alteration in functional aspects (such as mutations in genes coding for apically located transporters) as well as structural aspects (tight junction components) can also result in strong impairment in liver function and cause diseases (Gissen & Arias, 2015). Knowledge about the establishment of hepatocyte polarity in vivo remains elusive. It is therefore hard to tell whether the different model systems in place are effectively recapitulating

this process. However key features of polarity establishment have been identified over the years and are likely to be important also in hepatocyte polarity establishment.

The most studied in vitro system of polarity establishment is Madin-Darby Canine Kidney (MDCK) cells. After an initial cell division, a midbody remain between these cells, actin polymerization is then increased at this position, and contribute to recruit the protein zonula occludens 1 (ZO-1). Acetylated tubulin at this location facilitates ZO-1 dependant Cingulin recruitment. At this point, the apical membrane initiation site (AMIS) is formed (Mangan et al., 2016). Apical surface proteins are initially distributed all over the cell membrane. In parallel of the AMIS formation these proteins are internalized and concentrated into a rab8/rab11 vesicular cluster called the apical recycling endosome (ARE). After AMIS formation polarity complexes and the exocyst complex enables apical surface delivery and the pre-apical patch (PAP) is formed (Bryant et al., 2010). Apical ion secretion then drive water to go through water channels at this location and hydrostatic pressure leads to the opening of a lumen (Ferrari et al., 2008).

This process leads to the formation of a closed compartment (lumen) shared by multiple cells. Each cell has one basal surface and one apical surface on opposite sides. This corresponds to a columnar polarity like the one observed in cholangiocytes, however, mature hepatocytes polarity has slightly different features. The transverse section of a canaliculi is formed by only two cells and the apical surface of each cell is forming a belt that separate several distinct basal domains (Figure 1.2-2). Therefore, the description of the process in MDCK cells is not enough to explain the establishment of hepatocyte polarity. The current view includes additional remodelling steps.

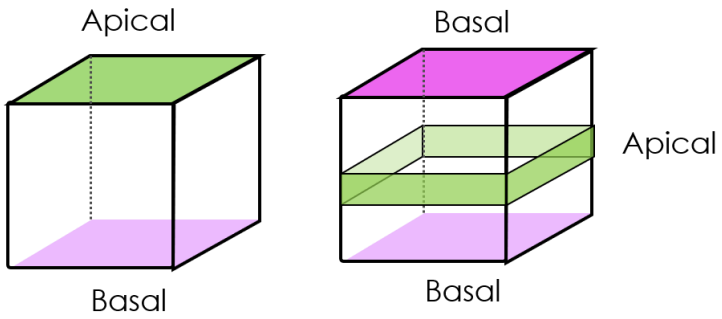

Figure 1.2-2: Schematic of columnar versus hepatocyte polarity

Left schematic represents a cell (full square) with a columnar like polarity, the apical (green) and basal (magenta) surfaces are on opposite side of the cell. Right schematic represents the hepatocyte polarity with the apical surface forming a belt between two distinct basal surfaces.

PAR1b overexpression in MDCK cells lead to the formation of a hepatocyte-like polarity (Cohen et al., 2007) it has then been further proposed that this may be due to a difference in adhesion behaviour that would impact the angle of cell division (Lázaro-Diéguez & Müsch, 2017). Cells showing this phenotype have several lumina, all situated between two cells. Thin sections of the developing liver show a polarity phenotype compatible with this process as a step at E17. In the same study a strong increase in bile canaliculi length is observed between E17 and E18 compared to later timepoints (Tanimizu Naoki et al., 2016). It has therefore been proposed that, initially hepatoblasts divide asymmetrically and generate multiple lumina, then at E17 a switch in the angle of cell division occurs leading to the connection of all lumina and the formation of the bile canaliculi network (Tanimizu & Mitaka, 2017) (Figure 1.2-3).

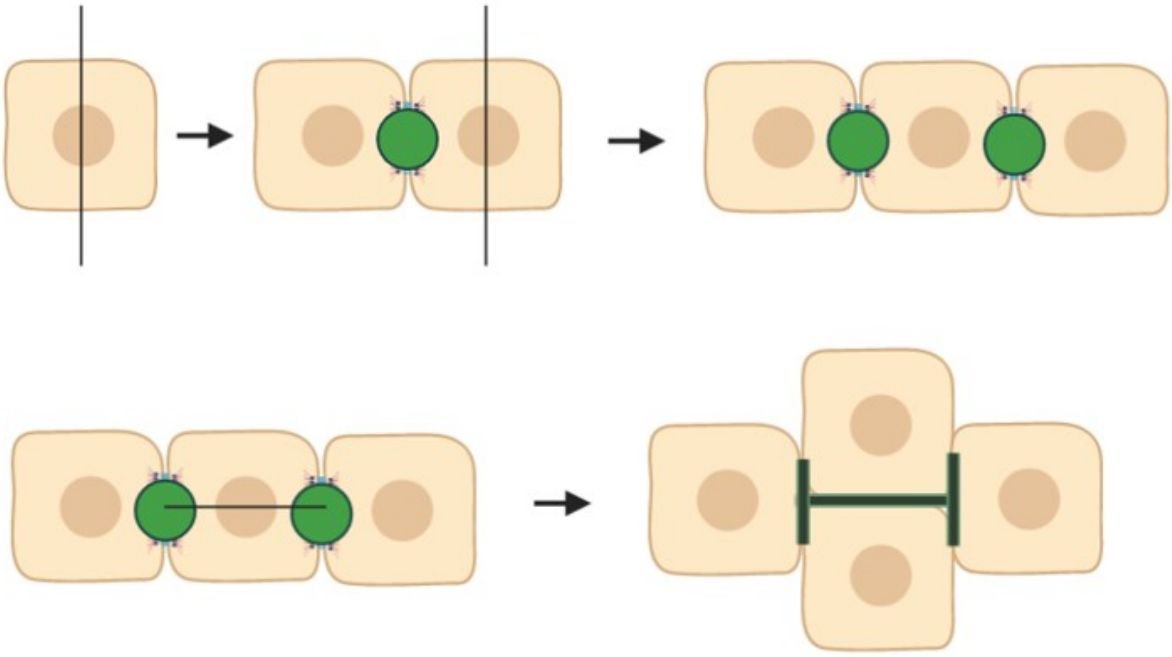

Figure 1.2-3: Schematic of the current view on hepatocyte polarity establishment.

Axes of cell division are shown as a black line crossing cells (yellow squares). Lumina are shown in light green, establish canaliculi network is shown as a dark green line. Basal surfaces are not represented. First asymmetric cell division would lead to the formation of multiple lumina (first row) then cell division would become symmetric to connect multiple lumina (second row).

These approaches are quite indirect and so far, no *in vivo* observation of the hepatocyte polarity establishment and bile canaliculi network formation has been performed. Additionally, even if cytokinesis has been proposed to be determinant in hepatocyte lumen positioning (Wang et al., 2014), it has been reported that only 25% of hepatoblasts are still dividing after E14 and almost all hepatoblasts are quiescent at E17 (Yang et al., 2017), it is therefore possible that a cell division independent process leads to hepatoblasts polarity establishment and very likely that bile canaliculi network connection is cell division independent.

We have therefore decided to directly address these questions:

- ***How is hepatocyte polarity established in vivo in mice?***
- ***How is the bile canaliculi network formed?***

For this we will use a combination of clearing and two photon microscopy in order to acquire images in a sufficient volume to appreciate the degree of network formation. We will first follow lumen formation over time to establish a sequence of events. We will then look at different markers to characterize the different steps in hepatocyte polarity acquisition.

At this point we should have a sufficient characterization of the process to evaluate the relevance of *in vitro* models regarding hepatocyte polarity establishment. Using such models, we will then try to understand the function of known polarity genes in the elaboration of hepatocyte polarity.

Finally, we will go back in vivo to try to identify further micro-environmental conditions leading to hepatic tissue architecture elaboration.

2 Material and methods

2.1 Experimental overview

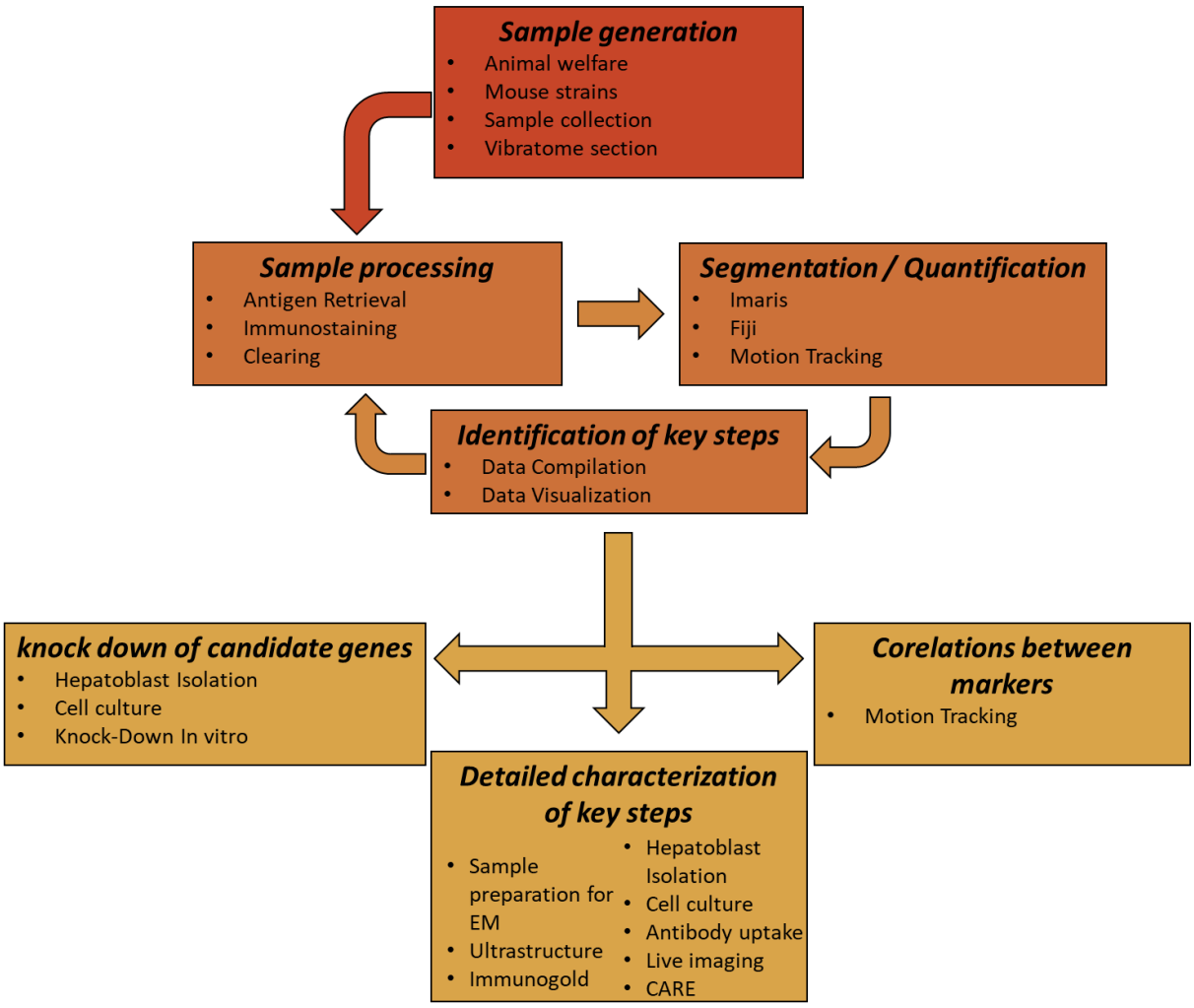

Figure 2.1-1: Workflow map

Map of the relationship between sections of the Material and methods chapter. Each box corresponds to a section of this chapter and within each box are listed the subsections. This map illustrates the workflow used to produce this document. In red the section sample generation corresponds to the mouse work from housing to sample production. In orange the first level of data generation leading to the identification of the key steps in hepatoblast polarization and network formation. Finally in yellow the steps addressing the questions asked in this document.

2.2 Sample generation

2.2.1 *Animal welfare*

As described in (Meyer et al., 2017), Animal experiments were performed on 8–12-week-old C57BL/6JOlaHsd (Harlan laboratories) mice at the MPI-CBG (Dresden, Germany). Experiments were conducted in accordance with German animal welfare legislation and in strict pathogen-free conditions in the animal facility of the MPI-CBG. Protocols were approved by the Institutional Animal Welfare Officer (Tierschutzbeauftragter), and all necessary licenses were obtained from the regional Ethical Commission for Animal Experimentation of Dresden, Germany (Tierversuchskommission, Landesdirektion Dresden).

2.2.2 *Mouse strains*

Strain	Description	Reference
C57BL/6JOlaHsd	Internal stock of BMS facility at MPI-CBG	--
Rosa mT/mG	Expresses ubiquitously a membrane Tomato florescent marker that can be recombined to a membrane GFP marker upon cre-lox recombination.	[63]

2.2.3 *Sample collection:*

Animal experiments were conducted in accordance with German animal welfare legislation in pathogen-free conditions in the animal facility of the MPI-CBG, Dresden, Germany. Mice were maintained in a conventional barrier animal facility with a climate-controlled environment on a 12-h light/12-h dark cycle, fed ad libitum with regular rodent chow. Protocols were approved by the Institutional Animal Welfare Officer (Tierschutzbeauftragter), and necessary licenses (Licence No. DD24.1-5131/394/42, DD24-5131/354/54) were obtained from the regional Ethical Commission for Animal Experimentation of Dresden, Germany (Tierversuchskommission, Landesdirektion Dresden)

Pregnant mice at different stages were sacrificed by cervical dislocation. The embryos were collected, and the liver was dissected in cold phosphate buffered saline (PBS). A solution of paraformaldehyde (PFA) 4% was mixed and filtered on the day of the collection, Tween20 was added to the solution after filtration at a final concentration of 0,1%. For embryos up to

E15 included the organs were placed in the PFA solution overnight at 4° on a rotating wheel. For embryos at E16 or later this step was prolonged to 2 overnight and the PFA solution was changed after the first night. The PFA was then removed and samples were quickly washed twice in cold PBS. A third washing in PBS at 4° was then done overnight on a rotating wheel. Finally, the PBS was removed, and the samples placed in a solution of PBS + 0,05% sodium azide for storage.

2.2.4 Vibratome sections:

The livers at E13 and later stages were embedded in 4% Agarose mixed in PBS. The septum transversum was placed at the bottom of the mould. The embedded samples were then glued on the sample holder with the septum transversum on the top side. The cutting was performed at a thickness of 100µm, an amplitude of 0.75 mm and a speed of 0,1 mm/s. Individual sections were then stored individually in PBS + 0,05% sodium azide until staining.

2.3 Sample processing

2.3.1 Immunostaining:

2.3.1.1 Tissue sections:

Sections were washed once in PBS and then permeabilized in PBS + Triton x100 0,5% for one hour. The sections were then incubated with primary antibodies in a solution of PBS+ Triton x100 0,3%+ Fish gelatin 0,2% for two days at room temperature. Sections were then washed 5 times 15 minutes in PBS+ Triton x100 0,2% before starting the incubation with secondary antibodies (in the same buffer as primary antibodies) for two days at room temperature. The sections were then washed 5 times 15 minutes in PBS+ Triton x100 0,2% and 3 times 5 minutes in PBS. The sections were then further processed through the clearing protocol.

2.3.1.2 Plated cells:

Cells were fixed overnight at 4° at different times after plating, using 4% PFA in PBS buffer with 0,1% Tween20. Cells were then permeabilized with a solution of PBS + Tritonx100 at 0,3%. Then cells were blocked using a solution PBS + Tritonx100 0,1% + Bovine serum

albumin (BSA) 3% for 2h at room temperature. Cells were then incubated overnight with primary antibodies in the blocking buffer. Cells were then washed 3 times 5 minutes with PBS + tritonx100 0,1%. Then cells were incubated overnight with secondary antibodies in the blocking buffer. Finally, cells were washed 3 times with PBS and imaged within a few days.

2.3.1.3 Antibodies:

Target protein	Concentration	Clonality	Species	Company / Lab
CD13	1/500	Monoclonal	Rat	Novus
ZO-1	1/100	Polyclonal	Rabbit	Invitrogen
Rab11	1/200	Polyclonal	Rabbit	Invitrogen
Prominin	1/200	Monoclonal	Rat	Huttner Lab
MRP2	1/500	Monoclonal	Rat	--
DppIV	1/100	Polyclonal	Goat	R&D Systems
Desmin	1/1000	Polyclonal	Goat	R&D Systems
E-Cadherin	1/200	Polyclonal	Rabbit	GeneTex
ß-Catenin	1/100	Polyclonal	Rabbit	Cell Signaling
Claudin 1	1/100	Polyclonal	Rabbit	Honigmann lab
JAM-A	1/50	Polyclonal	Rabbit	Honigmann lab
Occludin	1/100	Polyclonal	Rabbit	Thermofisher
Par3	1/100	Polyclonal	Rabbit	Knust lab
Desmoplakin	1/200	Polyclonal	Rabbit	Honigmann lab
Pericentrin	1/200	Polyclonal	Rabbit	Covance
β-Tubulin	1/100	Monoclonal	Rabbit	Abcam
phospho-Histone 3	1/500	Monoclonal	Rat	Abcam
HNF4α	1/50	Polyclonal	Goat	Santa Cruz
Flk1	1/1000	Polyclonal	Goat	R&D Systems
Fibronectin	1/5000	Polyclonal	Rabbit	Milipore
Laminin	1/1000	Polyclonal	Rabbit	Sigma-Aldrich

Secondary antibodies were used at the concentration of 1/1000. For actin staining we used Phalloidin labelled with Alexa 488 at a concentration of 1/200. Dapi was used at a concentration of 1/5000.

2.3.2 Antigen retrieval:

In order to stain tubulin we had to use an antigen retrieval step after fixation and before staining. MeOH was pre-cooled at -20°, the sections were then incubated with MeOH on dry ice for 5 minutes and then washed with cold PBS 5 times 5 minutes.

2.3.3 Clearing (SeeDB):

The clearing was performed following the protocol published by (Ke et al., 2013). Sections were incubated in increasing concentration of fructose on a rotating wheel at room temperature. Samples were placed in fructose 25% in distilled water for 6h then fructose 40% for 6 hours then fructose 60% overnight then fructose 80% overnight then fructose 100% overnight. Finally, samples were incubated in a See Deep Brain (SeeDB) solution overnight and then mounted in the same solution.

2.4 Segmentation / Quantification:

We used 3 different software to segment images depending on the question we were asking:

2.4.1 Imaris:

Imaris was used for its speed and ease to use. This software is also very powerful for visualization. It was used to segment canaliculi, ARE, Centrosomes and cell border for figures 2.4-2 and 2.4-3.

For canaliculi: we generated a colocalization channel based on CD13 and phalloidin. We then placed a threshold to capture most of the objects. At this point several ARE were still present in the pool. To remove them we sorted out the objects by ZO-1 intensity. Based on the histogram of the average intensity it was clear which ones were positives and which ones were negatives.

For ARE: we generated a colocalization channel based on CD13 and Rab11. We then placed a threshold to capture most of the objects. At this point several lumina were still present in the pool. To remove them we sorted out the objects by phalloidin intensity. Given that lumina display a very strong phalloidin staining it was clear based on the signal intensity histogram which ones were lumina and which ones were ARE.

For Centrosomes and cell borders we just aimed at providing clear visualisation objects, so we just placed a simple threshold on the signal intensity.

2.4.2 *Fiji:*

We used fiji to segment hepatoblasts and mitotic nuclei for its ease to use and ability to sort out segmented objects based on their morphology. Segmentation in fiji was used only for the study on mitosis. In our study we used the software (Schindelin et al., 2012) and the MorphoLibJ add on (Legland et al., 2016).

For hepatoblasts: the staining was generating a lot of non-specific staining on the edge of the tissue. This residual signal was strong and continuous, in order to exclude these objects from the analysis we applied several filters (Kuwahara and gaussian blur 3D) then we sorted out the objects of a size exceeding a single cell (2500 voxels with a voxel size 0,027 μm^3). The resulting binary image was then segmented in 3D to determine the amount of hepatoblasts and their location within the image.

For mitotic cells: the signal was extremely good, so we simply applied the same filters and then segmented the image directly. This led us to determine how many cells were dividing and where they were situated.

To determine the dividing hepatoblasts we looked for the overlap between dividing cells and hepatoblasts.

2.4.3 *MotionTracking:*

We used MotionTracking for the relative spatial distribution quantification for its versatility at the analysis level.

We corrected for channel misalignment using the phalloidin channel as a reference and then applied several gaussian blur filters to the images. We then segmented the CD13 channel and the basal cue candidate channel using an approach similar to (Morales-Navarrete et al., 2015).

2.5 Identification of key steps

2.5.1 *Data Compilation:*

For the lumina and ARE quantifications we exported the information about the segmented objects as csv files. All the files generated were then compiled and used as source for plotting using the python pandas, matplotlib and seaborn libraries.

2.5.2 *Data visualization:*

All the single plane image visualization and the maximum projections were obtained using Fiji. The 3D view on a dividing hepatoblasts presented in figure 2.5-2 was done using the ClearVolume add on (Royer et al., 2015).

2.6 Knock-Down of candidate genes

2.6.1 *Hepatoblast Isolation:*

Primary cell isolations were performed by Lenka Belicova and/or Sarah Seifert. These experiments were performed as described in Lenka Belicova's thesis. Time-pregnant mice (E12.5-E16.5) were sacrificed by cervical dislocation. Livers were dissected out from the embryos and pooled together. Typically, 20-30 livers of E13.5 embryos were collected for an isolation. The livers were transferred to 12 ml Liver perfusion media, fragmented by passing through 230 mm glass Pasteur pipette, and incubated for 20 min in a 37ºC water bath. After spinning at the 212 x g for 3 min, the media was exchanged for 12 ml Liver Digest Medium supplemented with10 µg/ml deoxyribonuclease I (DNAse I). The suspension was incubated for further 20 min and mixed each 5 min by a 10 ml pipette. After the digestion, the cells were separated from undigested pieces though 70 µm filter. Cells were collected by spinning at 260 g. After removing the supernatant, the erythrocytes were lysed by incubation with 12 ml of Red blood cell lysis buffer on ice for 5 min and by subsequent addition of 28 ml ice-cold After lysis media.

For the magnetic separation, the cell number was counted to prepare cell suspension of 100 x 106 cells/ml in magnetic cell isolation (MACS) buffer. Cells were divided into 2-3 Eppendorf tubes, so that the maximum volume per tube is 300 µl. Cells were incubated with Rat Anti-Mouse CD16/CD32 (dilution 1:100) for 10 min for blocking; and stained with a monoclonal antibody directed against Delta Like Non-Canonical Notch Ligand 1 and bound to Fluorescein isothiocyanate (anti-Dlk1 mAb-FITC) (dilution 1:40) for further 15 min on ice. After two washes with 1 ml of MACS buffer at 664 x g in a table-top centrifuge (4ºC), the cells were re-suspended in 150 µl MACS buffer and incubated with Anti-FITC MicroBeads (dilution 1:10) for 15 min on ice. The cells were washed once with 1 ml MACS buffer. The cells from the multiple tubes were pooled together into the total of 500 µl MACS buffer and loaded twice on a magnetic column. After three washes with 500 µl MACS buffer, the cells were removed from the magnetic field and eluted with 3 x 1 ml MACS buffer using the provided plunger. Finally, the eluted cells were

spun at 260 g, resuspended in 1ml Expansion media base (see page 78 for the recipe) and counted. Typically, an isolation will yield 1 – 2 million cells.

Material	Company
Liver Perfusion Medium (1X), liquid	Thermo Fisher Scientific
Liver Digest Medium	Thermo Fisher Scientific
DNAse I	Sigma-Aldrich
Mouse BD Fc Block	BD Biosciences
Anti-Dlk mAb-FITC	MBL
Anti-mouse CD326 EpCAM-FITC, clone G8.8	eBioscience
Anti-FITC MicroBeads	Miltenyi Biotec
Magnetic columns MS	Miltenyi Biotec
Falcon™ Cell strainer 70 µm	Corning

Solutions:

- *Red blood cell lysis buffer, pH 7.4:*

155 mM NH4Cl, 10mM KHCO3, 0.1 mM EDTA, filter-sterile

- *MACS buffer:*

0.5% BSA, 2 mM EDTA in PBS, filter-sterile

- *After lysis media:*

DMEM High Glucose (Cat. No. 41966-029, Gibco), 5% FBS (heat inactivated), 2 mM L-Glutamine (Cat. No. M11-004, PAA Laboratories), 1 x NEAA (Cat. No. 11140-050, Gibco).

2.6.2 Cell culture:

Cell culture was performed by Lenka Belicova and according the protocol described in her thesis. The culture wells were coated either with 10 µg/ml fibronectin solution in PBS or with 10 v/v % Matrigel in ice-cold PBS for at least 30 min at 37ºC. After coating, the wells were washes with PBS to remove unbound proteins.

Two culture protocols were used throughout this study. For live imaging, isolated cells were diluted in the Differentiation media and seeded on fibronectin-coated plates. For all the other experiments, cells were seeded on Matrigel coated-plates in the Expansion media, and

24h later, the media was exchanged for Differentiation media. In both cases media was supplemented with 4-5% Matrigel. The cells were incubated in standard culture incubator 37, 5% CO2.

Expansion Media composition	
	DMEM/F-12, GlutaMAX™ supplement
10 %	FBS, heat inactivated
1 X	ITS-X (100 X)
0.1 μM	Dexamethasone
10 mM	Nicotinamide
10 ng/ml	Mouse EGF
10 ng/ml	Human HGF
Differentiation Media composition	
	MCDB131, no glutamine
5 %	FBS, heat inactivated
2 mM	L-Glutamine (200 mM)
0.25 X	ITS-X (100 X)
0.1 μM	Dexamethasone

2.6.3 Knock-Down in vitro:

2.6.3.1 Design and synthesis of siRNA

Design and synthesis of siRNAs was done by Timofei Zatsepin (Skoltech, Moscow). Modified siRNAs were synthesized by solid phase phosphoramidite method, purified by Ion-Exchange High Performance Liquid Chromatography (IE-HPLC) and verified by Liquid chromatography–mass spectrometry (LC-MS) (Farzan et al., 2017). Design of siRNA was performed using in-house software, first by testing all available sequences on the specificity for the target in mouse transcriptome (RefSeq in Pubmed), followed by elimination of sequences with complementarity to mouse miRNA, GC content below 25% and higher than 75% and immune responsive ones (like UGU, UGUGU, etc.). In addition, sequences were filtered using Reynolds rules (Reynolds et al., 2004). Pyrimidines in the sense strand and before A in antisense strand (UA, CA) were 2'-O-methyl (shown by lower case letters in the sequence) and both strands were 3'-modified with phosphorothioate dithymidylate (TsT) to enhance nuclease stability. Upon arrival, dried siRNA pellets were resuspended in 10 mM Tris.HCl, pH 7.5 to concentration 100 μM and store at - 20ºC. The working aliquots were 10 μM and stored at 4ºC.

Gene	siRNA no.1 (sense/antisense)	siRNA no.2 (sense/antisense)	siRNA no.3 (sense/antisense)	siRNA no.4 (sense/antisense)
Pard3	cAUUGUGAGGAUuAACGAUTsT	UCGUuAAAUCcAUuAUcAATsT	CGUuAAAUCcAUuAUcAAUTsT	cAAGGAGcAAuAUGAAcAATsT
	AUCGUuAAUCCUcAcAAUGTsT	UUGAuAAUGGAUUuAACGATsT	AUUGAuAAUGGAUUuAACGTsT	UUGUUcAuAUUGCUCCUUGTsT
Tjp1	GcAuGAAAcuGGuAAAAuuTsT	AGAuGAAAcucuuAAuGAuTsT	AAAccuGAAuuGucuucAATsT	GccGGuGucuGAuAAuGAATsT
	AAUUUuACcAGUUUcAUGCTsT	AUcAUuAAGAGUUUcAUCUTsT	UUGAAGAcAAUUcAGGUUUTsT	UUcAUuAUcAGAcACCGGCTsT
Luciferase	cuuAcGcuGAGuAcuucGAdTsdT			
	UCGAAGuACUcAGCGuAAGdTsdT			

2.6.3.2 Transfection

Transfection was performed by Lenka Belicova and according the protocol described in her thesis, siRNAs were transfected with Lipofectamine™ RNAiMAX transfection reagent (cat. No. 13778075, ThermoFisher) using the reverse transfection protocol. The final concentration per well was 10 nM siRNA and 0.1 v/v% Lipofectamine™ RNAiMAX. E13.5 Dlk1+ cells were seeded into Matrigel precoated 96-well plates at the concentration 13 000 cells/100 µl/well on top of the 20 µl transfection mixture. The cells were seeded in the Expansion media without addition of the Matrigel. 24 h later, 80 µl of the Differentiation media supplemented with 12.5 v/v % Matrigel was added per well to obtain final 5% Matrigel concentration. Differentiation media (supplemented with 2% Matrigel) was exchanged once 72h post transfection.

2.7 Detailed Characterization of key steps

2.7.1 Antibody uptake:

Cells were taken out of the incubator after 2 days. No uptake control were fixed. All the other conditions were then incubated with CD13 antibody at 1/100 in culture media on ice for 15 minutes. The solution was then replaced with media without antibody and cells were fixed at different chase duration (0minutes, 15 minutes and 60 minutes). Cells were then stained either with primary antibody against rab11 or directly with secondary antibody.

2.7.2 Live Imaging:

The cells were taken out of the incubator and placed in a transparent media. On the microscope stand cells were provided with a constant flux of CO2 and heat. Images were taken starting 12h after plating up to 72h after plating. The cells were replaced every 24h. The images shown are taken at t0 corresponding to 24h after plating. The cells were then fixed in order to be stained later on to confirm the nature of the structures observed.

2.7.3 CARE:

In order to reduce the phototoxicity during live imaging we used the CARE approach (Weigert et al., 2018). We trained the network on a set of 200 images pairs (the same region taken at a low and then at a high laser intensity). We then applied the restoration on our live images (Figure 4.16-1). We believe that we can achieve a better result with a larger training set and will do so soon.

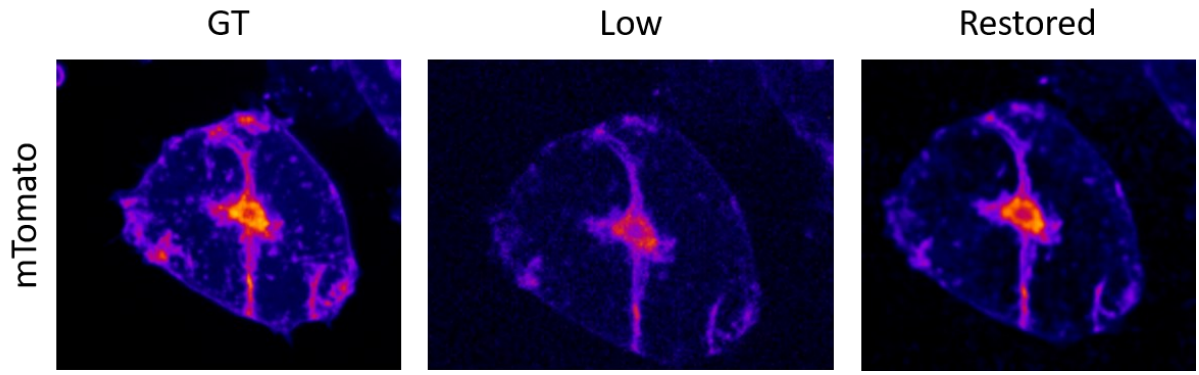

Figure 2.7-1: Content Aware image Restoration (CARE) validation set

The training was performed on the mTomato channel with 200 images taken at high exposure to be used as ground truth (GT) and images taken at the same location but at low exposure (Low). The result obtained after restoration is shown on the right (Restored).

2.7.4 Sample preparation for electron microscopy

Liver was dissected from E11-E16 stage mouse embryos and cut into a few pieces, which were immersion fixed in 1% glutaraldehyde in 200 mM HEPES, pH 7.4 for several days for the ultrastructural analysis, or in 4% PFA 200 mM HEPES, pH 7.4 for 24 hours for immunolabeling. After fixation, samples were further processed and imaged by Urska Repnik. Tissue was washed with dH2O, the residual fixative quenched with 0.1% glycine in dH2O, and

tissue cut into small pieces. All sections were analysed in a Tecnai T12 transmission electron microscope (ThermoFisher), operated at 100 kV and equipped with an axial 2k CCD camera (TVIPS).

2.7.5 Ultrastructure:

For the ultrastructural analysis tissue was postfixed with 1% osmium tetroxide and 1.5% potassium ferricyanide for 1 hour on ice, then contrasted en-bloc with 2% uranyl acetate for 2 hours at room temperature, dehydrated with a graded ethanol series: 70-80-90-96%, each for 10 min, and 4x 100%, each for 15 min, progressively infiltrated with epoxy resin and eventually polymerized at 60 °C for 2 days. Thin 70-80 nm sections were cut using a Leica Ultracut UCT ultramicrotome and deposited on formvar-coated, slot, copper grids. Sections were contrasted with 0.4% lead citrate for 1 min.

2.7.6 Immunogold:

For immunogold labelling, pieces were embedded in 12% bovine gelatine, and infiltrated with 2.3 M sucrose in dH2O on a rotating wheel at room temperature for at least 24 hours. Such cryo-protected pieces were mounted on pins and snap frozen in liquid nitrogen to become hard. 90-nm thin Tokuyasu thawed cryo-sections were prepared using a Leica FC6 cryo-ultramicrotome. Sections were transferred to formvar-coated, 100 mesh, hexagonal, copper grids. Grids were sequentially incubated on drops of:

1.) 1% glycine in PBS for 2 min to make sections hydrophilic,

2.) 1% cold water fish skin gelatine in PBS for 15 min to block non-specific binding,

3.) a rat Aminopeptidase N/CD13 antibody (clone ER-BMDM1, Novus NB100-64843) at 1:100 for 30 min,

4.) unconjugated bridging rabbit anti-rat IgG (Jackson ImmunoResearch) at 1:500 for 15 min,

5.) 10-nm protein A gold (UMC Utrecht) at 1:25 for 30 min.

Labelling reagents were diluted in 1% cold water fish skin gelatine in PBS, and PBS was used for washing after incubation with the labelling probes. After immunolabeling, grids were washed with dH2O and embedded in a thin layer of 0.2% uranyl acetate in 1.8% methyl cellulose prepared in dH2O

.

3 Results

3.1 Sequence of events

To understand the process of hepatoblast polarization we will first define a general timeline of events. Then, we will focus on polarization and try to identify key steps in this process. Finally, we will have a closer look on how polarized trafficking is established.

First, we will have to identify a timeframe for the study. To do so, we will follow the distribution of apical markers over time. It has been observed in our lab that apical markers are already expressed at E10. We have therefore started our study at this timepoint using an apical marker present at this stage. We used a protein found in the apical surface of hepatocytes: CD13 (also called Aminopeptidase-N). To qualify a structure as an apical surface we will confirm that it has reached the AMIS stage by looking for a common localization of CD13 and ZO-1 in the same region of the cell.

3.1.1 Discrepancies across the organ

Before any measurement, we had to ensure our observations were consistent between sections. In this regard we looked for differences across the organ and picked regions for imaging accordingly. As we are interested in apical surfaces, we looked at the distribution of an apical marker across sections.

Only looking at our apical surface marker (CD13), differences could be observed across the organ. The most striking difference was observed on frontal sections (Figure 2.1-1 A) illustrated here on the embryonic liver at E14 (Figure 2.1-1 B). Magnification reveals that CD13 stains structures and that this staining is more dispersed at the periphery of the organ (Figure 2.1-1 C) compared to the central region of the same section (Figure 2.1-1 D).

Further analysis of these structures will be performed later but for the moment we will assume that this corresponds to different stages of lumen formation as such differences are no longer observed in the adult.

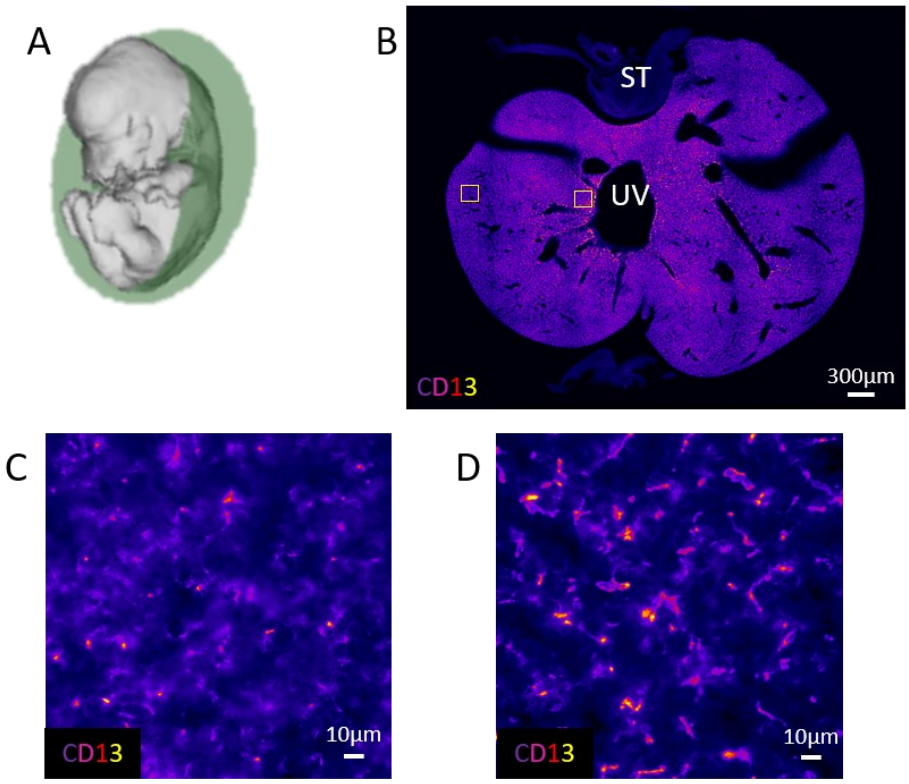

Figure 3.1-1: Discrepancies across the developing liver

A: section plane B: overview of a whole embryonic liver sectioned at E14 immunostained against CD13. The CD13 intensity is shown from blue (low) to yellow (high). The umbilical vein (UV) is located at the center of the section, the septum transversum (ST) is at the top. Magnified areas (C and D) are shown as squares. C: Maximum intensity projection over 90µm of the CD13 intensity in the magnification of the distal region. CD13 is mostly diffused. D: Magnification of the proximal region. CD13 is concentrated in distinct structures.

Similar discrepancies over space have been observed in the formation of bile ducts (Tanimizu Naoki et al., 2016). The distinction between these two regions can only be made from E13 to later timepoints because before this timepoint even the largest lobe is smaller than two fields of view. For the lumen analysis we have therefore made a distinction between the center (central region, close to the hilum) and the border (at the edge of a lobe).

These discrepancies can be due to several factors. A radial proliferation of hepatoblasts with daughter cells closer to the periphery. Based on clonal analysis at the organ scale (Weiss et al., 2016) it has been proposed that, due to the presence of radial clones, either hepatoblast initially proliferate this way or progenitors migrate radially. At a later developmental timepoint, it seems that hepatoblast tend to proliferate more locally and generate spotty cones. However, this study also confirms a strong drop in proliferation after E13.5, we would therefore expect a

consistent difference between center and border over time after this timepoint. This explanation is therefore not sufficient to explain the differences observed.

Another hypothesis would be a stimulation of canaliculi growth through factors present in the umbilical blood as it comes from the hilum and is progressively mixed with embryonic blood. A candidate would be bile salts, in the embryo these bile salts can only be eliminated through the placenta (Trauner & Boyer, 2003), they have been shown to stimulate canaliculi formation in vitro (Taurocholate in particular) (Fu et al., 2011) and we could reproduce these results (data not shown). If bile salt expression is reduced, bile would accumulate in the embryo and accelerate bile canaliculi formation. This hypothesis is interesting as it would connect the embryonic liver development to the nutritional environment of the mother, these aspects will be further discussed later when we will look at functional aspects of lumina.

3.1.2 Timeline overview

To identify an overall timeline of events we aimed at segmenting lumina in different regions of the organ every 24h from E10 until a network is formed. The lumina have been segmented through the colocalization of apical surface marker (CD13) (Figure 2.1-2 A) with a cell border marker (phalloidin) (Figure 2.1-2 B-C). We then sorted out the incomplete events by only keeping the segmented objects positive for a junctional marker (ZO-1).

With this approach we found object of extremely small size (down to the voxel size) we decided to keep only the ones that were clearly not artifact and put a threshold on minimal size at 8 cubic microns. With this criterion almost all the small structures had a spherical shape with an apparent empty space in the middle. We therefore classified them as lumina for this analysis and decided to come back on the identification of early steps later (Figure 2.1-2 D).

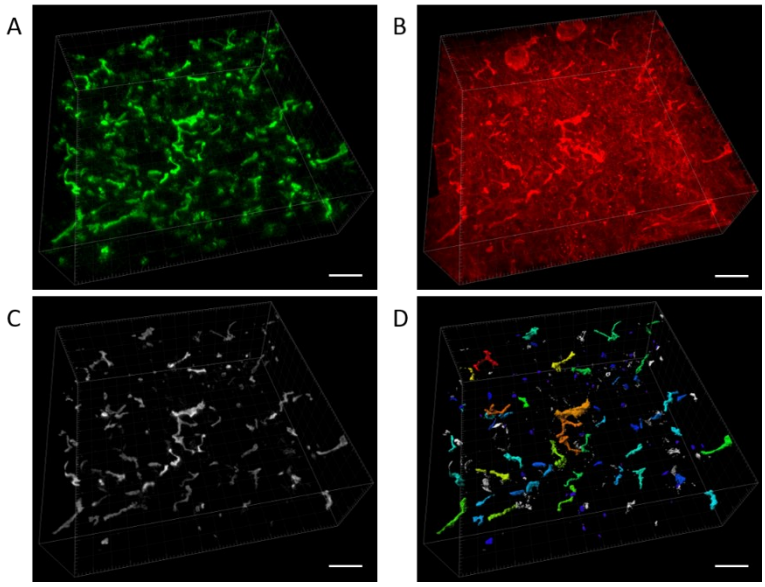

Figure 3.1-2: Segmentation strategy

A: Volume rendering of CD13 immunostaining at E14 close to the hilum. B: Phalloidin staining of the same image. C: Colocalization result between CD13 and phalloidin. D: Segmentation result all objects idenfied from the colocalization are shown. Only the ones kept after sorting out the ZO-1 negatives are coloured by size, the ones eliminated are shown in white. Scale bars: 100µm

We could observe that only very few lumina are formed at E10 and E11, the polarization process starts to be quite important starting at E12 (Figure 2.1-3 A). Also, for a given volume analysed, the number of lumina found increases until E14 at the border and E15 at the center of the organ. The number of distinct lumina found then decreases. On the other hand, the total lumen surface increases exponentially even between E15 and E16 (Figure 2.1-3 B). This strongly suggests that the lumina are getting connected and form a network around E15 (Figure 2.1-4).

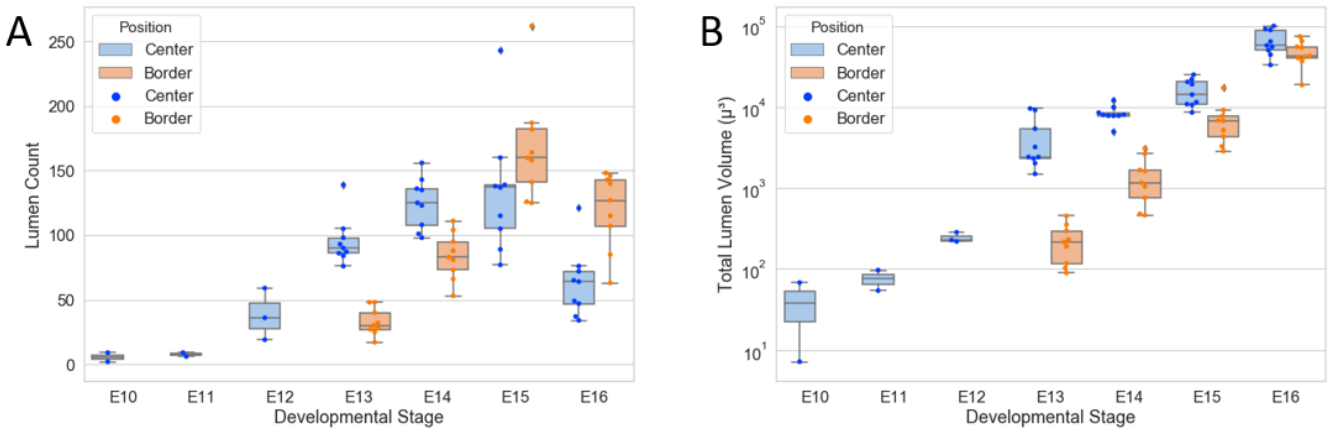

Figure 3.1-3: Lumen quantification

Each point correspond to an image. All the images were 150µmX150µmX80µm. Results are in duplicate for E10 and E11, triplicate for E12 each from individual plugs. Between E13 and E16 images were taken from 3 livers per plug for 3 different plugs. Boxes are showing the quartiles of the dataset while the whiskers extend to show the rest of the distribution, except for points that are determined to be "outliers" using a method that is a function of the inter-quartile range. A: The amount of lumen per volume increases and then decreases. B: Total lumen volume increases exponentially; logarithmic scale was used for the y axis. The difference between center and border seem to be reduced over time.

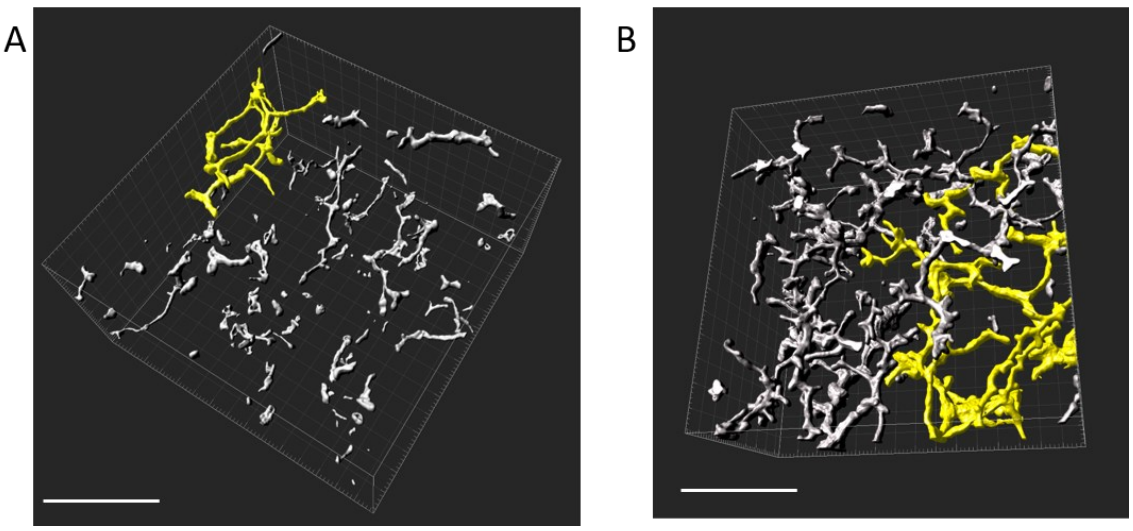

Figure 3.1-4: Network formation

Volume rendering of segmented lumina at E15 (A) and E16 (B) close to the hilum. The volume of the image is delimited by a box. All lumina are shown in white and the largest continuous lumen is shown in yellow. Scale bar: 50µm.

Additionally, we could observe that at E15 in some cases, ZO-1 bridges are connecting distinct lumina (Figure 2.1-5). This could provide a potential mechanism for the formation of the bile canaliculi network. However, it seems to be quite rare and would require more evidence to be conclusive.

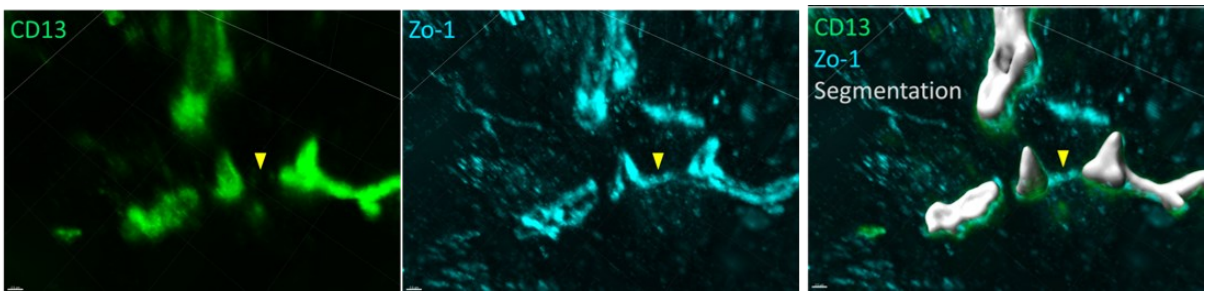

Figure 3.1-5: Junctional bridge between lumina

Volume rendering of images taken on a E15 embryonic liver slice. The sample was stained with phalloidin (not shown) and antibodies directed against CD13 and ZO-1 the lumen segmentation result is shown in grey. The yellow arrowhead shows a line of ZO-1 connecting two distinct lumina.

Our observations have provided us with a good overview on the different steps leading to the formation of the bile canaliculi network. It appears that hepatoblasts are likely to be continuously generating new lumina between E12 and E14 in the center and between E12 and E15 in the border of the organ. Therefore, in order to identify key steps in Hepatoblast polarization we must focus on this timeframe.

3.1.3 Timeline of polarization

Looking closely at the distribution of apical and junctional markers at E14 we could identify several patterns that resemble steps in polarization described in the literature (Figure 2.1-6 A). We could find structures that correspond the PAP (Figure 2.1-6 C) but no clear AMIS and interestingly on the other hand we could find clusters of apical markers close to the cell border in absence of ZO-1 (Figure 2.1-6 B). At this point it is not clear whether if CD13 is reaching the cell surface of if we observe a cluster of vesicles. Additionally, we are only looking at one junctional marker therefore we will have to confirm that this process happens in absence of any junctional component. But this observation leads us to believe that the restriction of CD13 localization can occur in absence of ZO-1. Also, assuming that the process of lumen formation is incremental we propose that this may occur before ZO-1 recruitment to the location.

We also observed that ZO-1 can form discrete clusters around a CD13 positive region at the cell border (structure 3 in Figure 2.1-6 D). This would correspond either to an advanced stage of PAP or to an established lumen. However, in the shown example no clear space is visible within the lumen suggesting an apical surface rather than an open lumen but here we do not have the resolution to address this.

Finally, it seems that even in presence of a lumen CD13 can be found clustered close to the cell border away from the lumen (structure 4 in Figure 2.1-6 D). This has to our knowledge never been described, it resembles a second lumen formation process starting after a first one is complete. If we can confirm this, it could explain the generation of multiple lumina in hepatoblasts and therefore the emergence of multipolarity.

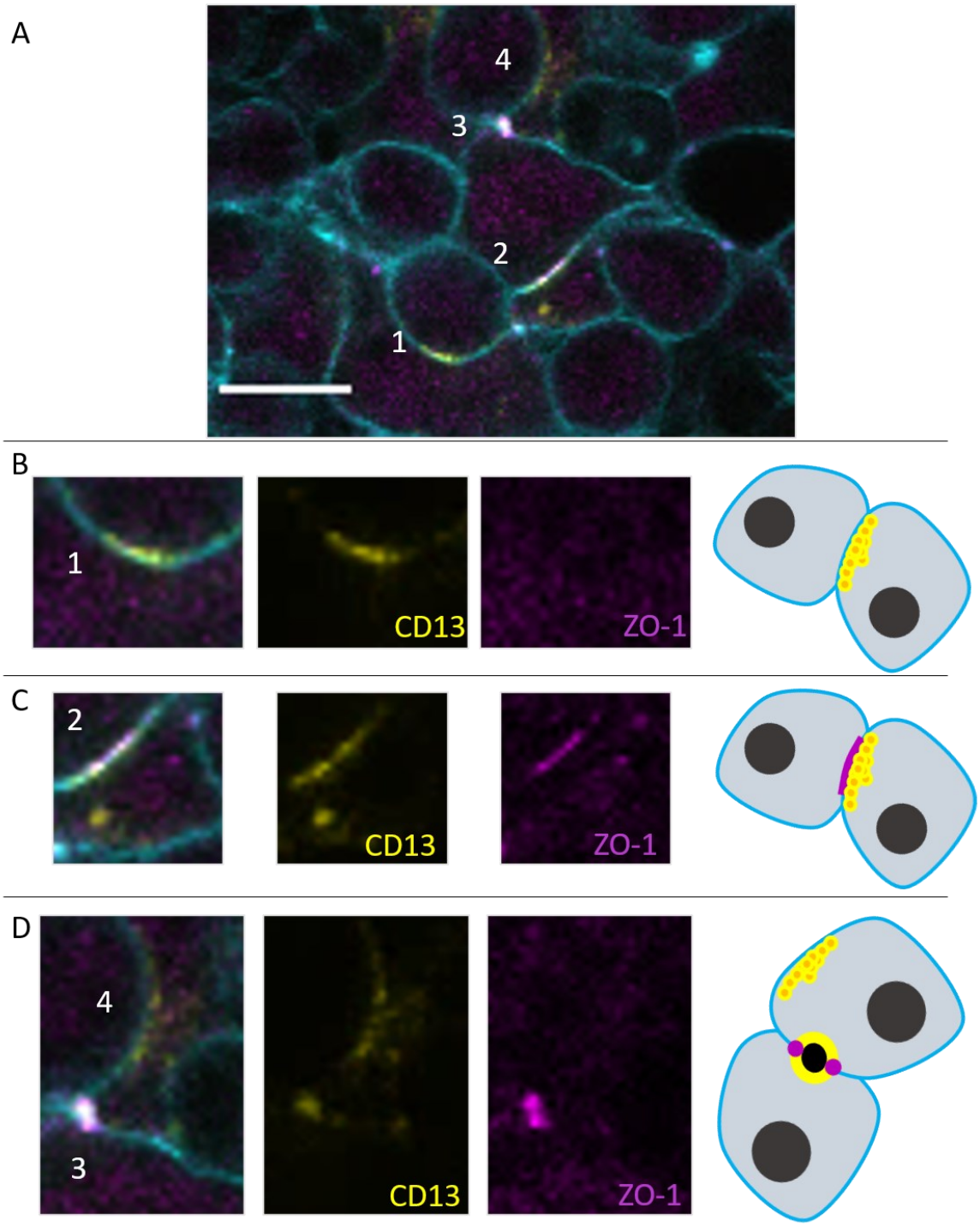

Figure 3.1-6: Polarization steps

Single plane image taken at E14 close to the hilum. Immunostaining against CD13 (yellow) and ZO-1 (magenta) counterstained with phalloidin (cyan) to visualize the cell border. A overview showing four distinct structures (1-4) scale bar: 10µm. B magnification of the structure 1 and associated schematic, CD13 is clustered close to the cell border in absence of ZO-1. C: Canonical PAP, CD13 and ZO-1 are clustered at the cell border. D: structure3: Advanced PAP or early lumen, ZO-1 forms spots on the edges of the structure and CD13 is located between the spots. Structure4: Similar to the structure 1 but in a cell already showing an advanced PAP or a lumen.

3.2 Apical component distribution prior to lumen formation

In MDCK cells the apical surface components are initially distributed evenly across the cell surface, after cell division the apical components are internalized and then redirected to a specific location. This is done through a rab11 positive compartment called the Apical Recycling Endosome (ARE) (Bryant et al., 2010).

3.2.1 ARE Timeline in vivo

We could observe a similar surface distribution of CD13 at E11,5 in some samples in hepatoblasts (Figure 2.2-1 A) in other samples CD13 was clustered intracellularly. At E12,5 in all samples, we could find CD13 in clearly intracellular spherical clusters positive for rab11 (Figure 2.2-1 B). At E13,5 the clusters were mostly at the cell border and spanning toward the inside of the cell (Figure 2.2-1 C). As a result of this shift toward the cell border the clusters seem to flatten.

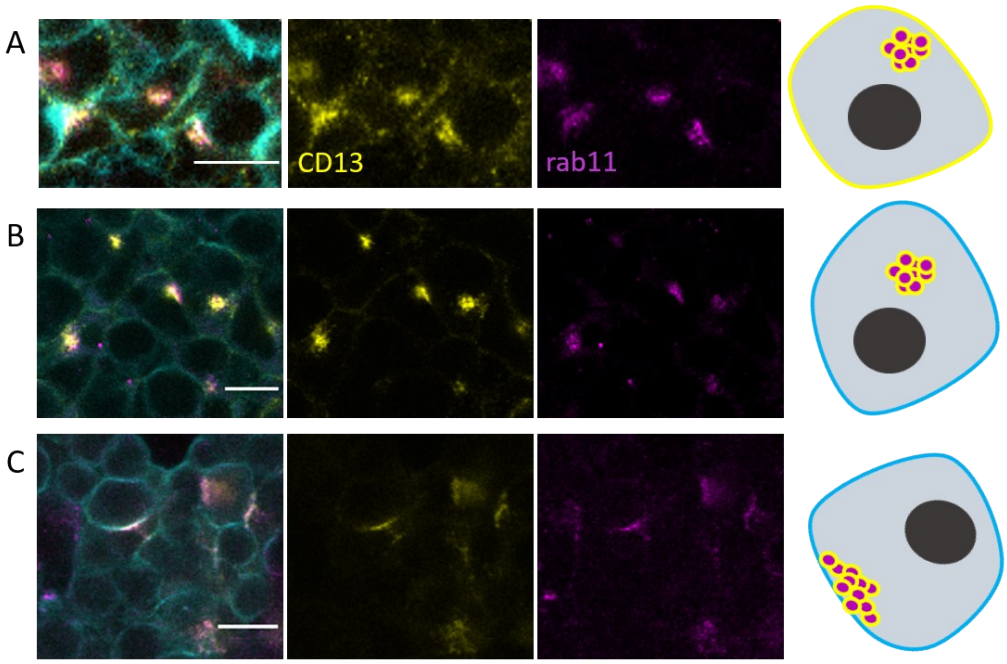

Figure 3.2-1: ARE localization at early developmental stages

Single plane image of immunostaining against CD13(yellow) and rab11(magenta) stained with phalloidin(cyan) and schematic of the typical marker distribution. A: at E11,5 CD13 is all over the cell border and within a rab11 positive vesicle cluster (ARE). B: At E12,5 CD13 is concentrated within the ARE. The cluster is spherical and close to the nucleus. C: At E13,5 CD13 is still in the ARE but the ARE is now flat and close to the cell border. Scale bar: 10µm.

To quantify this shift in distribution, we have segmented the colocalization between CD13 and rab11. We then sorted out the individual vesicles by only keeping large objects, this way we only kept clusters of vesicles (ARE). We then sorted out the few established lumina in the pool of segmented objects by only keeping the objects with a low total phalloidin intensity (established lumina having a strong phalloidin signal) (Figure 2.2-2).

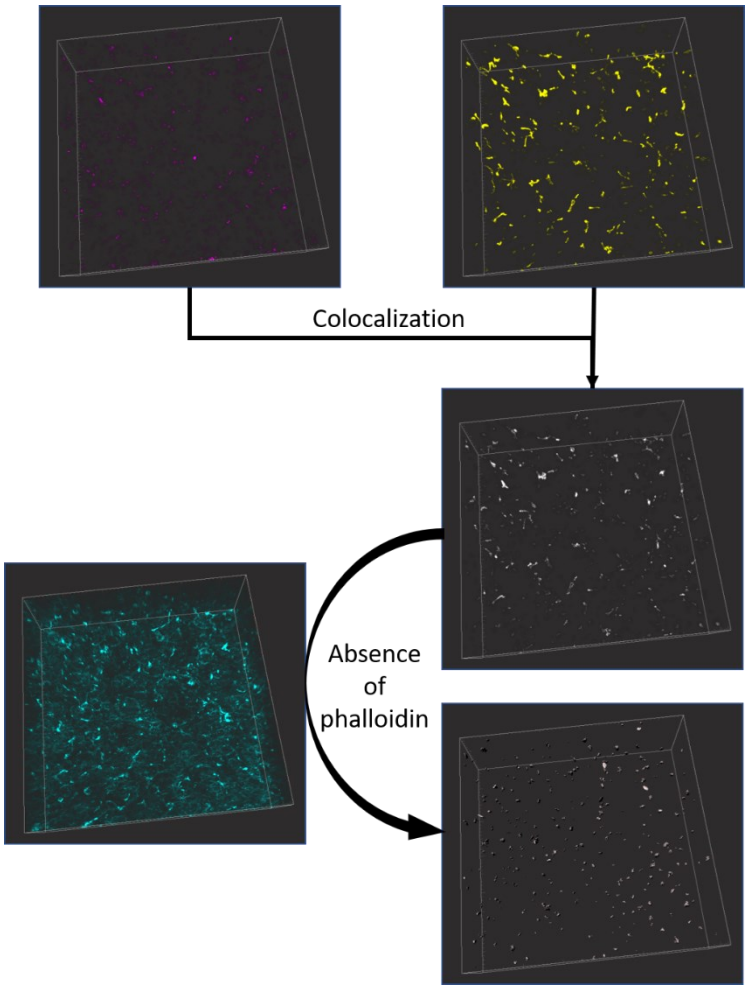

Figure 3.2-2: ARE segmentation strategy

Volume rendering of complete images (white box). First, we generate a colocalization image based on CD13 and Rab11 images. Then the remaining lumina are sorted out based on the total phalloidin intensity.

This way we could observe that for a given volume of tissue analysed between E10 and E13, a similar number of clusters could be found (Figure 2.2-3 A). A reduction could be observed between E13 and E14. This transition corresponds to the migration of the erythropoiesis from the Aorta-Gonad-Mesonephros region to the embryonic liver. This result in a dilution of hepatoblasts across the tissue.

However, we could not observe such a reduction in lumen density, the reduction in ARE density could therefore also be the result of an increase in polarization.

The density of ARE then stabilizes between E13 and E15. It is then reduced again between E15 and E16. This second reduction cannot be explained by the hepatoblast density as erythropoietic progenitors tend to leave the liver around these time points. It cannot be explained by an increase in polarization either, as the quantity of lumen is reduced in this interval. As we exclude the recycling endosomes close to established lumen this second reduction of ARE number could be due to a reduction or an arrest of polarization.

By measuring the sphericity of these clusters (Figure 2.2-B), we could observe that between E10 and E12, when few lumina can be found, the clusters are quite spherical. When more and more lumina are formed, the clusters shape is very variable with a quite homogeneous distribution of both spherical and flat. Finally, the few remaining clusters at E16 are spherical and this coincides to fewer polarization events.

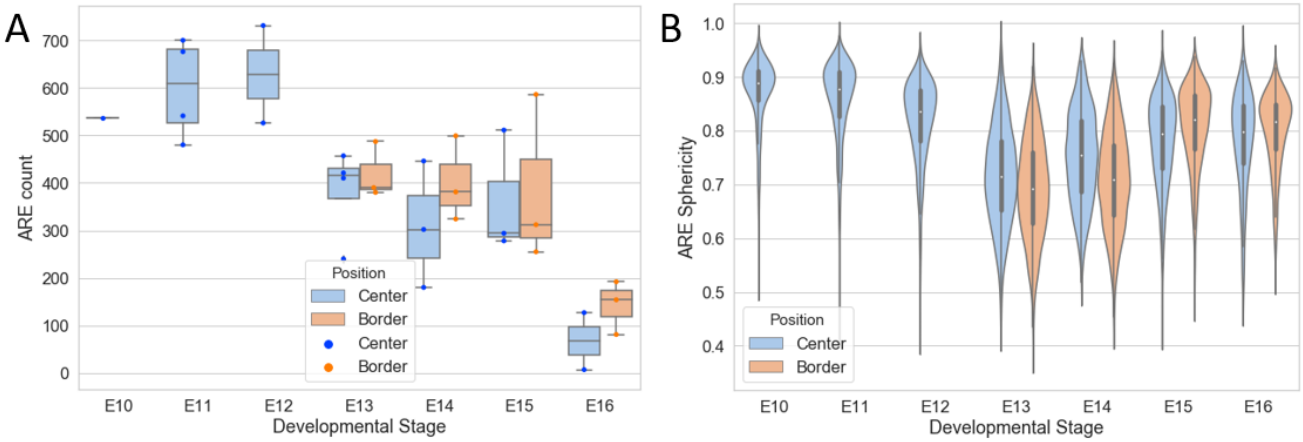

Figure 3.2-3: ARE quantifications

Each point corresponds to an image. All the images were 150µmX150µmX80µm. Data collection is not fully complete, results are in duplicate for E10-E12 and triplicate for E13-E16. A: Box plot are drown as previously described. We observe a stepwise decrease in ARE count per isovolumetric image. B: Kernel density estimate based on pooled lumen from all images per stage. The quartile (thick bar) and whisker (thin bar) values are shown as black bars, median value is shown as a white dot. ARE shape distribution is shifted toward a less spherical value around E13 and later increases.

3.2.2 Apical targeting in hepatoblasts in vivo

The timings suggest that CD13 is present early in the ARE, especially when compared to junction components clustering at the cell border. In adult mouse hepatocytes CD13 is sent to the apical surface via transcytosis (Ihrke et al., 1998) however we don't know which

trafficking route is active at this stage. We have therefore decided to look at the distribution of other apically targeted proteins (Table 2-1) to get hints about the active routes and to confirm that we are looking at AREs.

Apical Marker	Function	Distribution	
		Before lumen formation	After lumen formation
CD13	Peptidase	Intracellular polarized	Apical
Prominin	Glycoprotein	Could not detect	Apical
MRP2	Bile salt transporter	Intracellular polarized	Apical
DppIV	Peptidase	Intracellular polarized + Basal	Apical + Basal

Table 3-1: Apical surface marker distribution at early stages

Distribution pattern of apical surface markers observed at E14. The distinction between before and after lumen formation was done visually based on phalloidin pattern. Only markers showing consistent pattern over at least two separate experiments on different samples are listed. Intracellular polarized correspond to an ARE like pattern close to the cell border.

Prominin is a glycoprotein, its precise function is not known but it is apically distributed in neuro-epithelia at early stages, it is then removed after complete differentiation. We could detect it in small lumina but not intracellularly in ARE. As described in other systems we could not detect prominin at later stages (E18) after network formation.

Dipeptidyl Peptidase IV (DPPIV) is a well characterized peptidase, in the adult it is produced by hepatocytes and undergo transcytosis (like CD13). After synthesis, the protein is first targeted basally and then sent to the apical surface (Barr et al., 1995). The distribution of DPPIV in the embryonic liver suggest that, during development, the protein could also be expressed in stellate cells (Figure 2.2-4 A) and in endothelial cells (data not shown). In hepatoblasts, the protein seems to be present all over the cell surface but is concentrated in the ARE (Figure 2.2-4 B). Notably the ARE can be found close to the cell border and directed towards a cell negative for DPPIV, this will be further discussed later.

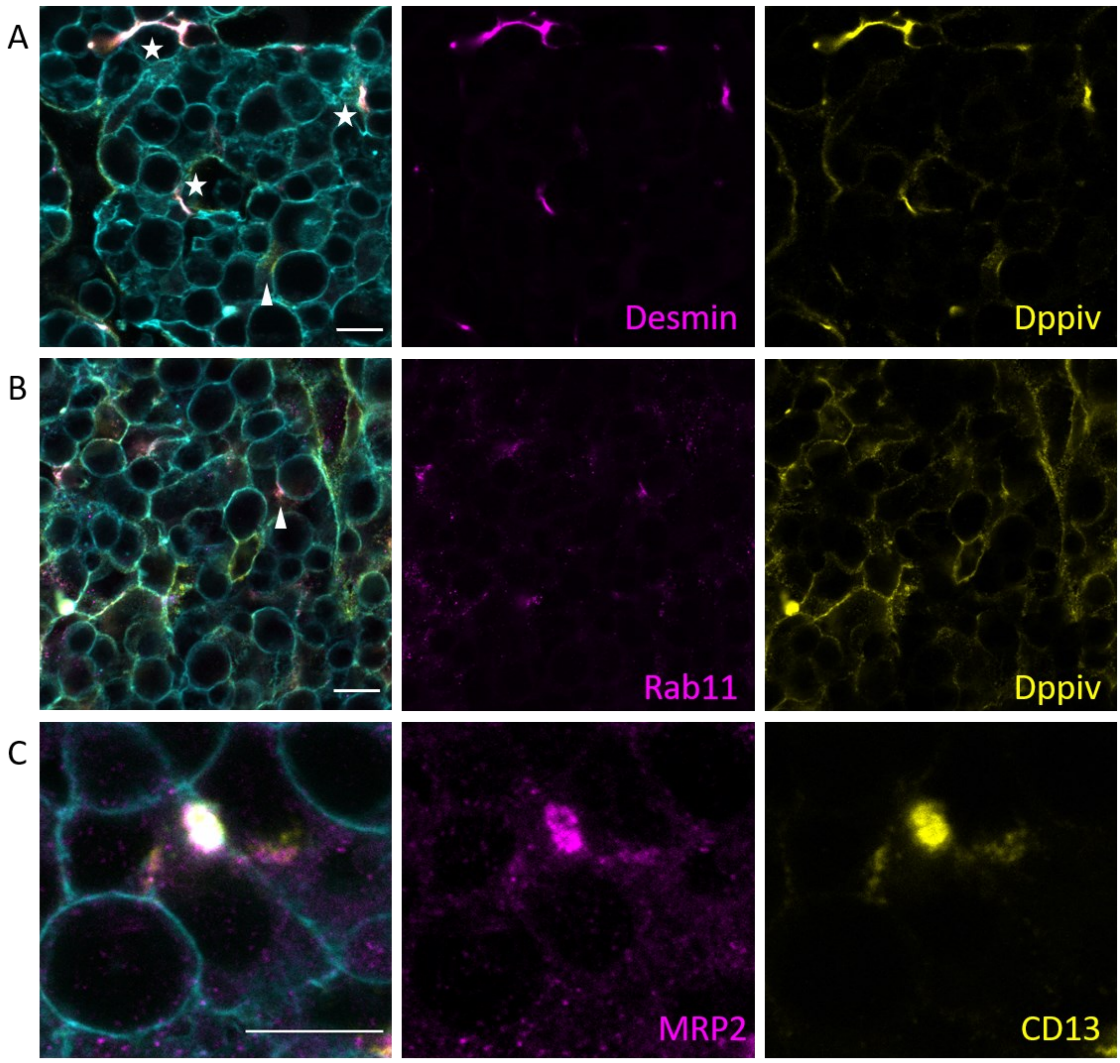

Figure 3.2-4: Apical surface marker distribution

Single plane immunostaining at E14,5. A: Stellate cells (marked with Desmin in magenta) are strongly positive for DppIV (Yellow) and underlined by white stars. B: DppIV colocalize with rab11 vesicle clusters. C: MRP2 colocalize with CD13 both on intracellular vesicle clusters and on established lumina. White arrowheads are pointing examples of ARE like structures close to the cell border. Scale bars: 10µm.

Multidrug Resistance Protein 2 (MRP2) is an active transporter that secrete bile salts and xenobiotics in the adult bile canaliculi network. We could find this protein also colocalizing with CD13 intracellularly at early stages. This protein also seems to be present at the apical surface in small lumina before network formation (Figure 2.2-4 C). As opposed to DPPIV and CD13, MRP2 is directly sent to the apical surface after synthesis and is not thought to transit through the basal side.

These results are suggesting that both apical targeting and transcytosis could be active and involve the ARE at this stage. The presence of MRP2 suggested that direct secretion could occur through this compartment. On the other hand, this cell region seems to also cluster rab4 vesicles (data not shown) further suggesting a recycling activity. However, at this point it is not clear whether if this compartment is actively recycling or if it is accumulating apical components. To address this, we have decided to perform uptake experiments *in vitro*.

3.2.3 Apical targeting in hepatoblasts in vitro

In these experiments we decided to use primary cells isolated from the embryonic liver. Using a Matrigel sandwich culture system it was possible to polarize these cells in a way that resemble hepatocyte polarity. To validate this model, we have compared the early stages of polarization *in vitro* with what we found in vivo.

Looking at the distribution of ZO-1 briefly after plating we could find that in the case of hepatoblast duplet it was mostly localized at the cell interface (Figure 2.2-5 A,B,C). CD13 was first distributed all over the cell border (Figure 2.2-5 A), Then it gets concentrated intracellularly (Figure 2.2-5 B) and finally it can be found between the two cells in structure lined by ZO-1; a lumen (Figure 2.2-5 C).

We also looked at the distribution of rab11. First it forms a cluster in cytoplasm positive for CD13 (Figure 2.2-5 D); the ARE. The cluster can also be found close to the cell-cell interface (Figure 2.2-5 E); this resembles a polarization event. Finally, it can be found just below established lumina like in vivo (Figure 2.2-5 F). We could confirm that these cells recapitulate the steps in hepatoblast polarization observed in vivo, and therefore likely to be suitable assess the activity of the ARE.

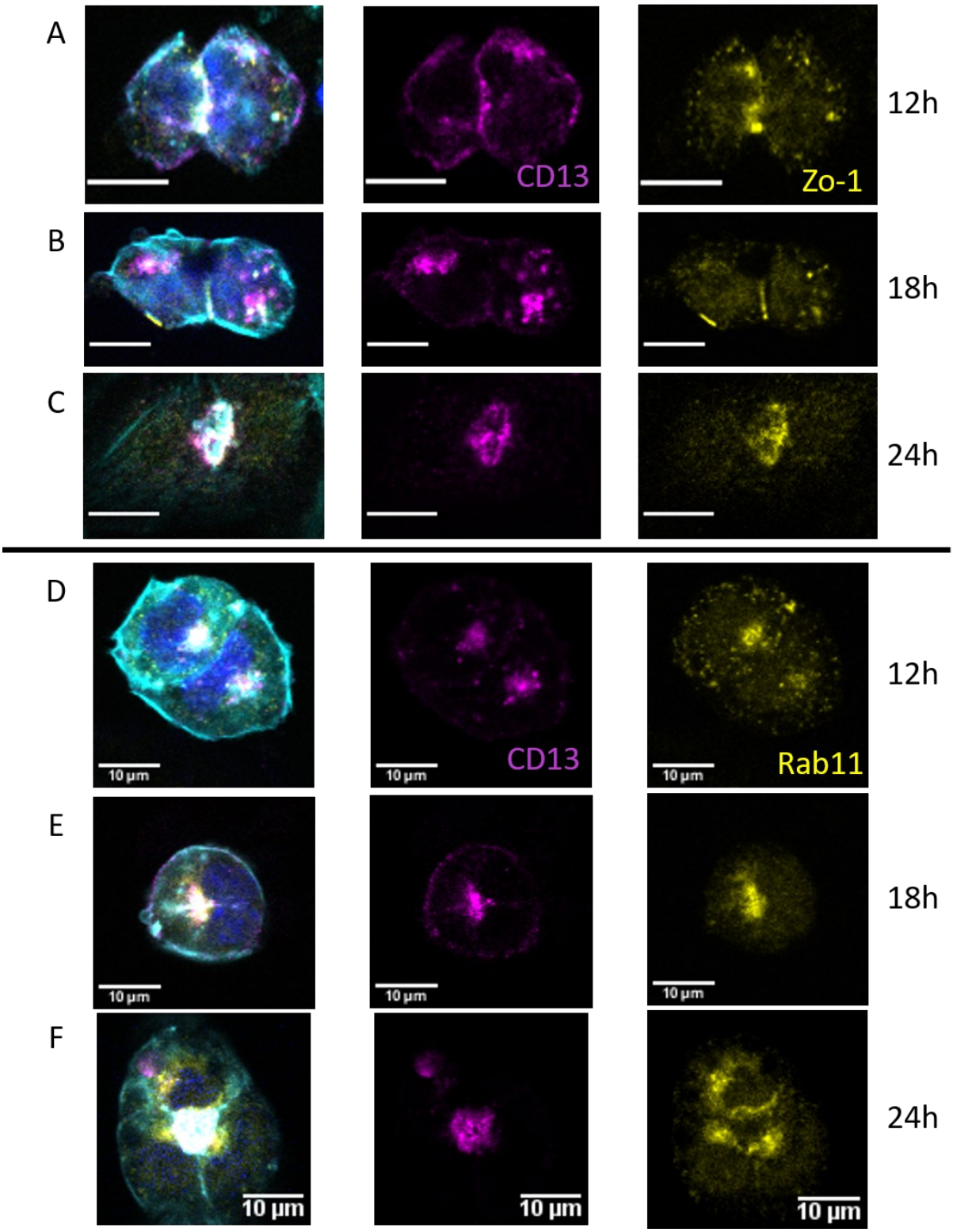

Figure 3.2-5: Early steps of polarization in vitro

Single plane images of representative cells for each timepoint. Cells were fixed 12h (A,D), 18h(B,E) and 24h(C,F) after Matrigel overlay. Cells were then stained with phalloidin (cyan) Dapi (blue) and immunostained against CD13 (magenta) and either ZO-1 or Rab11 (yellow).

We then performed an uptake of CD13 antibody in live cells. The cells were exposed to the antibody for 30 minutes on ice, the media was then changed, and the cells were placed back in the incubator. The hepatoblasts were then fixed after different chase time and stained with a secondary antibody. The cells incubated with primary antibody were all showing stronger fluorescence compared to their respective controls without primary antibody (Figure 2.2-6 A,B). Without chase the antibody is evenly distributed inside and at the cell surface (Figure 2.2-6 B). At 15 minutes, the antibody gets clustered inside the cell in a compartment resembling the ARE (Figure 2.2-6 C). This effect was even stronger after 1h of chase (Figure 2.2-6 D).

The CD13 intensity seems to decrease overtime at the cell border facing the ECM (Figure 2.2-6 E). This is probably the result of the internalization of the antibody along with CD13. Interestingly the decrease is much less important at the border between two hepatoblasts, this could be due to the presence of two cell borders at this location. However, the intensity seems to increase at this location between 0 minutes and 15 minutes chase. This suggest that CD13 is targeted towards this area.

Additionally, we could confirm that the intracellular compartment containing CD13 was rab11 positive (Figure 2.2-6 F) and therefore likely to be the ARE. The uneven distribution of CD13 at the cell border and its concentration within the ARE suggest that this compartment is active before lumen formation. It also opens the possibility that CD13 could be maintained at the cell border between two hepatoblasts.

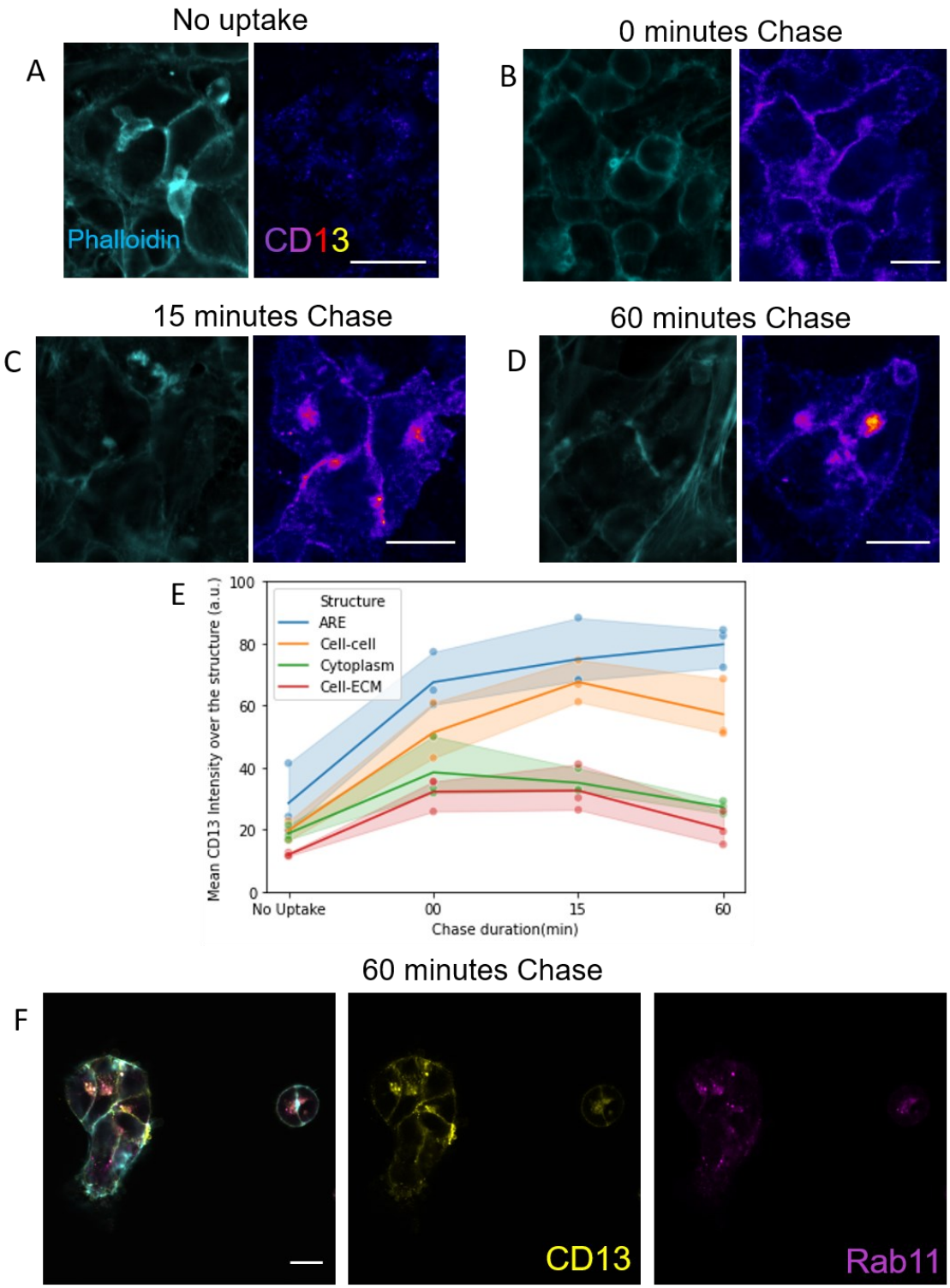

Figure 3.2-6: CD13 antibody uptake

Cells were exposed to CD13 antibody for 1h on ice, the antibody was washed, and cells were placed back in the incubator for different duration before fixation. A-D: Single plane image of cells stained with a secondary antibody against the incubated primary and phalloidin. E: Estimation of expected quantification of CD13 intensity in different cell locations at different timepoints (quantification was only performed on shown images). F: immunostaining against Rab11 on cells incubated with CD13 primary. Scale bars: 10µm

The ARE therefore seem active even before lumen formation. If the distribution of the CD13 antibody on the lateral side suggest that no junction was present we need to confirm this in vivo. To do so we used electron microscopy (EM) and immunogold on EM to look for junctional structures at the vicinity of ARE.

Using EM, we could identify large cluster of vesicles in the perinuclear region (Figure 2.2-7 A) and close to the cell border (Figure 2.2-7 B). Similar clusters could be found below established apical surfaces (Figure 2.2-7 C). In absence of clear lumina, no junctions could be found close to the vesicle clusters. These vesicles are forming clusters like ARE and the vesicles shape are compatible with tubulation observed in recycling endosomes.

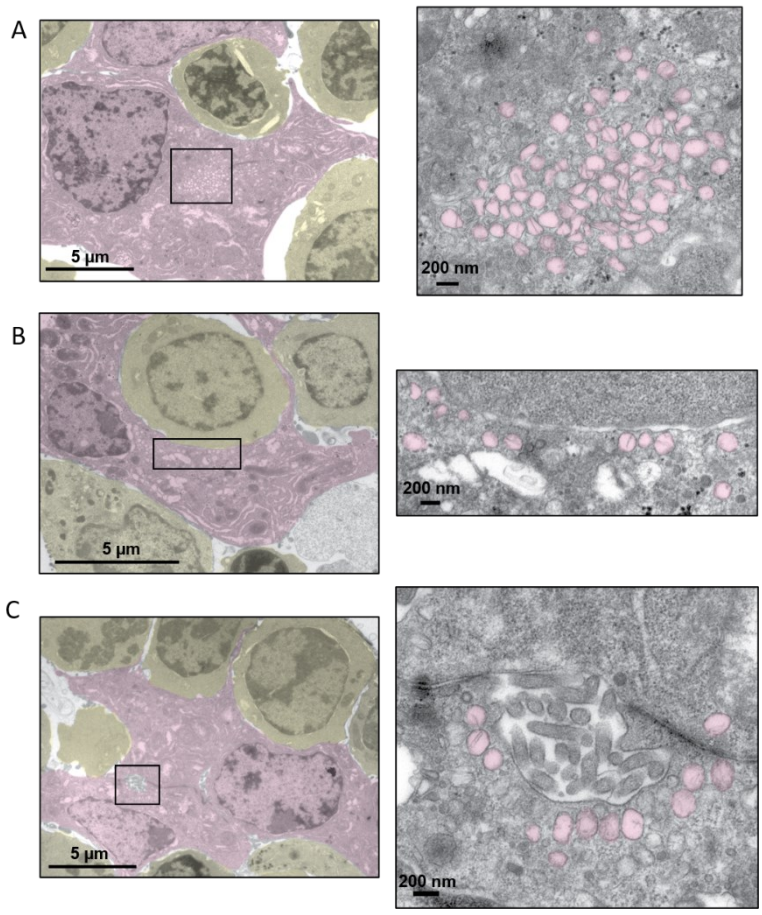

Figure 3.2-7: Electron microscopy images of the early steps of polarization

Epon sections of E14 embryonic livers were imaged by electron microscopy. Left column shows large fields of view, hepatoblasts are pseudocolored in magenta and other cell types are in yellow. The magnified area is shown as a black rectangle. On the right column the magnified area are shown, vesicles of interest are pseudocolored in magenta. A: Perinuclear vesicle cluster B: Vesicle cluster close to the cell border. C: Vesicle cluster lining an established lumen.

We then used immunolabelling to confirm that these vesicles clusters were containing CD13. We could detect the antibody in established lumina as expected (Figure 2.2-8 A) and also in vesicle clusters close to the nuclei (Figure 2.2-8 B). We could also find CD13 in vesicles close to the cell border. Interestingly, not only no junctional structures could be found in the proximity of these vesicles, but they seem to be positioned towards different cell types. These other cells are more spherical and possess less cytoplasm. These cells could therefore be erythropoietic progenitors. This hypothesis is compatible with the observation that DPPIV could be found in vesicular cluster positioned toward a DPPIV negative cell (Figure 2.2-8 B).

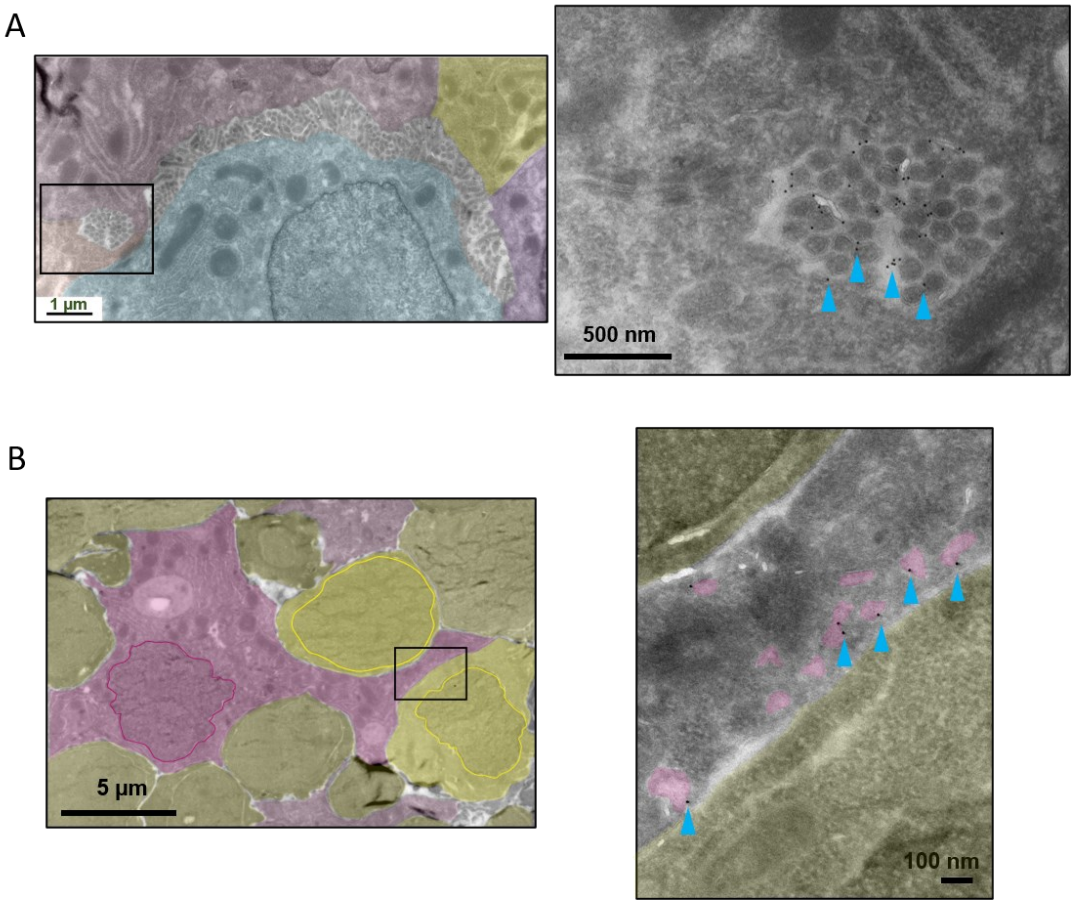

Figure 3.2-8: Immunogold on electron microscopy images of early steps of polarization

Tokayasu sections of E14 embryonic livers were labelled with immunogold directed against CD13 and then imaged by electron microscopy. A: Left image shows a large field of view, each colour corresponds to a different hepatoblast. A black square mark the magnified area. Right image is the magnified area gold particles are shown with cyan arrowheads. CD13 is located almost exclusively inside the lumen. B: Left image shows a large field of view, hepatoblasts are pseudo-coloured in magenta, other cell types are in yellow. A black square mark the magnified area. Right image is the magnified area gold particles are shown with cyan arrowheads. Other cell types are pseudo coloured in yellow, vesicles are in magenta. CD13 is located in a vesicle cluster close to the cell border.

At this point we could observe that the ARE clusters multiple apical surface components potentially from different trafficking route. It is positioned next to the cell border toward different cell types. This raises the question of how this compartment is positioned and this point will be further discussed later. This compartment seems also to be actively recycling some components at the plasma membrane and it appeared to be active in absence of junctions. We have therefore decided to investigate this possibility by knocking down candidate genes by taking advantage of our in vitro system.

3.3 Junctions involvement in lumen formation

The canonical view of polarization in MDCK cells includes the establishment of tight junctions prior to apical components delivery (Mangan et al., 2016). This process is thought to include ZO-1 and a fully mature tight junction. However, the results of the uptake experiment suggest that the ARE could be active even if the tight junction is not complete and the fence function is not yet established. Notably, in hepatocytes cell lines, a different set of tight junction proteins have been proposed to be involved in the process of vesicle delivery at the midbody location (Kojima et al., 2001).

3.3.1 Junctional markers in vivo

In order to clarify the degree of junction maturation at different steps of polarization we went back in vivo and looked at different junctional markers before and after lumen formation (Table 2-2).

Apical Marker	Junction type / localization	Distribution	
		Before lumen formation	After lumen formation
E-Cadherin	Adherens junctions / Transmembrane	Not consistent	Lateral
ß-Catenin	Adherens junctions / Intracellular	Not consistent	Lateral
Claudin 1	Tight junctions / Transmembrane	Could not detect	Sub-apical (only visible at late stages)
JAM-A	Tight junctions / Transmembrane	Not consistent	Could not detect
Occludin	Tight junctions / Transmembrane	Not consistent	Sub-apical
ZO-1	Tight junctions / Intracellular	Absent	Sub-apical
Par3	Tight junctions / Intracellular	Seems to corelate with ARE location	Apical + sub-apical (could not detect on late stages)
Desmoplakin	Desmosomes / Transmembrane	Not consistent	Lateral

Table 3-2: Junctional markers in vivo

Correlation between ARE location and junction marker distribution at E14. The distinction between before and after lumen formation was done visually based on phalloidin pattern. Only markers showing consistent pattern over at least two separate experiments on different samples are listed. The late stages mentioned correspond to E17 when most of the network is established. Not consistent: the ARE is directed towards it sometimes but not always and the marker can be found away from ARE. The Claudin 1 staining was quite weak, it is hard to conclude on the absence before lumen formation.

We could not corelate the location of Adherens junction components with the relocation of the ARE to the cell border. Adherens junctions could be present where the ARE is directed but they could also be found away from this location (Figure 2.3-1 A). It was also the case for

transmembrane components of tight junctions this could mean that these components are present before the ARE relocation to the cell border.

The distribution of Intracellular components of tight junctions was quite interesting. ZO-1 could only be found around established lumen but was also clearly present on small lumina. This suggest that it could be involved in the establishment of the fence function. However, we could find ARE located to the cell border in absence of ZO-1 suggesting that ZO-1 is not involved in the relocation of the ARE. Par3 is not strictly a component of tight junctions however it has been shown to interact with them in the early steps of their establishment. It appeared that in most cases, when the ARE was located at the cell border Par3 was also present (Figure 2.3-1 B). Par3 was also present at the apical surface of early lumina and was spread over the expected location of tight junctions. We have therefore decided to investigate further the function of ZO-1 and Par3 in the early steps of lumen formation.

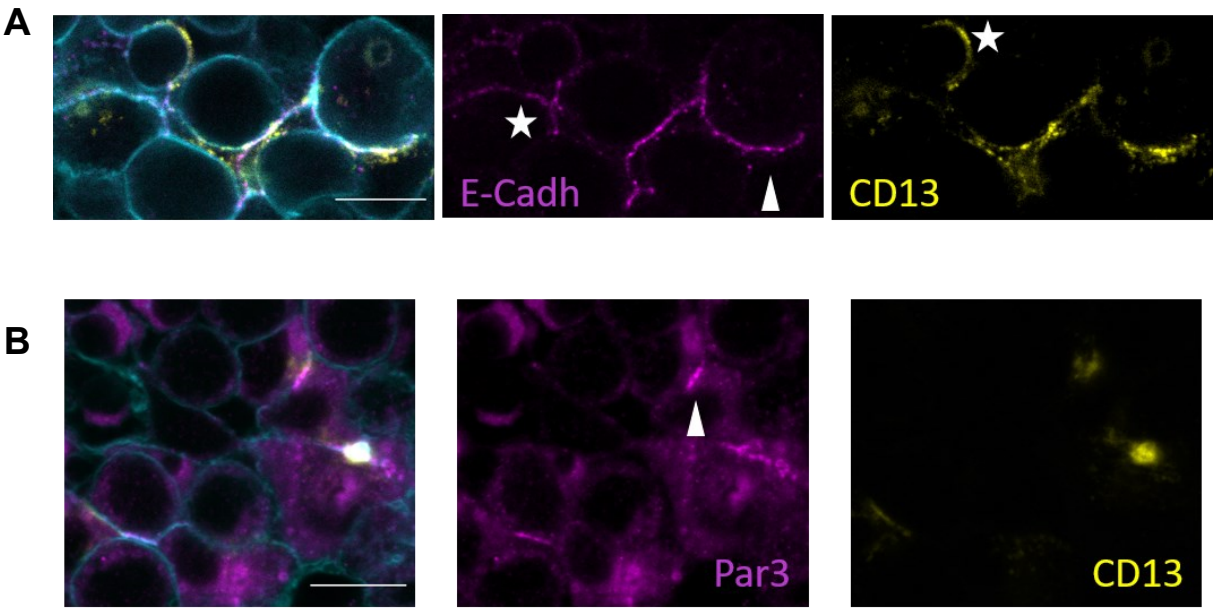

Figure 3.3-1: Junctional markers distribution in vivo

Single plane image of staining performed on E14 embryos. A: immunostaining against E-cadherin (magenta) and CD13 (Yellow) also stained with phalloidin (cyan). Stars indicate location where a marker is present but not the other, this correspond to the “not consistent” pattern described in table2. B: immunostaining against Par3 (magenta) and CD13 (Yellow) also stained with phalloidin (cyan). The presence of a local accumulation of Par3 at the cell border seem to corelate to the presence of CD13 in this region. Arrowheads points a possible ARE close to the cell border based on CD13 staining. Scale bars: 10µm

3.3.2 Junction function in vitro

We used primary hepatoblasts isolated from embryonic livers at E14. The knock-down (KD) was performed using naked small interfering ribonucleic acid (siRNA) and a transfection reagent for 24h. The Matrigel overlay was added upon washing of the transfection reagent on the second day. This approach implies to let the cells for 24h as a monolayer before applying the overlay.

We observed that in these conditions, primary hepatoblasts were able to generate columnar polarity as a monolayer. In response to the overlay the cells would then translocate the apical surface as a whole to the previously lateral side (Data not shown). This process involves a compartment resembling the vacuolar apical compartment (VAC) described in other systems (Vega-Salas et al., 1987).

However, after this phenomenon occurs the cells are still generating new lumina. We have therefore decided to use this simple KD system despite the possible artifacts in order to identify candidate genes involved in the generation of new lumina. We would then use a different approach to confirm the identified phenotype. This second approach will be discussed later.

We then assessed the knock down by immunofluorescence (Figure 2.3-2) and/or Reverse transcription-quantitative polymerase chain reaction (RT-qPCR) (Data not shown). First, we looked 24h hours after Matrigel overlay. We used the mock KD condition to evaluate the non-specific staining from the secondary antibody (Figure 2.3-2 A). The laser intensity used was higher than the one used in previous experiments therefore some bleed-through can be observed.

Cells lacking Par3 were able to polarize (Figure 2.3-2 B), this could be due to insufficient KD. Notably we could not detect the protein using our antibody on control cells. On the other hand, we could confirm the KD compared to control condition by RT-qPCR (Data not shown). This explanation is therefore unlikely. It is possible that the positioning of the VAC uses a different machinery than the positioning of the ARE. If Par3 is involved in the relocation of the ARE to the cell border we would expect the cells to no longer be able to generate new lumina in Par3 KD condition. The best way to assess this using the current system is to quantify the number of lumina per cells around 48h after overlay. At this timepoint the hepatoblasts have generated new lumina but the lumina are not yet connected. These quantifications are not complete yet. Finally, 24h after Matrigel overlay the differences between ZO-1 KD and control condition were not striking. The ZO-1 KD cells were able to lead the ARE to the cell border (Figure 2.3-2 C). But we could not find established lumina, so we decided to observe these cells at a later timepoint.

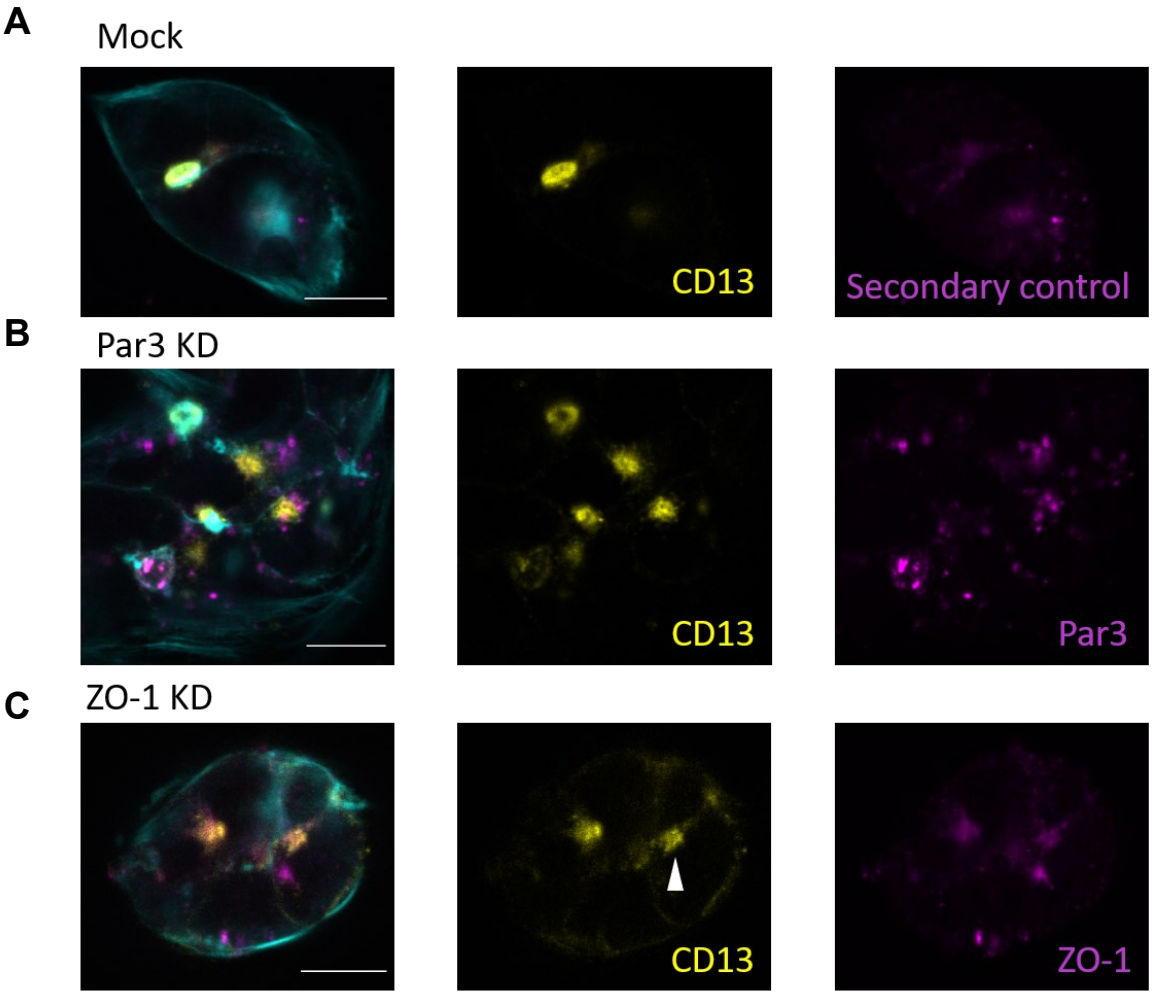

Figure 3.3-2: Knock down in vitro

Single plane images taken on cells isolated from E14 embryonic livers. Cells were treated with transfection reagent upon plating and let 24h before washing and adding the Matrigel overlay. The staining was performed on cells fixed 24h after the overlay. Cells were stained using antibody against CD13(yellow) and either the knock down target or no primary for the mock condition. The same secondary antibodies were used in all conditions. The magenta channel was acquired at high laser intensity. A: mock condition. no primary was used on the magenta channel and serves as secondary control. A lumen is visible in between the two cells. B: Par3 KD, multiple lumina are visible. C: ZO-1 KD, no lumen is visible on this field of view, CD13 is likely located in the ARE, the arrowhead points toward a possible ARE close to the cell border. Scale bars: 10µm.

3.3.3 ZO-1 function in polarity establishment

We then looked at the effect of ZO-1 knock down 36h after Matrigel overlay. At this point, clear defects in lumen formation could be observed (Figure 2.3-3). In the non-targeting siRNA control (luciferase siRNA shown in Figure 2.3-3 A), large lumina can be found between cells.

The cells lacking ZO-1 however were only showing sparse small lumina (Figure 2.3-3 B). We could also observe some intracellular lumina, these structures resemble the VACs like structures mentioned earlier. This could reveal that ZO-1 is required for VAC delivery to the lateral side but it does not necessarily imply a function in de novo lumen formation.

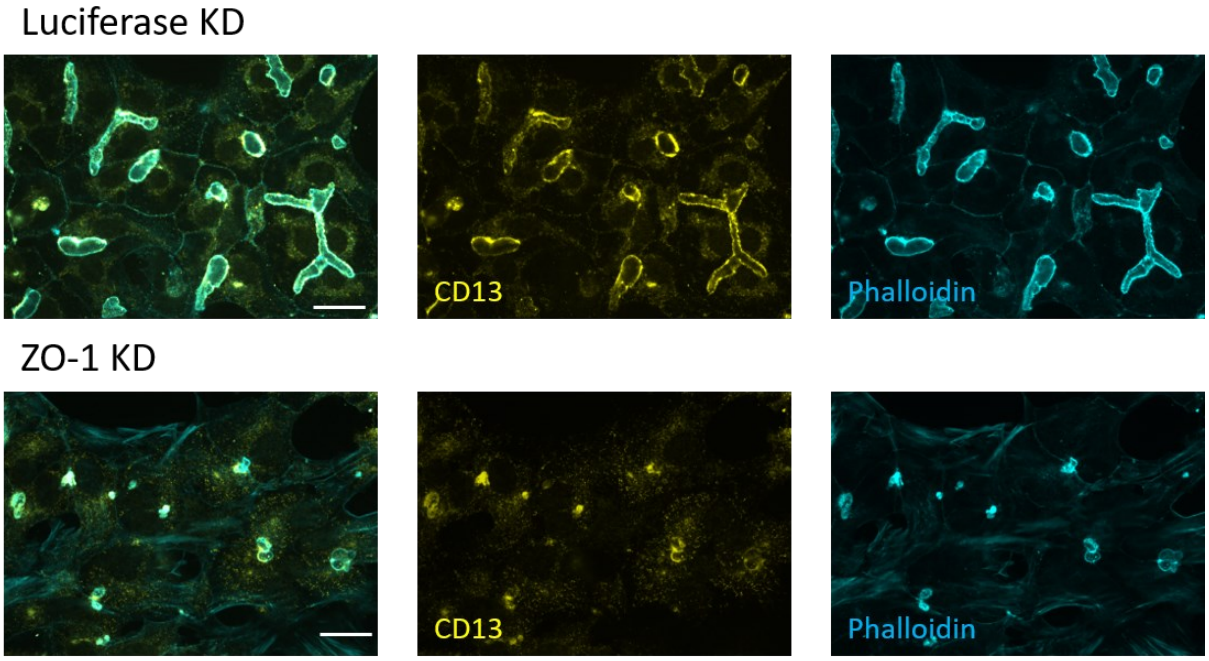

Figure 3.3-3: Lumen defects in ZO-1 KD cells

Single plane images taken on cells isolated from E14 embryonic livers. Cells were treated with transfection reagent upon plating and let 24h before washing and adding the Matrigel overlay. The staining was performed on cells fixed 36h after the overlay. Cells were stained using antibody against CD13(yellow) and with phalloidin. A: non targeting siRNA (designed against luciferase) at this stage lumina are formed and quite developed. B: ZO1-KD. Lumina are underdeveloped and not properly shaped.

In order to look for a potential defect in early steps of lumen formation we took a closer look at the ARE located close to the cell border. In the luciferase KD condition (Figure 2.3-4 A) almost all of them were directed towards a clear patch of occludin (Figure 2.3-4 B). In the ZO-1 KD condition (Figure 2.3-4 C) this did not appear to be the case. We could find multiple occurrences of occludin patches with no detectable CD13 (Figure 2.3-4 D). We could also find CD13 clusters close to the cell border in absence of occludin (Figure 2.3-4 E). We could not observe this in control KD or in mock conditions.

It could reveal that ZO-1 is required to coordinate junction formation and vesicle delivery. To confirm this, we will have to perform the KD in a way that prevents columnar polarity acquisition. This is possible using siRNA embedded in lipid nano particles. Using this approach, we can perform the KD while the hepatoblasts are in Matrigel sandwich (data not

shown). This has been done in our lab in order to KD other genes and we are planning to apply this method to ZO-1 as soon as possible.

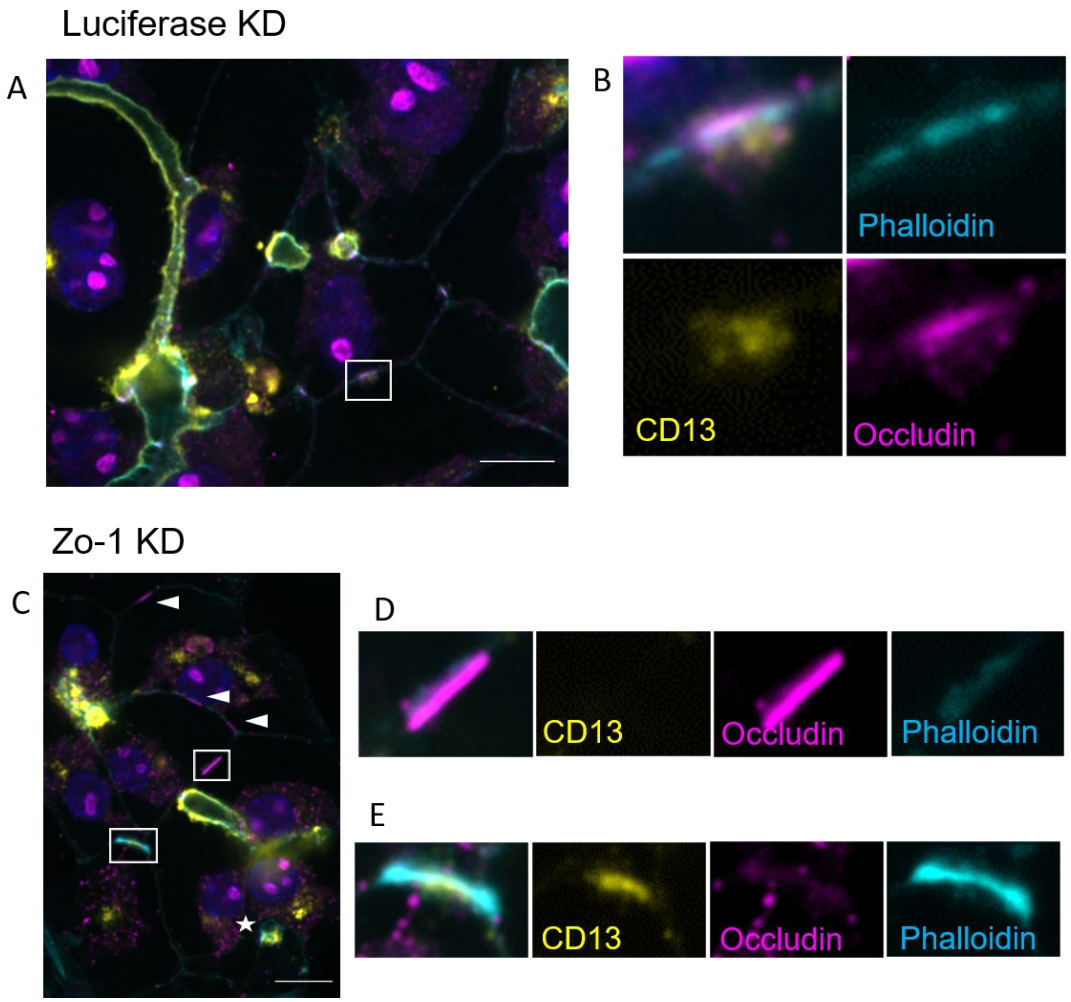

Figure 3.3-4: Polarization defects in ZO-1 KD cells

Single plane images taken on cells isolated from E14 embryonic livers. Cells were treated like described previously. The staining was performed on cells fixed 36h after the overlay. Cells were stained using antibody against CD13(yellow), Occludin(magenta) and with phalloidin. A: Luciferase KD, cells can form proper PAP. The magnified region is shown as a white square. B: Magnified region from A, this structure corresponds to a PAP. C: ZO1-KD. Incomplete PAP formation can be observed in multiple places. Either Occludin is present in absence of CD13 (arrowheads and D) or CD13 is present but no occludin can be found (star and E). D,E: magnified region from C

It has been proposed in other systems that ZO-1 would be required for apical components delivery. However, in hepatoblasts the situation could be different. We could observe that apical component delivery was likely to occur before junction formation. On the other hand, it appeared that upon ZO-1 KD the delivery was no longer occurring where junctions are located after their formation. It is therefore possible that ZO-1 is required to focus the delivery of apical

component at the right place after junction formation. The slight differences to the descriptions in other systems could be linked to specificity in hepatocyte polarity acquisition. In order to evaluate this possibility, we need to go back in vivo and look for the next steps in the process of hepatoblast polarity emergence during liver development.

3.4 Multipolar polarity acquisition

We have described to far the steps involved in polarization of hepatoblasts in vivo. We stopped at the point where a lumen is formed. At this stage, the hepatoblasts displays a clear apical surface. However as mentioned in introduction this does not correspond the hepatocyte polarity found in the adult liver.

3.4.1 Early multipolar polarity

Starting from a lumen the hepatoblasts will have to refine their polarity in order to establish an elongated belt-like apical surface. There are two possibilities for that. First, they could elongate the existing surface along their periphery. Second, they could generate several apical surfaces and then connect the distinct surfaces.

Both hypotheses assume that lumina grow as tubes. In a case or in the other if lumina were to expand in all directions their growth or their fusion would lead to large spheres. Going back to the lumen quantifications performed previously we can verify this. However, we will still make one reasonable assumption, the lumina tend to grow, and large lumina are not directly formed as such but start small and grow afterwards. This assumption is backed up by the observation that the largest lumen observed in each volume is larger over time (Figure 2.4-1 A). This effect becomes clear starting at E12 and there is an even stronger difference between E15 and E16 when the lumina start to connect and form a network.

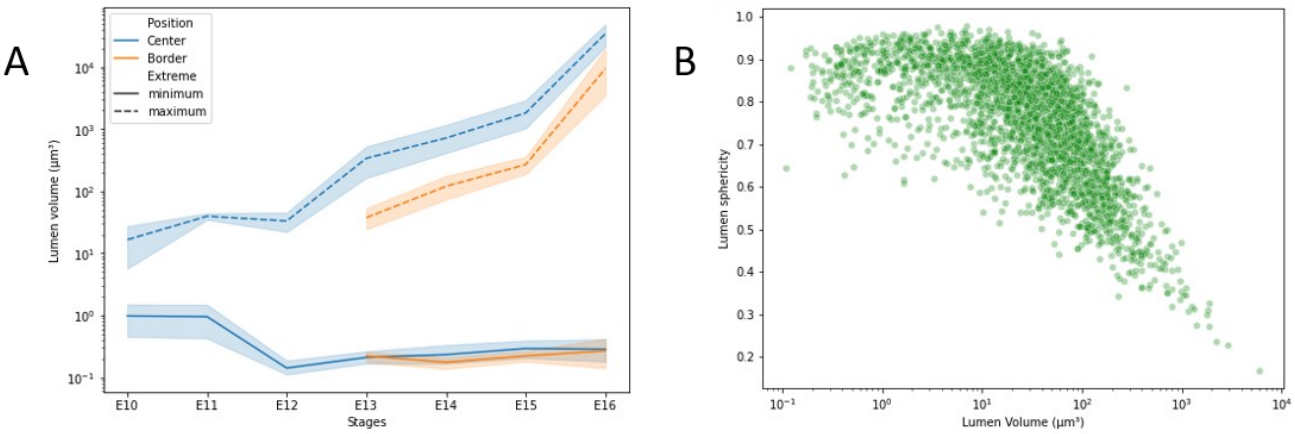

Figure 3.4-1: Lumen quantifications

Additional lumen quantifications based on the dataset described in part1. A: Smallest and largest lumen volume found at different stages. The hard lines capture the mean values over several images, the error bands show the 95% confidence interval. B: Scatterplot showing the relation between lumen sphericity and lumen volume at E15. Each dot represents a lumen, lumina form 18 different images are pooled on the figure (center and border of all replicates).

Based on this we can now look at the relation between sphericity and volume at a late stage and see whether if these parameters are related. We can then observe that at E15 below 100µm³ the lumina are quite spherical (Figure 2.4-1 B). For larger lumina however, it appears that the volume and the sphericity are strongly anti-corelated. The larger the lumen the less spherical it will be. This observation suggests strongly that lumina of at least 100µm³ grow as tubes. The same observation can be made at all stages were lumina of this size can be found (E13-E16, data not shown).

The two hypotheses are still valid. We can however note at this point that consistently small lumina can be found at every timepoint considered (Figure 2.4-1 A). This suggests that lumina are formed continuously over the considered timeframe. The formation of multiple lumina fits better with the hypothesis that an hepatoblast would polarize several times and then connect its lumina.

The most direct approach to assess this is to look directly in the organ if cells with multiple lumina can be found. It turned out to be the case, looking at E15 we could identify clear instances of cells completely included in the volume of the image that have formed distinct lumina with independent junctions and apical surfaces (Figure 2.4-2). This observation strongly supports the hypothesis we wanted to test. Notably these cells already have a multipolar polarity no longer compatible with a columnar polarity.

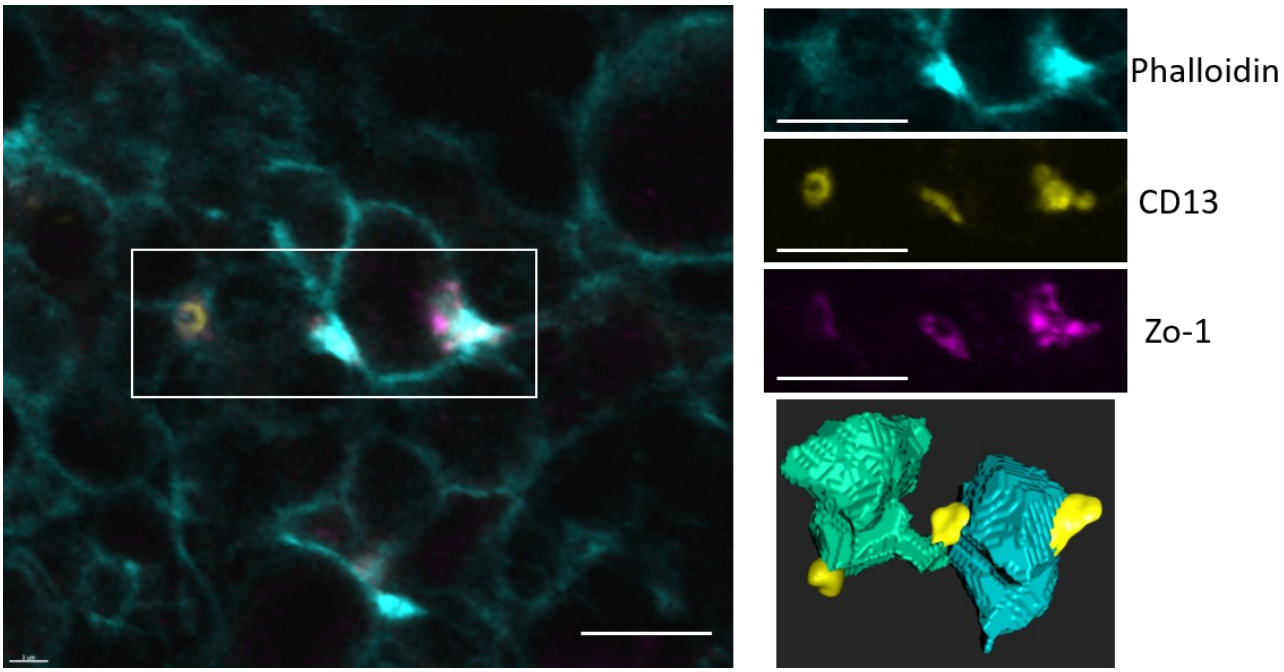

Figure 3.4-2: Multiple lumina in vivo

Single plane fluorescence image of multipolar hepatoblasts at E15 and 3D reconstruction of the hepatoblasts in focus and their lumina. Images on the right column are the individual channels of the region highlighted by a white rectangle on the overview on the left side. Liver sections have been stained with phalloidin and antibodies against CD13 and ZO-1. Structures positives for these 3 markers are considered lumina. On the 3D reconstruction (bottom right) we can clearly see that lumina are distinct in 3D. Scale bars: 10 µm

3.4.2 Multiple lumen generation

The presence of multiple lumina around one hepatoblast also raises the question of how cells achieve this polarity. It is possible that the hepatoblast repeat the polarization process described earlier. We have therefore looked for ARE away from lumina in polarized hepatoblasts. We could find such structures at multiple stages. The ARE were indeed rab11 positive and contained CD13. They could mostly be found close to the cell border and away from lumina. Interestingly it appeared that the centrosome was present at the ARE and not at the lumen (Figure 2.4-3).

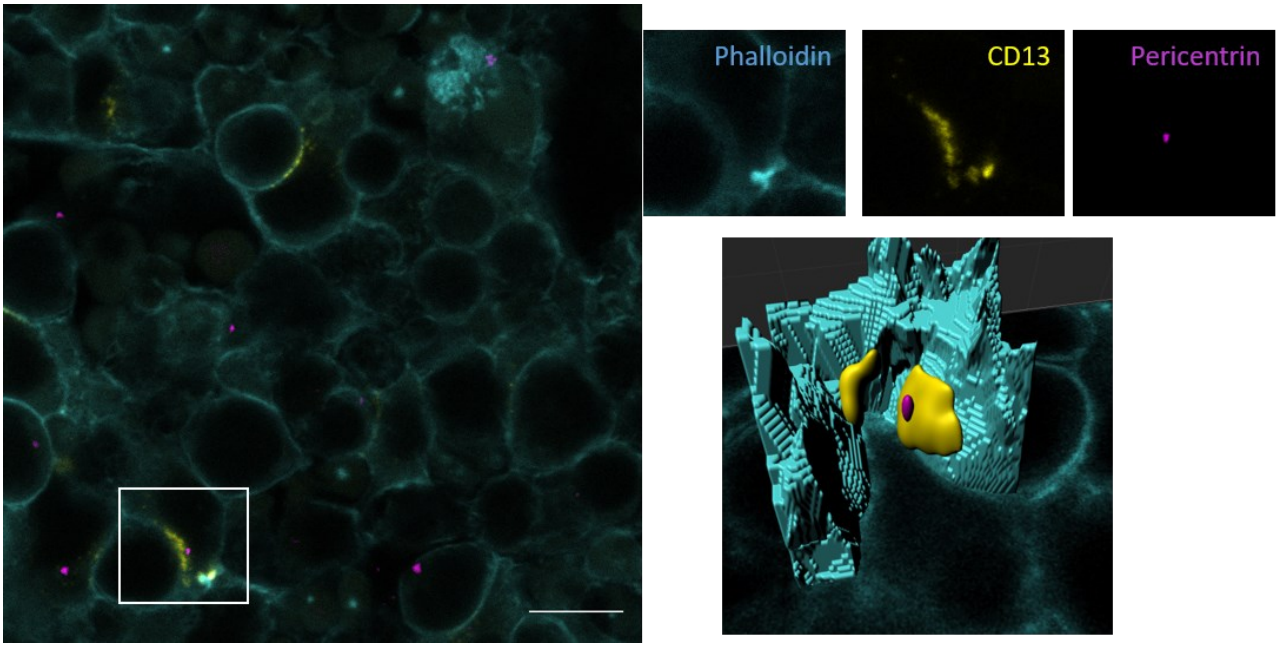

Figure 3.4-3: ARE away from lumen

Single plane immunofluorescence image and local 3D reconstruction. Liver slice from a E14 embryo has been stained with phalloidin (cyan) and antibodies directed against CD13 (yellow) and Pericentrin (magenta). On the left: an overview of the region with all channels overlaid, the magnified region is shown as a white square. On the top right: individual channels of the magnified region showing the tip of a lumen and an ARE with the centrosome. Bottom right: 3D rendering of the reconstructed region. CD13 is segmented in yellow, Pericentrin in magenta and cell borders in the considered region are segmented in cyan. The lumen is the yellow object on the left and the ARE is the yellow object on the right.

This observation led us to believe that hepatoblasts could displace the ARE as a cluster from a cell border to another. They could then generate multiple apical surfaces by repeating the same polarization process.

3.4.3 Live imaging in vitro

We could find similar structures in vitro on primary hepatoblasts cultured in Matrigel sandwich. Therefore, to confirm that hepatoblasts would move the ARE as a cluster we have decided to image this process live in vitro. Before imaging we must first characterize live imaging markers that will be required for our observation and set up post processing pipeline to find a balance between laser intensity and image quality.

We need to be able to visualize two structures: lumina and ARE. For the lumina we already know that they are expected to be decorated with an actin rich mesh. We have therefore

focused our attention on our mouse line expressing Lifeact bound to green fluorescent protein (lifeact-GFP). Lifeact is a small peptide with a strong affinity for filamentous actin. As expected, we could easily identify lumina on cells carrying this transgene (Figure 2.4-4 A).

For the ARE we used another transgenic mouse line: the mTmG. This mouse line expresses by default a membrane-targeted tandem dimer Tomato (mT) ubiquitously (Muzumdar et al., 2007). Upon Cre expression the tomato sequence and the associated stop codon is excised, and a membrane targeted enhanced GFP (EGFP) is expressed instead (the sequence is located right after the Tomato stop codon). Here we simply used the mT as a marker for membranes. Interestingly it is present not only on cell border membranes but also seem to have affinity for vesicular membranes. We can clearly see one cluster of vesicles per cell that is strongly positive for the marker. It is positive for Rab11 (Figure 2.4-4 B) and for CD13 (Figure 2.4-4 C) this fits the description of the ARE. We will therefore use this transgene to track this compartment. To have cells expressing these two markers we can cross these two mouse lines and isolate cells from the double positive embryos.

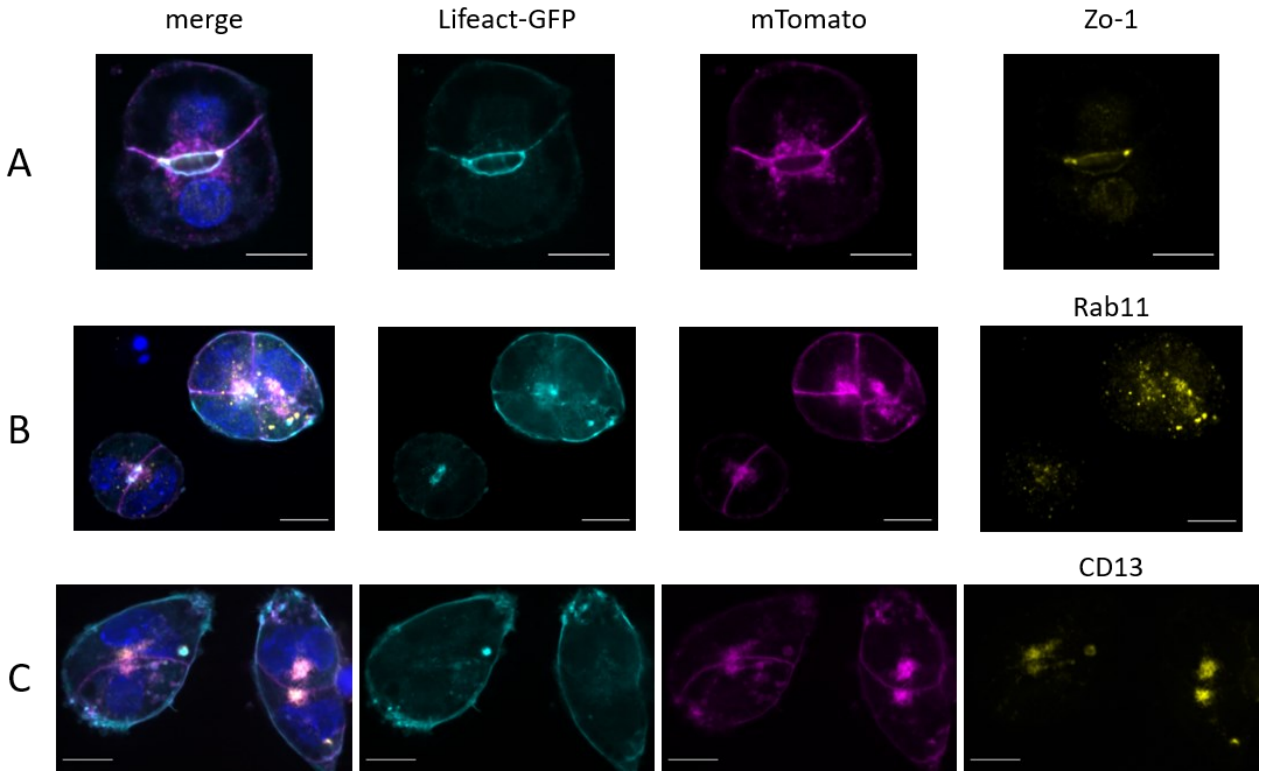

Figure 3.4-4: Live imaging markers

Cells were isolated from the liver of a double positive embryo and then plated for 24h. The cells were then stained with antibodies against ZO-1(A), Rab11(B) or CD13(C). A: Lifeact-GFP is stronger on the central structure, this structure is a lumen as confirmed by the ZO-1 staining on both sides. B: the intracellular mTomato vesicular clusters are positive for Rab11. C: The intracellular mTomato vesicular clusters are positive for CD13

We then wanted to minimize the laser exposure. To achieve this, we have decided to use the content aware image restoration (CARE) (Weigert et al., 2018) method. This method relies on machine learning to generate a neuronal network able to restore image resolution. After training, the network can improve the spatial resolution of low exposure images. We generated 100 pairs of images (same image taken at low exposure and high exposure) to train the network and applied the restoration on 25 control images. This corresponds to a first attempt at the method. A larger training set is required for optimal results. However, it appeared sufficient for a first attempt at a full experiment. With the laser intensity and exposure used for the low exposure set, under controlled CO2 and temperature conditions, we could image cells for up to 72h continuously with no cell death observed (data not shown). We therefore decided to proceed with the experiment under these conditions.

We used this pipeline to image cells 24h after plating. We could see several interesting events occurring. First, we could follow lumen formation (Figure 2.4-5). At the beginning of the image video, we could see a cluster of vesicles close to the cell border near a dense patch of actin, over time the cluster of vesicle disappears and is replaced by a clear lumen between the two considered cells.

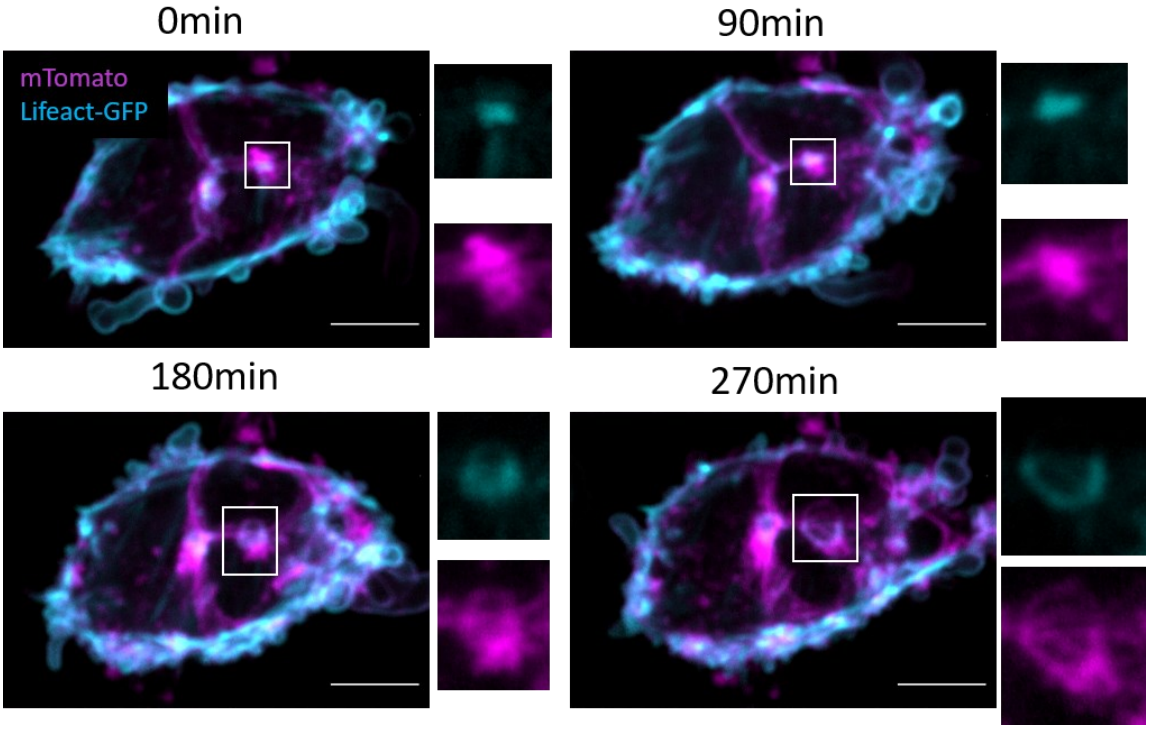

Figure 3.4-5: Live imaging of lumen formation and expansion

Cells were isolated from the liver of a double positive embryo and then plated for 24h before imaging. The time since the beginning of the recording is shown for each image. The magnified region is shown as a white square on the first overview overlaid image. Individual channels are magnified on the same region for each timepoint. Scale bars: 10 µm

Looking at another cell cluster we could see that ARE can move across the cytoplasm of a cell while remaining grouped as a cluster (Figure 2.4-6). In the first isolated frame, ARE are present on both polarizing cells next to the common cell-cell interface. In the second isolated frame, one of the clusters leaves the site while the other one remains. In the third frame both clusters are away from the initial site, one of them has reached another cell border, at the initial site a lumen is clearly formed.

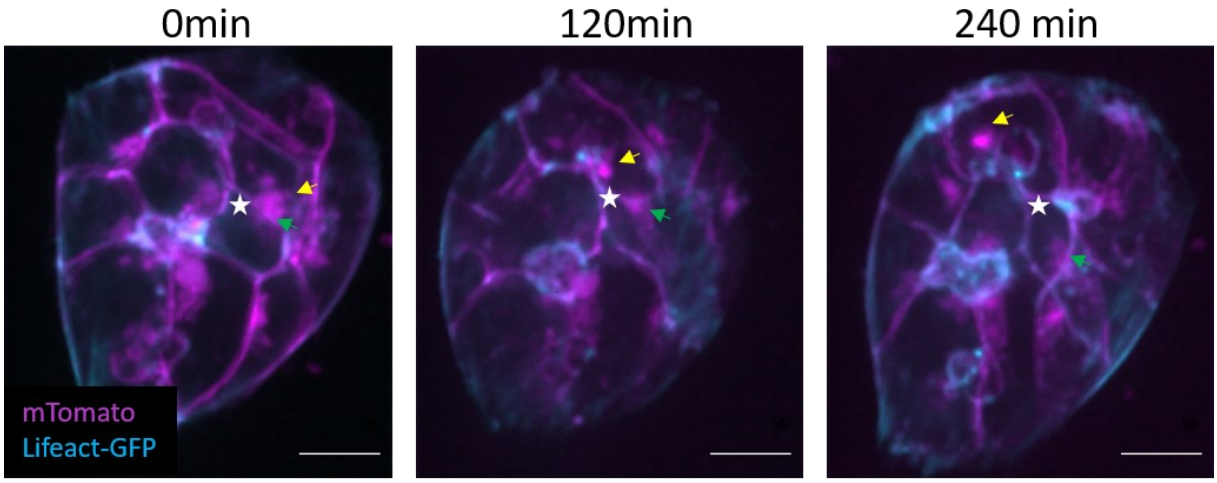

Figure 3.4-6: Live imaging of ARE movement

Cells were isolated from the liver of a double positive embryo and then plated for 24h before imaging. The time since the beginning of the recording is shown for each image. The polarization location is shown with a white star. Two ARE are shown with a yellow and a green arrow. Scale bars: 10 µm

Unfortunately, the experiment was interrupted before we could observe two consecutive polarization events, but we believe that we will be able to image the entire process soon. For the moment, this observation strongly supports our current view on the process of hepatoblast polarity formation.

Altogether the results presented so far led us to a model for hepatocyte polarity emergence and bile canaliculi network formation in the developing liver (Figure 2.4-7). We believe that initially hepatoblasts accumulate most of the apical components in a rab11 positive vesicle cluster: the ARE. Hepatoblasts then moves the ARE to the cell border in a cell autonomous manner. A single hepatoblast is capable of this independently of the cell type on the other side of the targeted cell border. The compartment is potentially active at this stage. It is currently unclear what defines the cluster location. Eventually two hepatoblasts position their cluster at the same location. At this point a tight junction is formed and the cells proceeds with the formation of a lumen. The ARE cluster is then moved away from the lumen. It is not clear at which point of the polarization process this occurs, but we could see that it may happen in early

steps of polarization. We could also see that it is not necessarily happening at the same time for the two cells sharing the nascent lumen. The ARE then reaches out for another cell border location and proceed with a second polarization event. After a second lumen formation the hepatoblast is multipolar, it then connects its multiple lumina by expanding them as tubes.

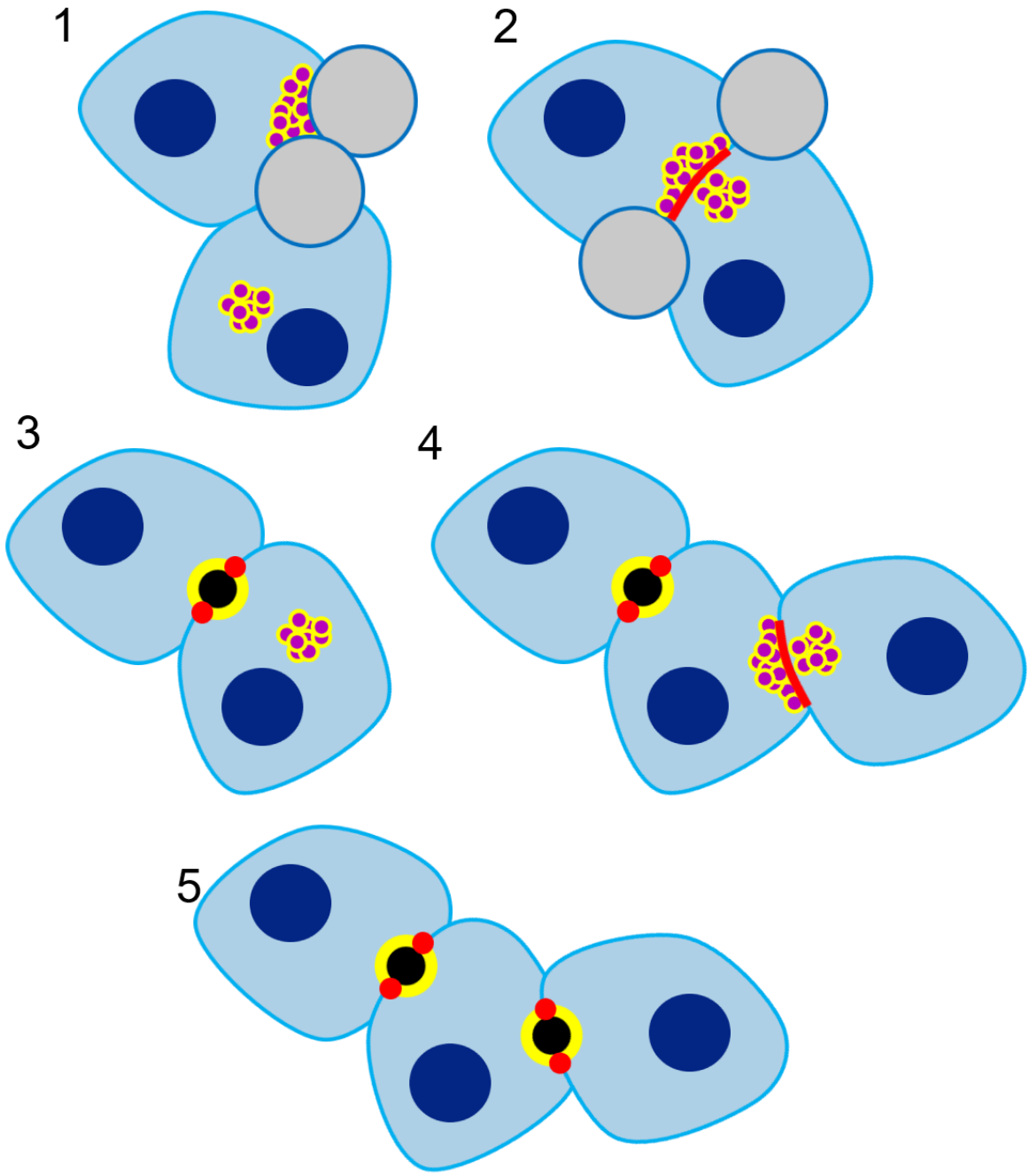

Figure 3.4-7: Proposed model

Schematic of a possible model for hepatocyte polarity formation and bile canaliculi network formation. The hepatoblasts are shown in blue (nuclei= dark blue, cytoplasm= light blue, Cell border= cyan). The erythropoietic progenitors are shown in grey. Apical surface is shown in yellow. Rab11 positive vesicles are shown in magenta. Tight junctions are shown in red.

Several steps in the process remain unclear. In order to achieve polarization two hepatoblasts need to position their ARE in a common location for the formation of a lumen. This cellular process is potentially a crucial point in the elaboration of the liver tissue architecture. A better understanding of this key step would bridge the gap between individual cell behaviour and tissue scale organization.

3.5 Polarized trafficking orientation cues

The mechanism leading to the positioning of the apical surface is still unclear and debated in most systems. The most fundamental property of polarity is asymmetry. Therefore, it is thought that the determination of apical surface location is guided by an asymmetric distribution of components. The relative importance of each factor is under debate, but cell division and ECM distribution appear to play a prominent role in lumen location determination in MDCK cells. We therefore looked first for cell division events and verify if our observation matches the model predictions. Then we looked at different basal markers in relation to apical marker distribution to see if a potential link could be found.

3.5.1 Cell division

First, we looked at the possibility that cell division could help direct polarization. As discussed in introduction, it has been proposed for hepatoblasts to play a key role in both positioning of the lumina and formation of the bile canaliculi network. Initially a lumen would be formed between daughter cells: a midbody would remain after cell division, leading to a spatial landmark for lumen formation (Wang et al., 2014). Then, asymmetric cell division would lead to multiple lumen generation: one daughter cell would inherit a pre-existing lumen and the new lumen would be formed between daughter cells. Finally, cells with multiple lumina would divide symmetrically, the cell division plane would cross all lumina and cytokinesis would bring them together (Tanimizu & Mitaka, 2017).

Looking at the proportion of hepatoblasts positives for a mitotic marker (phospho-Histone3) we found 3% (+/- 1,5) of hepatocytes in mitosis at E14 (data not shown). This result is compatible with the measure that, at E14, 25% of hepatoblasts are in proliferation (Yang et al., 2017). For each sample we found similar proportions of dividing hepatoblasts between center and border. In the adult liver, fluctuations of hepatocyte polyploidy have been corelated to the circadian rhythm (Wang et al., 2017). We therefore verified whether proliferation may depend

on the cell cycle. We collected embryos every 3h between E13 and E14, assessed the developmental progression based on Theiler stage characteristics (Theiler, 1989). Only one sample per timepoint was analysed but no striking variations could be found.

The connection between cell division and lumen formation has been proposed to be mediated by midbody deposition. We therefore looked for such a structure in the vicinity of the ARE. One of the characteristic features of the midbody is the presence of a microtubule bundle arising from the cell border. We could find such bundles in the developing liver (Figure 2.5-1) however the cells with a midbody were negative for CD13. Moreover, no midbody could be found where CD13 was located near the cell border. Overall, we could not find any correlation between midbody deposition and ARE positioning close to the cell border.

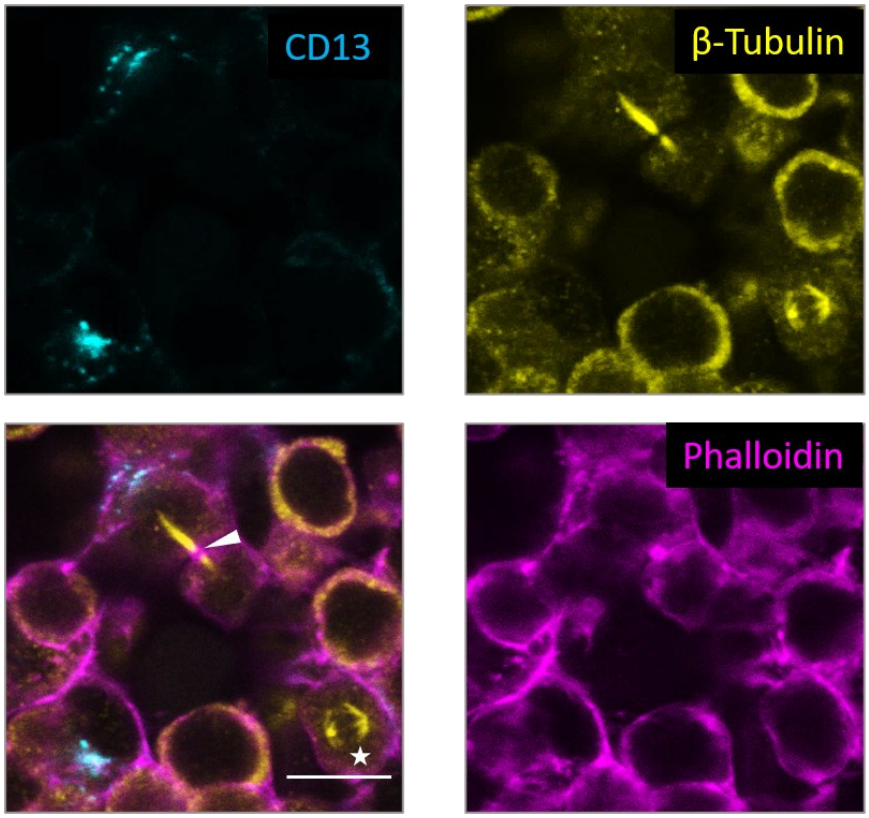

Figure 3.5-1: Midbody formation in vivo

Embryonic liver sections at E14. Sections were stained with phalloidin (Magenta) and antibodies directed against CD13 (Cyan) and β-Tubulin (Yellow). A mitotic spindle (white star) and a midbody (white arrowhead) are visible through their associated tubulin structures. Scale bar: 10µm

Cell division is also proposed to be involved in lumen connection in cells with multiple lumina. It is then expected that the plane of cell division would cross all lumina in order to connect them. However, regardless of the number of lumina, cell division appeared to be asymmetric. And it seemed to also be the case for cells with multiple lumina (Figure 2.5-2).

At this point the model expects the plane of cell division to cross both lumina, however in this example only one lumen is crossed by this plane. Our observations were not coherent with the cell division model of lumen and network formation, further observations and quantifications would be required to conclude on a role of cell division for the network formation.

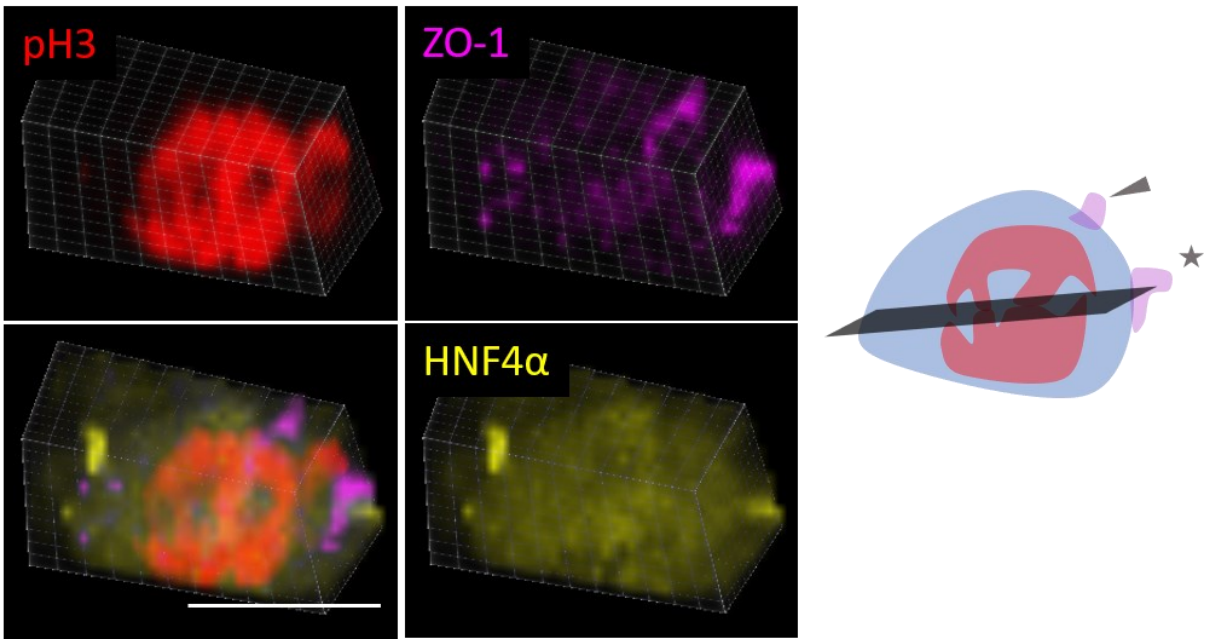

Figure 3.5-2: Asymmetric cell division in vivo

Embryonic liver sections at E14. Sections were stained with antibodies directed against HNF4α (Yellow), ZO-1 (Magenta) and phospho-Histone 3 (Red). The schematic underlies that the cell division plane (black) cross one of the lumina (star) but not the other (arrowhead). Scale bar: 10µm

3.5.2 Basal cues

Secondly, we looked at the distribution of basal markers with regards to apical markers. It has been shown in MDCK cells that integrins can sense the ECM and direct the apical surface formation away from it (Yu et al., 2005). It is therefore possible that some basal signal may push polarized trafficking of apical markers away. In the adult liver the basal surface of hepatocytes faces the sinusoids, around these blood vessels ECM components can be found

(mainly Fibronectin and Laminin). The ECM is thought to be secreted by stellate cells (marked by Desmin); these cells are also located close to blood vessels in the adult.

However, in the embryo, when lumina are formed at E14, the vasculature is scarce and still not fully formed (Figure 2.5-3 A). Fibronectin and Laminin are distributed all across the tissue (Figure 2.5-3 B,C) and so are stellate cells (Figure 2.5-3 D). The spatial separation of these components gave us the chance to look for an anti- correlation of apical marker distribution with each of these components individually.

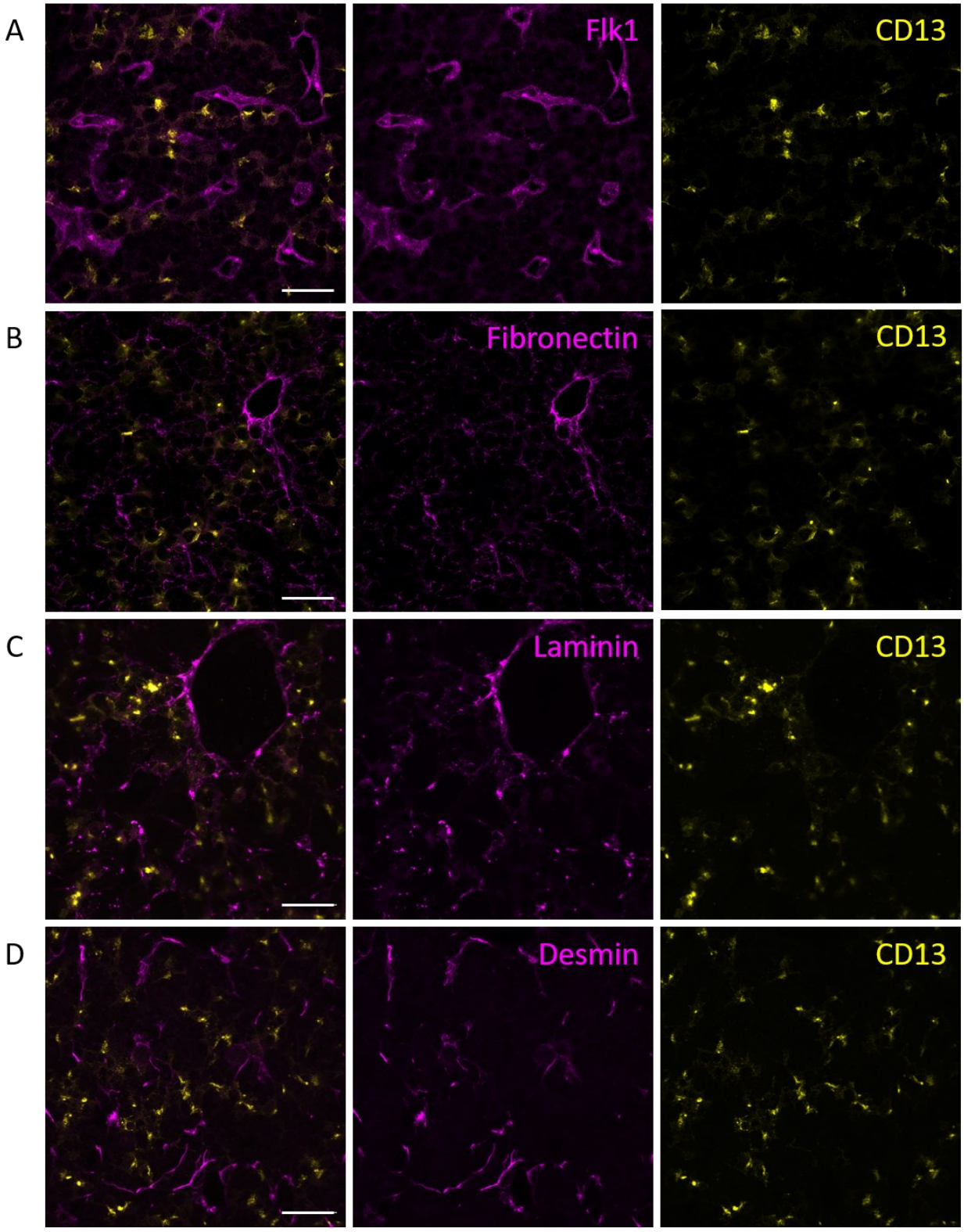

Figure 3.5-3: Basal markers in vivo

Maximum projections over 10µm of embryonic liver sections at E14. Sections were stained with CD13 (Yellow) and multiple basal markers (Magenta). Scale bars: 50µm

This was done by starting from each cluster of apical markers and measure the distance to the closest (d0) and the second closest (d1) basal marker cluster (Figure 2.5-4 A). If the apical marker is located in the middle of two basal marker clusters, then d0 = d1, if not we will measure d1>d0 (in the example Figure 2.5-4 B, green histogram: d1 = 2 x d0).

We measured these distances in simulated noisy images using motion tracking and obtained references histograms of these scenarios (Figure 2.5-4 B). We then measured these values on real data. Starting with the distance between CD13 clusters and Laminin clusters (Figure 2.5-4 C), however we could not obtain enough datapoints to observe a trend comparable to the simulated scenarios. With foetal liver kinase 1 (Flk1) (an endothelial cells specific surface receptor) (Figure 2.5-4 D) we could clearly see that the pic of the distribution occurs before 0,8 (d1/d0). Suggesting that in most cases the CD13 clusters are not located in the middle of two blood vessels.

For Desmin (staining stellate cells in the liver) (Figure 2.5-4 E) and for Fibronectin (Figure 2.5-4 F) it appeared that the maximum of the distribution is close to 1. Suggesting that in most cases the CD13 clusters are located in the middle of two stellate cells or two patches of fibronectin.

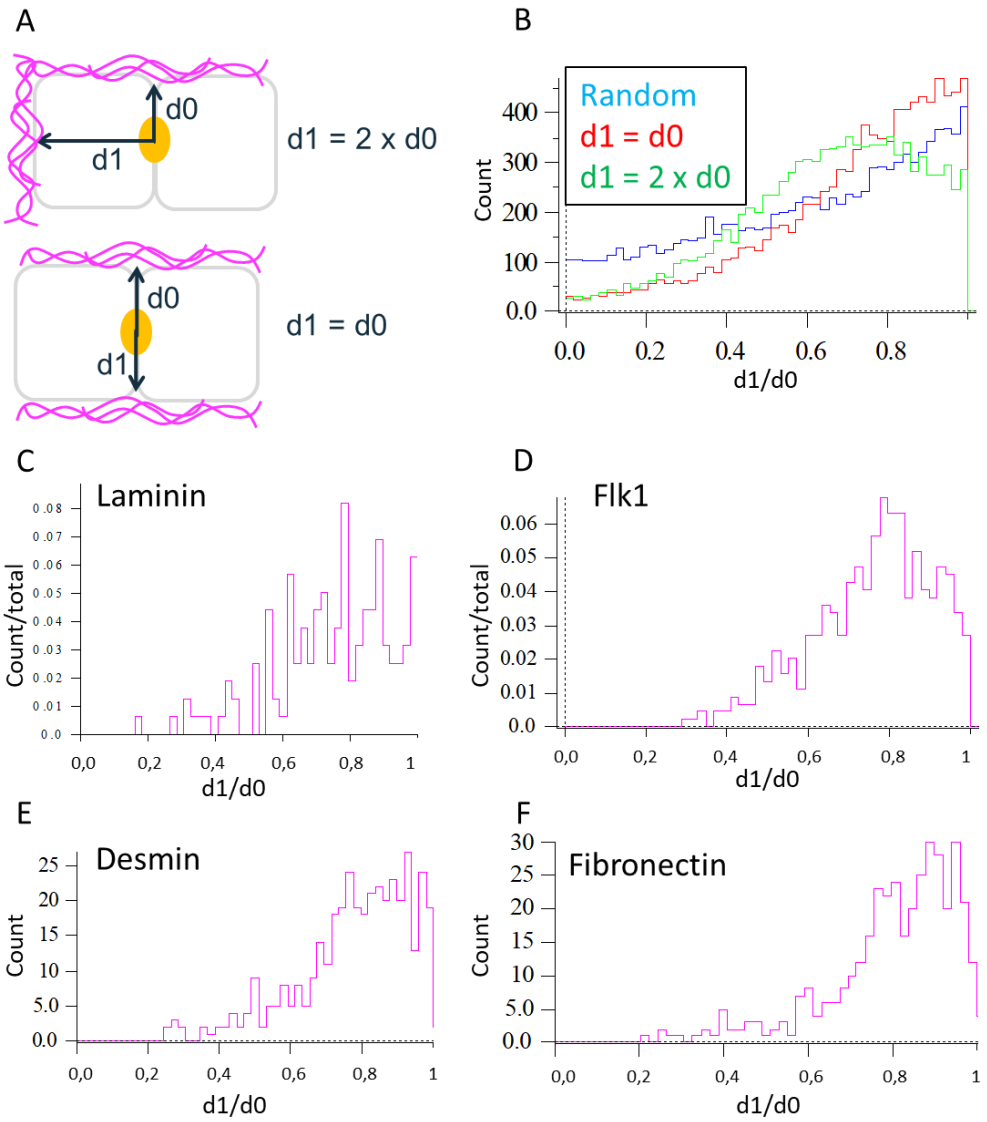

Figure 3.5-4: Relative spatial distribution of apical and basal markers in vivo

A: Schematic defining the distances between the apical surface (yellow) and the first (d0) or second (d1) basal surface (magenta). B: Distribution of the measurements obtained from simulated images when d1=d0 (red), d1=2 x d0 (green) or when no constrain was put (blue). The x axis corresponds to the ratio d1/d0 and the Y axis is either the number of measurements or the number of measurements over the total number of measurements. C-F: Same as B but using real images and measuring the distance between CD13 and Laminin (C), Flk1 (D), Desmin (E) or Fibronectin (F).

These measurements must be repeated in order to be conclusive. Nonetheless, based on these observations, it appears that the localization of apical marker may rather be connected to ECM distribution rather than cell division. Whether if the same trend can be observed for lumen connection remains to be determined.

4 Discussion

4.1 Discrepancies between the hilum and the periphery of the organ.

In our study the first observation was an apparent delay in polarization at the periphery compared to the proximal part of the organ; close to the hilum. This phenomenon was clearly visible in all samples. Several processes could cause such a delay. One would be that the proliferation could occur radially and the post mitotic, polarizing cells, would therefore be in the proximal part and the proliferating cells in the distal regions. However, when we looked for mitotic cells, we could not find strong differences in proliferation across the tissue. This explanation is therefore unlikely.

On the other hand, different factors coming from the maternal blood could enhance polarization. If these factors are quickly taken up a gradient could form across the organ along the vasculature. If this hypothesis is correct, we would expect that the gradient of polarization follows the vasculature and is not just along the proximal to distal axis. In our study we only used 100µm thick section in order to capture several cell layers and follow the network formation at the tissue scale. To capture a gradient along the vasculature we would need to image the complete vasculature and the surrounding tissue with sufficient resolution in order to follow small lumen formation.

Alternatively a factor could be accumulated in the blood but be produced by the embryo. Taurocholate is only excreted by the placenta at early stages of development and not at late stages (Iioka et al., 1993) it is also known to stimulate polarization of hepatoblasts (Fu et al., 2011). Furthermore, the efficacy of transporters in the placenta could be modulated based on maternal physiology. An accumulation of taurocholate in the maternal blood would reduce the export from the embryo. It is therefore possible that the bile acid mix present in the maternal blood modulates the development of the hepatoblasts according to the external nutritional environment. This could occur at least up to the point where the bile canaliculi network is formed.

4.2 Bile canaliculi network formation

We found that the bile canaliculi network was formed around E16. At this timepoint it appeared that the differences across the tissue were reduced compared to earlier timepoints. It seemed that at some point the lumen density was such that all the individual lumina collapse

into a network. It would be interesting to look at the problem from the perspective of available space by looking at cell surfaces. We could determine this way a threshold for the establishment of the bile canaliculi network. This could lay ground to further studies on the network remodelling towards the adult architecture through a better understanding of the initial conditions.

At the onset of network formation, we could also observe a potential mechanism for directed lumen fusion. In some cases, we could find ZO-1 bridges connecting distinct lumina. This seemed to occur between lumina formed by one cell and its neighbours. This observation not only supports the idea that multiple lumina would be connected to achieve the hepatocyte polarity but also provides with a potential mechanism for this process. However, for the moment, we do not have more supportive evidence. And we were unable to observe this phenomenon *in vitro*.

Interestingly this very phenomenon was expected and specifically looked for in the process of gut development in zebrafish (Alvers et al., 2014). The authors have found that, in this context, basolateral adhesion complexes separate lumina. It would be interesting to look for a similar phenomenon in a closer system such as the pancreatic duct network formation. It would be surprising that this process is hepatocyte specific as for the rest of the bile canaliculi network establishment we have been able to identify key steps that are conserved in other systems.

4.3 Early polarization steps: trafficking

As described in MDCK cells (Bryant et al., 2010) it seems that hepatoblasts initially direct at least some apical surface components to their surface in absence of polarity. We could find CD13 located at the cell surface at E11,5. We could observe this distribution in some samples but not in all of them. At this stage we cannot section the organ as we do for other samples. It is therefore possible that this inconsistency in the results is due to incomplete penetration of the antibodies in the organ. It could also be a very transient step when CD13 starts to be expressed.

In MDCK cells the Podocalyxin protein is showing this pattern. We tried to detect this protein in our samples and the staining appear to work on the gut and on hepatoblasts *in vitro*. Unfortunately, we could not detect this protein in hepatoblasts *in vivo*. So far only CD13 has shown this pattern in the tissue. This could be because CD13 is trafficked through transcytosis and is therefore expected to be, at least transiently, present on the basal side. It would therefore be interesting to look for the distribution of a protein directly targeted to the apical side, such as MRP2, at this stage.

Right after we found CD13 to be relocated to a rab11 vesicle cluster located in the perinuclear region. It is at this point that the apical recycling endosome (ARE) become clearly identifiable. Visually it seemed that there were only one ARE per cell. We were not able to segment individual cells along with ARE clusters so we could verify this. However, the density of hepatoblasts (estimated when we looked for dividing hepatoblasts) seem to match the pic density of ARE. Therefore, we are not expecting multiple ARE per hepatoblasts to be common. On the other hand, upon suggesting that ARE could be involved in multiple polarization event we looked for possible structure that could attract the ARE to the cell border.

ZO-1 appeared to be a good candidate. It seemed to be involved in a closely related process in MDCK cells (Mangan et al., 2016). However, it appeared quickly that the ARE was reaching the cell border in absence of ZO-1 *in vivo*. Interestingly this was not the case with primary hepatoblasts *in vitro* when they group as duplets. It tends to occur right after plating, most likely following a cell division. Once polarized or in larger groups however, hepatoblasts *in vitro* displace their ARE towards cell borders in absence of ZO-1. This allowed us to start assessing the activity of this compartment.

We only performed a preliminary experiment to assess the possibility that CD13 would be concentrated in this compartment. We found that after a pulse of labelled antibody directed against CD13, the fluorescent intensity seemed to transiently increase at the ARE but also at the hepatoblasts cell-cell interface whereas it decreased at the cell-ECM interface. This could suggest that the recycling process of apical components is already asymmetric at this stage. These results are preliminary, and the experiment needs to be repeated. We would need to perform a fluorescence recovery after photobleaching (FRAP) experiment and compare the recovery time in these 3 locations in order to really validate this hypothesis. This potential asymmetry in the recycling could be mediated or at least be visible through the positioning of the ARE towards a specific border, away from the perinuclear region.

Interestingly we found that, *in vivo,* the ARE could be directed toward Ter119 positive erythropoietic progenitors. We could also observe ARE directed towards other non-hepatoblasts cells lacking this marker, we were not able to identify these other cells. It would be interesting to see whether an asymmetric recycling could be found in this context as well. If the positioning of the ARE is done in response to the ECM this may lead to an asymmetric trafficking not towards other hepatoblasts but simply as far as possible from the ECM. It would then occur toward any obstacle that is not covered in ECM. We have tried to achieve this organization *in vitro* through co-seeding primary hepatoblasts with erythrocytes or with silica beads. So far, we could not get hepatoblasts in contact with these obstacles.

4.4 Early polarization steps: junctions

We found that at epithelial cadherin (E-cadherin) was specifically located at the interface between hepatocytes. It appeared that a primitive lateral side could be organized early in the polarization process. Interestingly E-Cadherin puncta could be seen below these interfaces. This could correspond to a lateral recycling or targeting. We know that these puncta are not rab11 positive, but it could be interesting to see if these puncta correspond to rab4 positive vesicles.

E-Cadherin turnover has been shown to be linked to mechanical constrained on the tissue. *In vitro* hepatoblasts take a circular shape but *in vivo* these cells appear to be deformed by the other cells in the tissue. It is therefore possible that hepatoblasts *in vivo* are under a lot of mechanical stress and this may impact the E-cadherin organization. Moreover, it has been shown in other systems that mechanical stress sensed by E-cadherin is involved in tight junction positioning (Rübsam et al., 2017). It would be interesting to see if the crowded environment of the embryonic liver tissue influences the maturation of junctions.

The impact of mechanical stress is likely to be limited, junction do form and mature *in vitro* in absence of tissue crowding. In this context it appeared that ZO-1 is required to achieve hepatocyte polarity. In the ZO-1 KD cells we could still find occludin staining resembling junction plates in between cells. It remains to be determined whether if these structures correspond to a tight junction. In these cells the ARE could reach the cell border but it appeared that the presence of the ARE to the cell border and the formation of junction like structure was not sufficient to form a lumen. We believe that ZO-1 is filling this gap, either by co-ordinating the trafficking at the junction location. ZO-1 could, for instance, help anchor the centrosome to this location. Or by directly or indirectly regulating trafficking at the junction site. By either preventing apical surface components removal or by enhancing delivery at this location.

It has been proposed in other systems that ZO-1 through cingulin recruitment is involved in Rab11 vesicle targeting at the lumen initiation site (Mangan et al., 2016). In our system it appears that the ARE is directed towards the border and that vesicles could be delivered to the cell-cell interface in absence of ZO-1. However, a similar mechanism could enhance the delivery of vesicles locally to form a lumen when junctions are formed. This would be important in order to initiate lumen formation.

4.5 Multipolar polarity establishment

Looking at lumen growth we could find that they seem to grow as tubes. At this point we made the assumption that lumina tend to grow. When we looked at this process *in vitro*, we observed that lumina shape is extremely dynamic. We could observe lumina splitting, fusing, growing, and shrinking. The overall trend leading to larger and larger lumina is therefore likely to be a general tendency at the population level for lumen to grow rather than a rule for every individual lumen to grow.

To achieve multipolar polarity, we also found that hepatoblasts polarize multiple times. Upon looking for hepatoblasts with multiple lumina we only found cells with two lumina. We were not able to find hepatoblasts with 3 or more lumina. This raises the question of whether if this is a limitation from the polarization system or if this can occur under rare circumstances. It could be that there is usually not enough space for hepatoblasts to polarize 3 times or that the cell exhausts its capacity after two rounds of polarization. Yet the capacity to move the ARE offers cells the capacity to polarize more than once.

The ARE appeared to always be formed around the centrosome. This may lead us to a potential mechanism for ARE movement. In the context of primary cilia formation, the centrosome has been shown to move, pushed away from the ECM where microtubules are stabilized (Pitaval et al., 2017). A very similar process could occur in our system.

4.6 ARE positioning

We were not able to connect cell division to the positioning of the ARE *in vivo*. However, the angle of cell division is probably important regarding the establishment of others features of the organ. For instance, we have not looked at the lobular organization, the angle of cell division could make sense at the tissue level in the establishment of the lobule. Some ECM components are differentially distributed along the metabolic axis, it is possible that the angle of cell division is influenced by some ECM components, as it has been shown in MDCK cells (Lázaro-Diéguez et Müsch, 2017).

We could find correlation between the ECM distribution and the CD13 distribution at the tissue scale. In this analysis we looked at the complete CD13 staining, in both lumina and ARE. This observation needs to be refined to make the distinction between both, but we expect to find the same result with both structures. If this is confirmed it would suggest that the ARE is positioned as far away as possible from the ECM. It would be interesting to complete this

correlation by interfering with the ability of cells to sense Fibronectin. We could knock down Integrin in these cells and see if the ARE movement to the cell border is impaired.

4.7 Conclusion / Outlook

We have identified the timeline of events from hepatoblasts polarity initiation to bile canaliculi network formation. We found that the hepatocyte polarity is achieved by the combination of oriented lumen growth as tubes and multiple lumen formation. The lumina then fuse, potentially via the formation of junctional bridges between lumina, to form a network.

The generation of multiple lumina seems to be allowed by the capacity of hepatoblasts to move their ARE after the formation of a lumen. This movement is possibly guided by the ECM and driven by microtubules dynamics. We found that the ARE of hepatoblasts seem to be actively recycling in absence of tight junctions. And finally, that ZO-1 is required in order to locally increase apical surface components during lumen formation.

The aim of this study is to contribute to a basic understanding in the different processes involved in the formation of a functional bile canaliculi network during development. We hope that this could serve as a reference for the study of any kind of liver developmental disorder and for the development of in vitro model systems.

5 Summary

Background: The liver occupies a central function in homeostasis maintenance. Its functions depend on a fine architecture allowing each parenchymal cell, the hepatocytes, to contact both the vasculature and to contribute to the formation of the bile canaliculi network. To separate two compartment, epithelial cells like hepatocytes must develop a specific organization: polarity. In the liver, the bile canaliculi network and vasculature are organized as two tightly intertwined networks. To achieve contact with both, the hepatocytes must acquire a complex polarity composed of multiple axes.

The study of this organization is the focus of intense research. A lot of attention is put on the understanding of the established structure in the adult organ and the regeneration of this structure in case of injury. With a progressing understanding of this organization comes the interrogation on how it is established during development. Furthermore, a proper understanding of the establishment process is central to develop reliable in vitro systems or organ-on-a-chip approaches.

Questions:

In this context we have decided to address the following questions:

- *When and how is multipolar polarity established.*

- *Can this establishment be correlated to any extracellular cue in vivo.*

Methods: To address these questions we have fixed, stained, imaged, and reconstructed large volumes of embryonic liver tissue at several consecutive stages of development. We looked at polarized trafficking and junctional markers to follow polarity establishment. We looked at ECM and cell division markers to correlate cues susceptible to guide polarization. We also performed in vitro experiments to further explore the hypotheses formulated along the way based on in vivo observations.

Conclusion: This study led us to conclude that multipolar polarity arises from both lumen tubular elongation and multiple lumen formation. The formation of multiple lumina involves the movement of a Rab11 vesicular cluster and independent junctional plate formation. Our study suggests that ZO-1 could be involved in the synchronization between vesicular cluster movement and junction plate formation. Finally, we could not link cell division to polarization, however, we could correlate fibronectin distribution to potential early polarization events.

6 Zusammenfassung

Einleitung: Die Leber hat eine zentrale Rolle im Stoffwechsel inne. Ihre Funktionen sind von ihrem Feinaufbau abhängig, bei dem jede einzelne Leberzelle, auch Hepatozyt genannt, Kontakt zu Blutgefäßen hat, aber gleichzeitig auch zu der Ausbildung von Gallenkanälchen beiträgt. Um diese zwei Bereich getrennt zu halten müssen Epithelzellen, wie die Hepatozyten, eine spezifische Organisation entwickeln: Die Polarität. In der Leber sind das Gallenkanälchensystem und die Blutgefäße als zwei eng miteinander verschlungene Netzwerke organisiert. Um Kontakt mit beiden Systemen sicherzustellen, müssen Hepatozyten eine komplexe Polarität mit mehreren Axen annehmen.

Die Untersuchung dieser Organisation ist der Fokus von intensiver Forschung. Dabei wird viel Aufmerksamkeit auf das Verständnis der bestehenden Strukturen im ausgewachsenen Organ, sowie auf die Regenerierung dieser Strukturen im Falle einer Verletzung gelegt. Mit dem fortschreitendem Verständnis der grundlegenden Organisation kommt ein Interesse an der Aufklärung wie diese während der embryonalen Entwicklung entstehen. Des Weiteren ist ein detailliertes Verständnis der Entstehungsprozesse zentral für die Entwicklung von zuverlässigen in vitro Systemen und organ-on-a-chip Techniken.

Fragestellung:

In diesem Zusammenhang, haben wir entschieden uns den folgenden Fragestellungen zu widmen:

- Wann und wie etabliert sich multipolare Polarität
- Kann diese Entstehung in vivo zu einem extrazellulärem Signal korreliert werden

Methoden: Um diesen Fragen nachzugehen, haben wir große Volumina von embryonalen Lebergewebe während mehreren aufeinanderfolgenden Entwicklungsstadien fixiert, angefärbt, abgebildet und rekonstruiert. Dabei haben wir den polarisierten Vesikeltransport und verschiedene Zellkontaktproteine untersucht, um der Polaritätsentwicklung zu folgen. Des Weiteren haben wir die extrazelluläre Matrix, sowie als auch Kennzeichen für Zellteilung untersucht, um Signale zu korrelieren, die die Entstehung der Polarität leiten könnten. Es wurden auch in vitro Experimente durchgeführt, um die Hypothesen, die auf Grund der Beobachtungen in vivo formuliert werden konnten, im Detail zu erkunden.

Schlussfolgerung: Diese Studien haben uns zu der Erkenntnis geführt, dass multipolare Polarität auf Basis von der Verlängerung von röhrenförmigen Lumina, sowie also auch in Abhängigkeit von der Bildung von mehreren Lumina entsteht. Die Entstehung von mehreren Lumina schließt den Transport eines Clusters an Rab11 Vesikeln und eine davon unabhängige Bildung einer Scheibe von junktionalen Proteinen ein. Letztendlich konnten wir keine Verbindung zwischen Zellteilung und Polarisierung herstellen, wir konnten jedoch die Verteilung von Fibronektin mit potenziellen zeitigen Ereignissen der Polarisierung korrelieren.

7 References

Alvers AL, Ryan S, Scherz PJ, Huisken J, Bagnat M. 2014. Single continuous lumen formation in the zebrafish gut is mediated by smoothened-dependent tissue remodeling. Development, 141(5):1110–1119 DOI: 10.1242/dev.100313.

Antoniou A, Raynaud P, Cordi S, Zong Y, Tronche F, Stanger B, Jacquemin P, Pierreux CE, Clotman F, Lemaigre FP. 2009. Intrahepatic bile ducts develop according to a new mode of tubulogenesis regulated by the transcription factor SOX9. Gastroenterology, 136(7):2325–2333 DOI: 10.1053/j.gastro.2009.02.051.

Asahina K, Tsai SY, Li P, Ishii M, Maxson RE, Sucov HM, Tsukamoto H. 2009. Mesenchymal origin of hepatic stellate cells, submesothelial cells, and perivascular mesenchymal cells during mouse liver development. Hepatol Baltim Md, 49(3):998–1011 DOI: 10.1002/hep.22721.

Banerjee S, Sousa AD, Bhat MA. 2006. Organization and function of septate junctions. Cell Biochem Biophys, 46(1):65-77 DOI: 10.1385/CBB:46:1:65.

Barr VA, Scott LJ, Hubbard AL. 1995. Immunoadsorption of Hepatic Vesicles Carrying Newly Synthesized Dipeptidyl Peptidase IV and Polymeric IgA Receptor. J Biol Chem, 270(46):27834-27844 DOI: 10.1074/jbc.270.46.27834.

Bedossa P. 1993. The cellular origin of extracellular matrix constituents. J Hepatol, 19(1):1-3 DOI: 10.1016/S0168-8278(05)80168-0.

Bhunchet E, Wake K. 1998. The portal lobule in rat liver fibrosis: a re-evaluation of the liver unit. Hepatol Baltim Md, 27(2):481-487 DOI: 10.1002/hep.510270223.

Bort R, Signore M, Tremblay K, Barbera JPM, Zaret KS. 2006. Hex homeobox gene controls the transition of the endoderm to a pseudostratified, cell emergent epithelium for liver bud development. Dev Biol, 290(1):44-56 DOI: 10.1016/j.ydbio.2005.11.006.

Bryant DM, Datta A, Rodríguez-Fraticelli AE, Peränen J, Martín-Belmonte F, Mostov KE. 2010. A molecular network for de novo generation of the apical surface and lumen. Nat Cell Biol, 12(11):1035–1045 DOI: 10.1038/ncb2106.

Cohen D, Tian Y, Müsch A. 2007. Par1b Promotes Hepatic-type Lumen Polarity in Madin Darby Canine Kidney Cells via Myosin II- and E-Cadherin–dependent Signaling. Mol Biol Cell, 18(6):2203-2215 DOI: 10.1091/mbc.E07-02-0095.

Douarin par NL. 1964. Induction de l'endoderme pré-hépatique par le mésoderme de l'aire cardiaque chez l'embryon de poulet. Development, 12(4):651-664.

Ebnet K, Suzuki A, Horikoshi Y, Hirose T, Meyer zu Brickwedde M-K, Ohno S, Vestweber D. 2001. The cell polarity protein ASIP/PAR-3 directly associates with junctional adhesion molecule (JAM). EMBO J, 20(14):3738-3748 DOI: 10.1093/emboj/20.14.3738.

Elias H. 1949. A re-examination of the structure of the mammalian liver; the hepatic lobule and its relation to the vascular and biliary systems. Am J Anat, 85(3):379-456, 15 pl DOI: 10.1002/aja.1000850303.

Farzan VM, Ulashchik EA, Martynenko-Makaev YV, Kvach MV, Aparin IO, Brylev VA, Prikazchikova TA, Maklakova SY, Majouga AG, Ustinov AV, Shipulin GA, Shmanai VV, Korshun VA, Zatsepin TS. 2017. Automated Solid-Phase Click Synthesis of Oligonucleotide Conjugates: From Small Molecules to Diverse N-Acetylgalactosamine Clusters. Bioconjug Chem, 28(10):2599-2607 DOI: 10.1021/acs.bioconjchem.7b00462.

Feracci H, Connolly TP, Margolis RN, Hubbard AL. 1987. The establishment of hepatocyte cell surface polarity during fetal liver development. Dev Biol, 123(1):73–84.

Ferrari A, Veligodskiy A, Berge U, Lucas MS, Kroschewski R. 2008. ROCK-mediated contractility, tight junctions and channels contribute to the conversion of a preapical patch into apical surface during isochoric lumen initiation. J Cell Sci, 121(21):3649–3663 DOI: 10.1242/jcs.018648.

Fu D, Wakabayashi Y, Lippincott-Schwartz J, Arias IM. 2011. Bile acid stimulates hepatocyte polarization through a cAMP-Epac-MEK-LKB1-AMPK pathway. Proc Natl Acad Sci, 108(4):1403–1408 DOI: 10.1073/pnas.1018376108.

Garcia MA, Nelson WJ, Chavez N. 2018. Cell-Cell Junctions Organize Structural and Signaling Networks To Regulate Epithelial Tissue Homeostasis. Cold Spring Harb Perspect Biol, 10(4) DOI: 10.1101/cshperspect.a029181.

Gissen P, Arias IM. 2015. Structural and functional hepatocyte polarity and liver disease. J Hepatol, 63(4):1023-1037 DOI: 10.1016/j.jhep.2015.06.015.

Hamazaki Y, Itoh M, Sasaki H, Furuse M, Tsukita S. 2002. Multi-PDZ Domain Protein 1 (MUPP1) Is Concentrated at Tight Junctions through Its Possible Interaction with Claudin-1 and Junctional Adhesion Molecule. J Biol Chem, 277(1):455-461 DOI: 10.1074/jbc.M109005200.

Haruna Y, Saito K, Spaulding S, Nalesnik MA, Gerber MA. 1996. Identification of bipotential progenitor cells in human liver development. Hepatol Baltim Md, 23(3):476–481 DOI: 10.1002/hep.510230312.

Ihrke G, Martin GV, Shanks MR, Schrader M, Schroer TA, Hubbard AL. 1998. Apical Plasma Membrane Proteins and Endolyn-78 Travel through a Subapical Compartment in Polarized WIF-B Hepatocytes. J Cell Biol, 141(1):115-133.

Iioka H, Hisanaga H, Akada S, Shimamoto T, Yamada Y, Sakamoto Y, Moriyama IS, Ichijo M. 1993. Characterization of human placental activity for transport of taurocholate, using brush border (Microvillous) Membrane vesicles. Placenta, 14(1):93-102 DOI: 10.1016/S0143-4004(05)80252-8.

Isern J, Fraser ST, He Z, Baron MH. 2008. The fetal liver is a niche for maturation of primitive erythroid cells. Proc Natl Acad Sci U S A, 105(18):6662-6667 DOI: 10.1073/pnas.0802032105.

Jung J, Zheng M, Goldfarb M, Zaret KS. 1999. Initiation of Mammalian Liver Development from Endoderm by Fibroblast Growth Factors. Science, 284(5422):1998–2003 DOI: 10.1126/science.284.5422.1998.

Kamiya A, Kinoshita T, Ito Y, Matsui T, Morikawa Y, Senba E, Nakashima K, Taga T, Yoshida K, Kishimoto T, Miyajima A. 1999. Fetal liver development requires a

paracrine action of oncostatin M through the gp130 signal transducer. EMBO J, 18(8):2127–2136 DOI: 10.1093/emboj/18.8.2127.

Kaylan KB, Ermilova V, Yada RC, Underhill GH. 2016. Combinatorial microenvironmental regulation of liver progenitor differentiation by Notch ligands, TGFβ, and extracellular matrix. Sci Rep, 6:23490 DOI: 10.1038/srep23490.

Ke M-T, Fujimoto S, Imai T. 2013. SeeDB: a simple and morphology-preserving optical clearing agent for neuronal circuit reconstruction. Nat Neurosci, 16(8):1154–1161 DOI: 10.1038/nn.3447.

Kojima T, Kokai Y, Chiba H, Osanai M, Kuwahara K, Mori M, Mochizuki Y, Sawada N. 2001. Occludin and claudin-1 concentrate in the midbody of immortalized mouse hepatocytes during cell division. J Histochem Cytochem, 49(3):333–339.

Kordes C, Sawitza I, Götze S, Häussinger D. 2013. Hepatic stellate cells support hematopoiesis and are liver-resident mesenchymal stem cells. Cell Physiol Biochem Int J Exp Cell Physiol Biochem Pharmacol, 31(2-3):290-304 DOI: 10.1159/000343368.

Kruepunga N, Hakvoort TBM, Hikspoors JPJM, Köhler SE, Lamers WH. 2019. Anatomy of rodent and human livers: What are the differences? Biochim Biophys Acta BBA - Mol Basis Dis, 1865(5):869-878 DOI: 10.1016/j.bbadis.2018.05.019.

Kubota H, Yao H, Reid LM. 2007. Identification and characterization of vitamin A-storing cells in fetal liver: implications for functional importance of hepatic stellate cells in liver development and hematopoiesis. Stem Cells Dayt Ohio, 25(9):2339-2349 DOI: 10.1634/stemcells.2006-0316.

Lázaro-Diéguez F, Müsch A. 2017. Cell-cell adhesion accounts for the different orientation of columnar and hepatocytic cell divisions. J Cell Biol, 216(11):3847–3859 DOI: 10.1083/jcb.201608065.

Lee PJ, Hung PJ, Lee LP. 2007. An artificial liver sinusoid with a microfluidic endothelial-like barrier for primary hepatocyte culture. Biotechnol Bioeng, 97(5):1340–1346 DOI: 10.1002/bit.21360.

Legland D, Arganda-Carreras I, Andrey P. 2016. MorphoLibJ: integrated library and plugins for mathematical morphology with ImageJ. Bioinformatics, 32(22):3532-3534 DOI: 10.1093/bioinformatics/btw413.

Li D, Friedman S. 1999. Liver fibrogenesis and the role of hepatic stellate cells: New insights and prospects for therapy. J Gastroenterol Hepatol, 14(7):618-633 DOI: 10.1046/j.1440-1746.1999.01928.x.

Luzzatto AC. 1981. Hepatocyte differentiation during early fetal development in the rat. Cell Tissue Res, 215(1):133–142 DOI: 10.1007/BF00236254.

Maiers JL, Peng X, Fanning AS, DeMali KA. 2013. ZO-1 recruitment to α-catenin--a novel mechanism for coupling the assembly of tight junctions to adherens junctions. J Cell Sci, 126(Pt 17):3904-3915 DOI: 10.1242/jcs.126565.

Mangan AJ, Sietsema DV, Li D, Moore JK, Citi S, Prekeris R. 2016. Cingulin and actin mediate midbody-dependent apical lumen formation during polarization of epithelial cells. Nat Commun, 7 DOI: 10.1038/ncomms12426.

Marchesini G, Petta S, Dalle Grave R. 2016. Diet, weight loss, and liver health in nonalcoholic fatty liver disease: Pathophysiology, evidence, and practice. Hepatol Baltim Md, 63(6):2032-2043 DOI: 10.1002/hep.28392.

Margagliotti S, Clotman F, Pierreux CE, Beaudry J-B, Jacquemin P, Rousseau GG, Lemaigre FP. 2007. The Onecut transcription factors HNF-6/OC-1 and OC-2 regulate early liver expansion by controlling hepatoblast migration. Dev Biol, 311(2):579-589 DOI: 10.1016/j.ydbio.2007.09.013.

Margagliotti S, Clotman F, Pierreux CE, Lemoine P, Rousseau GG, Henriet P, Lemaigre FP. 2008. Role of metalloproteinases at the onset of liver development. Dev Growth Differ, 50(5):331-338 DOI: 10.1111/j.1440-169X.2008.01031.x.

Matsumoto K, Yoshitomi H, Rossant J, Zaret KS. 2001. Liver Organogenesis Promoted by Endothelial Cells Prior to Vascular Function. Science, 294(5542):559–563 DOI: 10.1126/science.1063889.

van Meer G, Simons K. 1986. The function of tight junctions in maintaining differences in lipid composition between the apical and the basolateral cell surface domains of MDCK cells. EMBO J, 5(7):1455-1464.

Meyer K, Ostrenko O, Bourantas G, Morales-Navarrete H, Porat-Shliom N, Segovia-Miranda F, Nonaka H, Ghaemi A, Verbavatz J-M, Brusch L, Sbalzarini I, Kalaidzidis Y, Weigert R, Zerial M. 2017. A Predictive 3D Multi-Scale Model of Biliary Fluid Dynamics in the Liver Lobule. Cell Syst, 4(3):277–290.e9 DOI: 10.1016/j.cels.2017.02.008.

Monahan-Earley R, Dvorak AM, Aird WC. 2013. Evolutionary origins of the blood vascular system and endothelium. J Thromb Haemost, 11(s1):46-66 DOI: 10.1111/jth.12253.

Morales-Navarrete H, Nonaka H, Scholich A, Segovia-Miranda F, de Back W, Meyer K, Bogorad RL, Koteliansky V, Brusch L, Kalaidzidis Y, Jülicher F, Friedrich BM, Zerial M. 2019. Liquid-crystal organization of liver tissue. eLife, 8 DOI: 10.7554/eLife.44860.

Morales-Navarrete H, Segovia-Miranda F, Klukowski P, Meyer K, Nonaka H, Marsico G, Chernykh M, Kalaidzidis A, Zerial M, Kalaidzidis Y. 2015. A versatile pipeline for the multi-scale digital reconstruction and quantitative analysis of 3D tissue architecture. eLife, 4 DOI: 10.7554/eLife.11214.

Muzumdar MD, Tasic B, Miyamichi K, Li L, Luo L. 2007. A global double-fluorescent Cre reporter mouse. genesis, 45(9):593-605 DOI: 10.1002/dvg.20335.

Nagai H, Terada K, Watanabe G, Ueno Y, Aiba N, Shibuya T, Kawagoe M, Kameda T, Sato M, Senoo H, Sugiyama T. 2002. Differentiation of liver epithelial (stem-like) cells into hepatocytes induced by coculture with hepatic stellate cells. Biochem Biophys Res Commun, 293(5):1420-1425 DOI: 10.1016/S0006-291X(02)00406-0.

Pitaval A, Senger F, Letort G, Gidrol X, Guyon L, Sillibourne J, Théry M. 2017. Microtubule stabilization drives 3D centrosome migration to initiate primary ciliogenesis. J Cell Biol, 216(11):3713-3728 DOI: 10.1083/jcb.201610039.

Rappaport AM, Borowy ZJ, Lougheed WM, Lotto WN. 1954. Subdivision of hexagonal liver lobules into a structural and functional unit; role in hepatic physiology and pathology. Anat Rec, 119(1):11-33 DOI: 10.1002/ar.1091190103.

Reynolds A, Leake D, Boese Q, Scaringe S, Marshall WS, Khvorova A. 2004. Rational siRNA design for RNA interference. Nat Biotechnol, 22(3):326-330 DOI: 10.1038/nbt936.

Roh MH, Liu C-J, Laurinec S, Margolis B. 2002. The Carboxyl Terminus of Zona Occludens-3 Binds and Recruits a Mammalian Homologue of Discs Lost to Tight Junctions. J Biol Chem, 277(30):27501-27509 DOI: 10.1074/jbc.M201177200.

Román-Fernández A, Bryant DM. 2016. Complex Polarity: Building Multicellular Tissues Through Apical Membrane Traffic. Traffic, 17(12):1244–1261 DOI: 10.1111/tra.12417.

Rossi JM, Dunn NR, Hogan BLM, Zaret KS. 2001. Distinct mesodermal signals, including BMPs from the septum transversum mesenchyme, are required in combination for hepatogenesis from the endoderm. Genes Dev, 15(15):1998-2009 DOI: 10.1101/gad.904601.

Royer LA, Weigert M, Günther U, Maghelli N, Jug F, Sbalzarini IF, Myers EW. 2015. ClearVolume: open-source live 3D visualization for light-sheet microscopy. Nat Methods, 12(6):480-481 DOI: 10.1038/nmeth.3372.

Rübsam M, Mertz AF, Kubo A, Marg S, Jüngst C, Goranci-Buzhala G, Schauss AC, Horsley V, Dufresne ER, Moser M, Ziegler W, Amagai M, Wickström SA, Niessen CM. 2017. E-cadherin integrates mechanotransduction and EGFR signaling to control junctional tissue polarization and tight junction positioning. Nat Commun, 8(1):1250 DOI: 10.1038/s41467-017-01170-7.

Sasse D, Spornitz UM, Maly IP. 1992. Liver architecture. Enzyme, 46(1-3):8-32 DOI: 10.1159/000468776.

Schindelin J, Arganda-Carreras I, Frise E, Kaynig V, Longair M, Pietzsch T, Preibisch S, Rueden C, Saalfeld S, Schmid B, Tinevez J-Y, White DJ, Hartenstein V, Eliceiri K, Tomancak P, Cardona A. 2012. Fiji: an open-source platform for biological-image analysis. Nat Methods, 9(7):676-682 DOI: 10.1038/nmeth.2019.

Segovia-Miranda F, Morales-Navarrete H, Kücken M, Moser V, Seifert S, Repnik U, Rost F, Brosch M, Hendricks A, Hinz S, Röcken C, Lütjohann D, Kalaidzidis Y, Schafmayer C, Brusch L, Hampe J, Zerial M. 2019. Three-dimensional spatially resolved geometrical and functional models of human liver tissue reveal new aspects of NAFLD progression. Nat Med, 25(12):1885-1893 DOI: 10.1038/s41591-019-0660-7.

Shin K, Fogg VC, Margolis B. 2006. Tight junctions and cell polarity. Annu Rev Cell Dev Biol, 22:207-235 DOI: 10.1146/annurev.cellbio.22.010305.104219.

Suzuki K, Tanaka M, Watanabe N, Saito S, Nonaka H, Miyajima A. 2008. p75 Neurotrophin Receptor Is a Marker for Precursors of Stellate Cells and Portal Fibroblasts in Mouse Fetal Liver. Gastroenterology, 135(1):270-281.e3 DOI: 10.1053/j.gastro.2008.03.075.

Tanimizu N, Mitaka T. 2017. Epithelial Morphogenesis during Liver Development. Cold Spring Harb Perspect Biol, 9(8):a027862 DOI: 10.1101/cshperspect.a027862.

Tanimizu Naoki, Kaneko Kota, Itoh Tohru, Ichinohe Norihisa, Ishii Masayuki, Mizuguchi Toru, Hirata Koichi, Miyajima Atsushi, Mitaka Toshihiro. 2016. Intrahepatic bile ducts are developed through formation of homogeneous continuous luminal network and its dynamic rearrangement in mice. Hepatology, 64(1):175–188 DOI: 10.1002/hep.28521.

Theiler K. 1989. The House Mouse: Atlas of Embryonic Development. Springer-Verlag, Berlin Heidelberg DOI: 10.1007/978-3-642-88418-4.

Trauner M, Boyer JL. 2003. Bile Salt Transporters: Molecular Characterization, Function, and Regulation. Physiol Rev, 83(2):633–671 DOI: 10.1152/physrev.00027.2002.

Tsukita S, Tanaka H, Tamura A. 2019. The Claudins: From Tight Junctions to Biological Systems. Trends Biochem Sci, 44(2):141-152 DOI: 10.1016/j.tibs.2018.09.008.

Vega-Salas DE, Salas PJI, Rodriguez-Boulan E. 1987. Modulation of the expression of an apical plasma membrane protein of Madin-Darby canine kidney epithelial cells: Cell-cell interactions control the appearance of a novel intracellular storage compartment. J Cell Biol, 104(5):1249-1259 DOI: 10.1083/jcb.104.5.1249.

Wang J, Mauvoisin D, Martin E, Atger F, Galindo AN, Dayon L, Sizzano F, Palini A, Kussmann M, Waridel P, Quadroni M, Dulić V, Naef F, Gachon F. 2017. Nuclear Proteomics Uncovers Diurnal Regulatory Landscapes in Mouse Liver. Cell Metab, 25(1):102–117 DOI: 10.1016/j.cmet.2016.10.003.

Wang T, Yanger K, Stanger BZ, Cassio D, Bi E. 2014. Cytokinesis defines a spatial landmark for hepatocyte polarization and apical lumen formation. J Cell Sci, 127(11):2483–2492 DOI: 10.1242/jcs.139923.

Weigert M, Schmidt U, Boothe T, Müller A, Dibrov A, Jain A, Wilhelm B, Schmidt D, Broaddus C, Culley S, Rocha-Martins M, Segovia-Miranda F, Norden C, Henriques R, Zerial M, Solimena M, Rink J, Tomancak P, Royer L, Jug F, Myers EW. 2018. Content-aware image restoration: pushing the limits of fluorescence microscopy. Nat Methods, 15(12):1090-1097 DOI: 10.1038/s41592-018-0216-7.

Weiss MC, Garrec J-FL, Coqueran S, Strick-Marchand H, Buckingham M. 2016. Progressive developmental restriction, acquisition of left-right identity and cell growth behavior during lobe formation in mouse liver development. Development, 143(7):1149–1159 DOI: 10.1242/dev.132886.

Willey A. 1894. Amphioxus and the Ancestry of the Vertebrates. Macmillan.

Yang L, Wang W-H, Qiu W-L, Guo Z, Bi E, Xu C-R. 2017. A single-cell transcriptomic analysis reveals precise pathways and regulatory mechanisms underlying hepatoblast differentiation. Hepatol Baltim Md, 66(5):1387-1401 DOI: 10.1002/hep.29353.

Yu W, Datta A, Leroy P, O'Brien LE, Mak G, Jou T-S, Matlin KS, Mostov KE, Zegers MMP. 2005. β1-Integrin Orients Epithelial Polarity via Rac1 and Laminin. Mol Biol Cell, 16(2):433–445 DOI: 10.1091/mbc.E04-05-0435.

Zihni C, Mills C, Matter K, Balda MS. 2016. Tight junctions: from simple barriers to multifunctional molecular gates. Nat Rev Mol Cell Biol DOI: 10.1038/nrm.2016.80.

Zong Y, Panikkar A, Xu J, Antoniou A, Raynaud P, Lemaigre F, Stanger BZ. 2009. Notch signaling controls liver development by regulating biliary differentiation. Development, 136(10):1727–1739 DOI: 10.1242/dev.029140.

8 Acknowledgements

I want to thank Prof. Dr. Marino Zerial for giving me the opportunity to pursue my PhD in his group, for his support and mentorship.

I would also like to thank Dr. Lenka Belicova and Dr. Hernan A. Morales Navarrete, they have been there to help and support me when I needed it both as colleagues and as friends.

I want to thank Prof. Dr. Wieland B. Huttner and Prof. Dr. Elisabeth Knust for being in my TAC committee and providing feedback throughout my PhD.

I am thankful to Dr. Anne Wuttke, Sarah Seifert, Dr. Fabian Segovia-Miranda, Dr. Giuseppe Ferrandino, Dr. Yannis Kalaidzidis, Dr. Kirstin Meyer, Dr. Jose Ignacio Valenzuela Iturra and Dr. Nereo Kalebic for their scientific feedback.

I am grateful for the help provided by people in the facilities making MPI-CBG such a great place to work.

I would like to thank the entire Zerial lab, current and former members I had pleasure to meet. The collaborative and friendly atmosphere made me always happy to come to work.